R. & M. No. 2992
(17,413)
A.R.C. Technical Report

MINISTRY OF SUPPLY

AERONAUTICAL RESEARCH COUNCIL
REPORTS AND MEMORANDA

Theoretical Load Distributions on Fin-Body-Tailplane Arrangements in a Side-wind

By

J. WEBER, Dr.rer.nat., and A. C. HAWK, B.A.

Crown Copyright Reserved

LONDON: HER MAJESTY'S STATIONERY OFFICE
1957
SEVENTEEN SHILLINGS NET

Theoretical Load Distributions on Fin-Body-Tailplane Arrangements in a Side-wind

By

J. Weber, Dr.rer.nat., and A. C. Hawk, B.A

Communicated by the Principal Director of Scientific Research (Air), Ministry of Supply

Reports and Memoranda No. 2992*

August, 1954

Summary.—A theory has been developed for calculating the distributions of sideforce and lift on fin-fuselage-tailplane arrangements in a side-wind but with the tailplane set at zero incidence. The analysis is limited to incompressible flow and has been further simplified by assuming that the geometrical arrangement is in each case such as to give constant induced sidewash. The results, which can be extended to other arrangements and to compressible sub-critical flow, are required for stability and stressing analyses. This paper is a continuation of an earlier note by the first author (Ref. 1), where the interference between fin and fuselage was considered. The addition of the tailplane introduced into the present report brings considerable changes in the load distribution as well as in the overall forces. The actual calculation procedure is very simple and quick since the main functions needed are presented in tables and charts for representative cases. The results for other geometrical arrangements can be obtained by interpolation.

1. *Introduction*.—The work described in this report belongs to a series of investigations of the mutual interference between the separate parts of combinations of lifting surfaces and bodies. This interference problem can be divided into two major parts: (i) the determination of the pressure distribution when the wing and body are at zero incidence (thickness effect); (ii) the determination of the load distribution when the wing is at a finite angle (either incidence or side-wash). Only the second problem is treated here; it can easily be solved for arrangements, for which the resulting trailing vortex system produces constant induced velocity along the wing span. In this case the load distribution can be calculated from the two-dimensional flow around the cross-section of the wake in the Trefftz-plane (which is situated far behind the wing for wings of large aspect ratio), if the induced velocity is known. The latter is determined from the given characteristics of the wing; *i.e.*, plan-form, angle of sweep and sectional lift slope.

This method has been applied by Nagel and Mangler[2,3] and Falkner and Darwin[4] to wings with end plates, by Rotta[5] to wings with single plates, by Hartley[6] to wings with tip tanks and by the first author to wings with fences[7] and to fin-fuselage arrangements[1]. The method is used in the present report to determine the load distribution for fin-tailplane-fuselage combinations. Recent experimental investigations are reported in Refs. 8 and 9.

Comparison with experimental results has demonstrated that the theoretical results obtained for combinations which give constant induced velocities can successfully be used to estimate the additional load distributions for other combinations. In Ref. 9 it has been shown for fin-fuselage

* R.A.E. Report Aero. 2518, received 1st March, 1955.

combinations without tailplane that the side-force distribution along the height of the fin and fuselage can be obtained with sufficient accuracy from the theoretical load distributions on a wing with a cylindrical body at one end, by adding the difference between the side-force calculated for a constant induced side-wash arrangement and the side-force for the isolated fin which gives constant induced side-wash to the side-force distribution on the given fin alone[9]. Differences between the side-forces on any given arrangement and those for the constant induced side-wash arrangement can be appreciable only when the aspect ratio is large. They will become smaller as the aspect ratio A is decreased, and in the limiting case $A \rightarrow 0$ the theory is exact for any arrangement. Experimental evidence has also shown that the fuselage need not be strictly cylindrical in the neighbourhood of and behind the fin to allow the application of the theoretical results which were obtained for cylindrical bodies. This means that the shape of the wake immediately behind the trailing edge matters most and not any alterations far behind; this is consistent with the fact that, for ordinary wings, the rolling-up of the trailing vortices far downstream can be ignored when calculating the induced velocity at the wing.

This report gives the side-force distributions along the height of fin and body and the spanwise lift distribution on tailplane and body for fin-tailplane-fuselage arrangements in a pure side-wind. The main flow is at zero incidence with respect to the axis of the fuselage. The fuselage is of circular cross-section, it is assumed to be cylindrical near the wing, and this cylindrical part is assumed long enough to ensure that the wake behind the system has the shape of a spanwise cross-section through fin-tailplane-fuselage. The tailplane can be attached either to the fuselage or to the fin. The method is applicable to tailplanes of straight cross-section without dihedral, except for tailplanes positioned near the fin-fuselage junction in which case the conformal transformation requires a curved cross-section. The chord of the tailplane is assumed to be about the same as that of the fin.

Numerical values of the induced side-wash, the side-force and the lift distributions are given in charts and tables for a series of representative cases. Tailplanes of various spans, varying from zero to three times the height of the fin outside the body, are considered at four spanwise positions: at the body centre-line, at the top of the fin and at $0 \cdot 5$ and $0 \cdot 75$ times the fin height away from the fin-fuselage junction. The body diameter varies between zero and the fin height. The special case of zero body diameter which has been treated by Rotta[5], and the case of zero tailplane span, dealt with in Ref. 1, are included. They are treated here by simpler conformal transformations than those of Refs. 1 and 5. The provision of these charts and tables means that the actual computation which remains to be done in any particular case is very small. The geometrical configurations considered should be sufficient to enable most practical cases to be calculated by interpolation.

Though the calculations are restricted to incompressible flow, the results can be applied to sub-critical compressible flow by employing the well-known Prandtl-Glauert procedure.

The same transformations of the Trefftz-plane can be used when calculating the load distribution for a main flow which has a side-wash angle and an incidence. This report deals with the case of zero incidence only. The general problem with the main flow at an angle of incidence and side-wash has been treated by Bryson[10] and Landahl[11] for the special case of a tailplane along the line of symmetry of the body by employing the slender-body theory.

2. *The Potential Function of the Flow in the Trefftz-Plane.*—The force distribution over the body, fin and tailplane is proportional to the local difference of the potential function on either side of the vortex sheet in the Trefftz-plane. To determine the flow in the Trefftz-plane is a two-dimensional problem, which can be solved by conformal transformation. The wake contour in the Trefftz-plane is moving with constant velocity $v_{y\infty}$ in the direction of the tailplane span. The flow around the moving wake contour is equal to the one around the non-moving contour in a parallel flow of velocity $-v_{y\infty}$, on which is superimposed a parallel flow of velocity $v_{y\infty}$.

First, a conformal transformation is determined which transforms the flow around the wake contour into the flow past a flat plate parallel to the uniform stream $-v_{y\infty}$, for which the potential function is known.

A rectangular system of co-ordinates x, y, z is chosen, with the x-axis along wind, the z-axis along the line of symmetry, and the origin on the body axis (*see* Fig. 1). Let R be the radius of the body, h the height of the fin outside the body, b the total span of the tailplane, and h_1 its distance from the body-fin junction, measured positively from body-fin junction to body-tailplane junction. Then the wake contour in the Trefftz-plane, $x = \infty$, may be taken as the circle $y^2 + z^2 = R^2$, the line $y = 0$, $R < z < R + h$ and the line $z = R + h_1$, $-b/2 < y < b/2$. To obtain dimensionless parameters all lengths are divided by h and throughout the section describing the conformal transformation R, b, h_1, y and z are written for R/h, b/h, h_1/h, y/h and z/h.

The transformation is performed in four steps. The position of certain points on the contour and their transforms are shown in Fig. 1, and the co-ordinates of the points are given in Table 1. The case of the tailplane lying in the line of symmetry of the body allows some simplification and is therefore dealt with separately in section 7.

In the first step, the ζ-plane where

$$\zeta = y + iz \qquad \text{(1)}$$

is transformed into the ζ_1-plane so that the circle ABCA is transformed into a slit along the z_1-axis from A_1 to C_1. This is done by the transformation,

$$\zeta_1 = \zeta - \frac{R^2}{\zeta}. \qquad \text{(2)}$$

This transforms the fin CG into the z_1-axis from C_1 to G_1 and the tailplane EFJ into a curve $E_1F_1J_1$. In the next transformation this curve is approximated by the arc of a circle through the points E_1, F_1, J_1. This means that the tailplane for which the calculations are performed is not exactly straight.

To show the accuracy of this approximation, a few tailplane shapes are plotted in Fig. 2, which become circular arcs in the ζ_1-plane by the transformation of equation (2). The results are given for arrangements with large body diameter compared with the height of the fin, since for these cases the deviations from a straight tailplane become larger than for small bodies. The figure shows that in those cases where the tailplane is not near the fin-body junction the difference between the calculated tailplane and the straight tailplane is negligible.

For tailplanes near the fin-body junction, the tailplane shapes that lead to circular arcs in the ζ_1-plane are not straight. This is no serious drawback for the practical application of the present calculation method since a straight tailplane on top of a fuselage of circular cross-section does not seem to be an aerodynamically good arrangement in view of the acute angle that would be formed at the tailplane-fuselage junction. For a tailplane near the fuselage-fin junction one will, therefore, either design a fuselage which has a non-circular cross-section in the neighbourhood of fin and tailplane or take a tailplane that is not straight. This means that tailplane shapes as in Fig. 2 are probably still reasonable for estimating the effect of the tailplane on the side-forces on fin and body. For the design of tailplanes near the top of the fuselage the shape of neutral tailplanes which do not affect the flow around fin and fuselage alone are of interest. Such shapes are plotted in Fig. 14.

By the second transformation the circular arc $E_1F_1J_1$ is transformed into a full circle and the z_1-axis from A_1 to D_1 and F_1 to G_1 into the z_2-axis from A_2 to D_2 and F_2 to G_2. The transformation is:

$$\zeta_1 - iz_{E1} = \zeta_2 + \frac{y_{E1}^2}{4}\frac{1}{\zeta_2}. \qquad \text{(3)}$$

With

$$\varkappa = z_{E1} = \frac{(h_1 + R)[h_1^2 + 2h_1R + 2R^2 + (b/2)^2]}{(h_1 + R)^2 + (b/2)^2} \quad \ldots \quad (4)$$

and

$$\lambda = y_{E1} = \frac{(b/2)[h_1^2 + 2h_1R + (b/2)^2]}{(h_1 + R)^2 + (b/2)^2} \quad \ldots \quad (5)$$

equation (3) can be written in the form:

$$\zeta_2 = \frac{1}{2}\left[\zeta_1 - i\varkappa \mp \sqrt{\{(\zeta_1 - i\varkappa)^2 - \lambda^2\}}\right] \quad \ldots \quad (6)$$

The minus sign holds for points on the z_1-axis below D_1 and for the lower side of the circular arc, the positive sign for points on the z_1-axis above F_1 and for the upper side of the circular arc.

The circle in the ζ_2-plane has the centre:

$$\zeta_2 = i\frac{\mu}{2} = i\frac{z_{D2} + z_{F2}}{2} = i\frac{R^2(b/2)^2}{2(h_1 + R)[(h_1 + R)^2 + (b/2)^2]} \quad \ldots \quad (7)$$

and the radius

$$r = \frac{z_{F2} - z_{D2}}{2} = \frac{1}{2}\sqrt{(\mu^2 + \lambda^2)}\,.$$

In the next step the circle is transformed into a straight line along the z_3-axis by the transformation

$$\zeta_3 = \zeta_2 - i\frac{\mu}{2} - \frac{1}{4}\frac{\mu^2 + \lambda^2}{\zeta_2 - i\frac{\mu}{2}}\,. \quad \ldots \quad (8)$$

Thus the whole wake contour is transformed into a slit along the z_3-axis from A_3 to G_3.

Finally, this slit is transformed into a slit along the y_4-axis by the transformation:

$$\zeta_4 = \sqrt{\left\{\left(\zeta_3 + i\frac{\varrho - \sigma}{2}\right)^2 + \left(\frac{\varrho + \sigma}{2}\right)^2\right\}} \quad \ldots \quad (9)$$

where

$$\varrho = -z_{A3} = +\frac{1}{2}\left[2R + \varkappa + \mu + \sqrt{\{(2R + \varkappa)^2 + \lambda^2\}} + \frac{\mu^2 + \lambda^2}{2R + \varkappa + \mu + \sqrt{\{(2R + \varkappa)^2 + \lambda^2\}}}\right] \quad (10)$$

and

$$\sigma = z_{G3} = \frac{1}{2}\left[\tau - \varkappa - \mu + \sqrt{\{(\tau - \varkappa)^2 + \lambda^2\}} + \frac{\mu^2 + \lambda^2}{\tau - \varkappa - \mu + \sqrt{\{(\tau - \varkappa)^2 + \lambda^2\}}}\right] \quad \ldots \quad (11)$$

with

$$\tau = z_{G1} = \frac{1 + 2R + 2R^2}{1 + R}\,. \quad \ldots \quad (12)$$

Thus the relation between points on the wake contour and on the slit in the ζ_4-plane is known. Points on the wake contour correspond to points on the z_3-axis. For any point on the body where $-R \leqslant z \leqslant R$, $y = \sqrt{(R^2 - z^2)}$, the relation reads:

$$z_3 = \frac{1}{2}\left[2z - \varkappa - \mu - \sqrt{\{(2z - \varkappa)^2 + \lambda^2\}} + \frac{\mu^2 + \lambda^2}{2z - \varkappa - \mu - \sqrt{\{(2z - \varkappa)^2 + \lambda^2\}}}\right] \quad \ldots \quad (13)$$

and for any point on the fin, where $y = 0$, $R \leqslant z \leqslant R + 1$, the relation is:

$$z_3 = \frac{1}{2}\left[\frac{z^2 + R^2}{z} - \varkappa - \mu \mp \sqrt{\left\{\left(\frac{z^2 + R^2}{z} - \varkappa\right)^2 + \lambda^2\right\}} + \frac{\mu^2 + \lambda^2}{\frac{z^2 + R^2}{z} - \varkappa - \mu \mp \sqrt{\left\{\left(\frac{z^2 + R^2}{z} - \varkappa\right)^2 + \lambda^2\right\}}}\right] \quad \ldots \quad (14)$$

with the negative sign holding for points of the fin between the body and tailplane

$$R \leqslant z \leqslant R + h_1$$

and the positive sign for points outside

$$R + h_1 \leqslant z \leqslant R + 1 .$$

The relation between corresponding points on the z_3-axis and the y_4-axis reads:

$$y_4 = \pm \sqrt{\{-z_3^2 - (\varrho - \sigma)z_3 + \varrho\sigma\}} . \quad \ldots \quad (15)$$

For the tailplane which has been replaced by a curve differing slightly from the straight line $z = R + h_1$, points of the same y-value on the actual and the replacement tailplane are correlated We find corresponding points on the tailplane and the y_4-axis by the relations:

$$z_3 = \frac{1}{2}\left[-(\varrho - \sigma) \pm \sqrt{\{(\varrho + \sigma)^2 - 4y_4^2\}}\right] \quad \ldots \quad (16)$$

$$y_1 = \frac{1}{2}\sqrt{\{\mu^2 + \lambda^2 - z_3^2\}}\left[1 + \frac{\lambda^2}{2\mu^2 + 2\mu z_3 + \lambda^2}\right] \quad \ldots \quad (17)$$

$$z_1 = \varkappa + \tfrac{1}{2}(z_3 + \mu)\left[1 - \frac{\lambda^2}{2\mu^2 + 2\mu z_3 + \lambda^2}\right] \quad \ldots \quad (18)$$

$$y = \frac{1}{2}\left[y_1 \pm \sqrt{\left\{\frac{1}{2}\left(y_1^2 - z_1^2 + 4R^2 + \sqrt{\{(y_1^2 - z_1^2 + 4R^2)^2 + 4y_1^2 z_1^2\}}\right)\right\}}\right] . \quad (19)$$

In equation (16) the positive sign has to be taken throughout, if $(\varrho - \sigma)/2 > \sqrt{(\mu^2 + \lambda^2)}$, *i.e.*, if the mid-point of A_3G_3 lies below D_3 (*see* Table 1). Points on the upper side of the tailplane (EF) are obtained for:

$$\sqrt{[-\mu^2 - \lambda^2 - \sqrt{\{\mu^2 + \lambda^2\}}(\varrho - \sigma) + \varrho\sigma]} < |y_4| < \sqrt{[-\mu^2 + (\varrho - \sigma)\mu + \varrho\sigma]} \quad \ldots \quad (20)$$

and points on the lower side (DE) for:

$$\sqrt{[-\mu^2 + (\varrho - \sigma)\mu + \varrho\sigma]} < |y_4| < \sqrt{[-\mu^2 - \lambda^2 + \sqrt{\{\mu^2 + \lambda^2\}}(\varrho - \sigma) + \varrho\sigma]}. \quad \ldots \quad (21)$$

If

$$\mu < \frac{\varrho - \sigma}{2} < \sqrt{(\mu^2 + \lambda^2)} ,$$

i.e., if the mid-point of A_3G_3 lies between D_3 and E_3, the points corresponding to the tailplane lie partly on the upper side of the slit along the y_4-axis and partly on the lower side. Points on the upper side of the tailplane are again obtained for y_4-values corresponding to equation (20), for which the positive sign in equation (16) is taken. For y_4-values in the range

$$\sqrt{[-\mu^2 + (\varrho - \sigma)\mu + \varrho\sigma]} < |y_4| < \frac{\varrho + \sigma}{2} \quad \ldots \quad (22)$$

and the positive sign in equation (16) part of the lower side of the tailplane is obtained. The remaining part corresponds to

$$\sqrt{[-\mu^2 - \lambda^2 + \sqrt{\{\mu^2 + \lambda^2\}}(\varrho - \sigma) + \varrho\sigma]} < |y_4| < \frac{\varrho + \sigma}{2} \quad \ldots \quad (23)$$

and the negative sign taken in equation (16).

With all transformations the behaviour at infinity is unchanged, this means that in the ζ_4-plane the flow at infinity is the same parallel flow with velocity $-v_{y\infty}$ as in the original ζ-plane. Since the slit in the ζ_4-plane lies along the parallel flow, the potential function for the flow around the fixed wake contour is

$$F_1(\zeta) = \phi_1 + i\psi_1 = -v_{y\infty} h\zeta_4 \, .$$

To obtain the flow around the moving wake we superimpose the potential for a parallel flow of velocity $v_{y\infty}$ in the ζ-plane

$$F_2(\zeta) = v_{y\infty} h\zeta \, ,$$

so that the total potential function for the wake moving with a velocity $v_{y\infty}$ is given by

$$\phi(y,z) = \phi_1 + \phi_2 = -[y_4(y,z) - y]v_{y\infty} h \qquad \ldots \quad (24)$$

where equations (13) to (15) give the relations between (y,z) and y_4 for points on the body and fin and equations (16) to (19) the relations between y and y_4 for the tailplane.

3. *The Side-force Distribution on Fin and Body and the Overall Side-force Coefficient.*—From the known flow in the Trefftz-plane the strength of the trailing vortices can be determined. The trailing vortices are related to the bound vortices on fin, fuselage and tailplane. Thus the latter can be calculated from the flow in the Trefftz-plane. The local side-force and lift are proportional to the difference of the potential function at corresponding points on the two surfaces of the vortex sheet in the Trefftz-plane.

The local coefficient of the side-force on the fin and body is given by the difference of the potential function in the wake, taken at two points of the same height:

$$C_Y = \frac{F_Y}{\frac{1}{2}\varrho V_0^2 c} = \frac{2}{cV_0} (\phi_{\text{left}} - \phi_{\text{right}}) \qquad \ldots \quad (25)$$

where c is the local chord, used as reference chord for the local side-force coefficient C_Y, and V_0 is the velocity of the main flow. From equations (24) and (25) for the fin, $R < z < R + h$:

$$C_{YF}(z)c(z) = 4\frac{v_{y\infty}}{V_0} |y_4(z)|h \qquad \ldots \quad (26)$$

and for the body, $|z| < R$:

$$C_{YB}(z) \, . \, c = 4\frac{v_{y\infty}}{V_0} h\left[|y_4(z)| - \sqrt{\left\{\left(\frac{R}{h}\right)^2 - \left(\frac{z}{h}\right)^2\right\}}\right]. \qquad \ldots \quad (27)$$

The coefficient of the overall side-force on the fin $\bar{C}_{YF}$ is obtained by integration. Referring $\bar{C}_{YF}$ to the fin area $h\bar{c}_F$, where $\bar{c}_F$ is the mean fin chord:

$$\bar{C}_{YF}\,\bar{c}_F = \int_{R/h}^{(R/h)+1} C_{YF}\, c \, d\left(\frac{z}{h}\right) \qquad \ldots \quad (28)$$

we find

$$\bar{C}_{YF} = \frac{v_{y\infty}}{V_0} A_F J_{YF} \qquad \ldots \quad (29)$$

where

$$A_F = \frac{h}{\bar{c}_F} \qquad \ldots \quad (30)$$

is the aspect ratio of the fin, and

$$J_{YF} = 4\int_{R/h}^{(R/h)+1} |y_4(z)| \, d\left(\frac{z}{h}\right). \qquad \ldots \quad (31)$$

J_{YF} is a function of R/h, b/h and h_1/h but independent of the aspect ratio. Values of J_{YF} are plotted in Figs. 4a to 4d.

The overall side-force on the body, also referred to the fin area $h\bar{c}_F$, is

$$\bar{C}_{YB} = \frac{v_{y\infty}}{V_0} A_F J_{YB} \quad \ldots \quad (32)$$

with

$$J_{YB} = 4\int_{-R/h}^{R/h} \left[|y_4(z)| - \sqrt{\left\{ \left(\frac{R}{h}\right)^2 - \left(\frac{z}{h}\right)^2 \right\}} \right] d\left(\frac{z}{h}\right)$$

$$= 4\int_{-R/h}^{R/h} |y_4(z)| \, d\left(\frac{z}{h}\right) - 2\pi\left(\frac{R}{h}\right)^2 . \quad \ldots \quad (33)$$

J_{YB} also is a function of R/h, b/h and h_1/h and independent of A_F. Values of J_{YB}/J_{YF} are plotted in Fig. 5.

The shape of the spanwise force distribution on the fin is by equations (26) to (33):

$$\frac{C_{YF}(z)c(z)}{\bar{C}_{YF}\bar{c}_F} = \frac{4|y_4(z)|}{J_{YF}} \quad \ldots \quad (34)$$

and for the body

$$\frac{C_{YB}(z)c}{\bar{C}_{YF}\bar{c}_F} = 4\,\frac{|y_4(z)| - \sqrt{\left\{ \left(\frac{R}{h}\right)^2 - \left(\frac{z}{h}\right)^2 \right\}}}{J_{YF}} . \quad \ldots \quad (35)$$

A few distributions of the side-force are plotted in Figs. 6a to 6c. For the fin, values of $C_{YF}\,c/\bar{C}_{YF}\bar{c}_F$ for various tailplane positions, body diameters and tailplane spans are given in Table 2. For the body the local side-force divided by the value at the fin-fuselage junction $C_{YB}\,c/(C_{YB}\,c)_{\text{junction}}$ is tabulated in Table 3.

The flow in the Trefftz-plane and from that the local and the total side-force are known if the side-wash velocity $v_{y\infty}$ at infinity is known. The value of $v_{y\infty}$ cannot be determined from the conditions in the Trefftz-plane alone, but has to be related to the conditions at fin, body and tailplane. This will be done in the following section.

4. *The Induced Side-wash Velocity*.—The next step in the calculation procedure is to relate the induced velocity $v_{y\infty}$ in the wake to the sideways component βV_0 of the main stream at the actual fin-tailplane position. For this purpose, the boundary condition at the fin can be used, which states that the sum of the induced side-wash and the effective side-wash produced by the bound vortices is equal and opposite to the geometric side-wash at the fin. The latter is the sum of $-\beta V_0$ and of $-\beta_B V_0$ which results from the cross-flow component of the flow around the isolated fuselage and which depends on the cross-sectional shape of the fuselage. The induced side-wash angle β_i at the fin-tailplane arrangement can be related to $v_{y\infty}$, whereas the effective side-wash angle β_e can be determined from the known distribution of the bound vortices. At this stage, the condition of constant induced side-wash can be expressed as requiring a certain 'plan-form' of the fin.

The strength of the bound vortices and therefore the local side-force coefficient of the fin are proportional to the sectional lift slope $a(z)$, as defined in Ref. 12, and hence also to the effective side-wash angle β_e:

$$C_{YF}(z) = \beta_e(z)a(z) . \quad \ldots \quad (36)$$

The boundary condition gives

$$\beta_e = \beta + \beta_B - \beta_i \quad \ldots \quad (37)$$

where β is the geometric side-wash angle of the fin. The additional side-wash angle β_B which is produced by the flow around the isolated body, is as explained in Ref. 13,

$$\beta_B = \beta\,\frac{1}{(z/R)^2} . \quad \ldots \quad (38)$$

In relating the induced side-wash $v_{y\,\infty}/V_0$ in the Trefftz-plane to the induced side-wash angle β_i on the actual fin-tailplane arrangement, we have to decide where the streamwise position of the Trefftz-plane is, since this has not yet been fixed. For fins of very large aspect ratio, the Trefftz-plane is obviously infinitely far behind the arrangement and $\beta_i = \frac{1}{2}v_{y\,\infty}/V_0$. For fin-tailplanes of very small aspect ratio, the Trefftz-plane may be considered as a section through the actual fin-tailplane arrangement, following R. T. Jones[14], and therefore $\beta_i = v_{y\,\infty}/V_0$. Generally, the side-wash angle β_i which the trailing vortices induce at the fin can be taken as proportional to the side-wash far downstream:

$$\beta_i = \frac{v_y}{V_0} = \frac{\omega}{2}\frac{v_{y\,\infty}}{V_0}. \qquad (39)$$

The value of ω depends on the chordwise load distribution and therefore mainly on the effective aspect ratio of the wing; $\omega = 1$ for wings of large aspect ratio, $\omega = 2$ for $A \to 0$. A method for calculating ω for isolated wings is given in Ref. 12. As discussed in Ref. 1, the same value of ω is taken for that part of the vorticity which is dependent on the geometric side-wash angle β as for the vorticity derived from the additional side-wash angle β_B, though the corresponding chordwise side-force distributions are different. A relation from which ω can be determined is given by equation (123) in section 8 of the present report.

Thus we obtain from equations (36) to (39) the following equation for the side-force coefficient:

$$\frac{C_{YF}(z)}{\beta} = a(z)\left[1 + \frac{1}{(z/R)^2} - \frac{\omega}{2}\frac{v_{y\,\infty}/V_0}{\beta}\right]. \qquad (40)$$

This is another relation between C_{YF} and $v_{y\,\infty}$ besides equation (26). The two relations together imply that, in order to obtain an arrangement which gives constant side-wash along the fin, the fin must have a certain planform. The variation of chord along the height of the fin which satisfies the condition of producing a constant side-wash distribution in the presence of fuselage and tailplane is found by combining equations (26) and (40):

$$\frac{c(z)}{h} = \frac{4\,\dfrac{v_{y\,\infty}/V_0}{\beta}\,|y_4(z)|}{a(z)\left[1 + \dfrac{1}{(z/R)^2} - \dfrac{\omega}{2}\dfrac{v_{y\,\infty}/V_0}{\beta}\right]}$$

$$= \frac{\dfrac{8}{\omega}\dfrac{\beta_i}{\beta}\,|y_4(z)|}{a(z)\left[1 + \dfrac{1}{(z/R)^2} - \dfrac{\beta_i}{\beta}\right]}. \qquad (41)$$

The chord distribution is a function of β_i/β and known quantities. Integrating $c(z)$ along the fin height gives a relation between the unknown β_i/β and the known quantities A_F, $a(z)$, R/h, b/h, and h_1/h:

$$\frac{\bar{c}_F}{h} = \frac{1}{A_F} = \frac{8}{\omega}\frac{\beta_i}{\beta}\int_{R/h}^{(R/h)+1} \frac{|y_4(z)|}{a(z)\left[1 + \dfrac{1}{(z/R)^2} - \dfrac{\beta_i}{\beta}\right]}\, d\left(\frac{z}{h}\right). \qquad (42)$$

To permit the evaluation of the integral in equation (42) we must know $a(z)$. For isolated wings the sectional lift slope is a function of the aspect ratio and for swept wings of the angle of sweep φ and the spanwise position (*see* Ref. 12). The attachment of a body to the wing alters not only the spanwise loading on the wing, but also the chordwise load distribution. This implies that the sectional lift slope is different from that of the wing alone. With fin-body-tailplane arrangements with straight fin the chordwise distribution of the side-force on the fin will be similar to that on an isolated fin of larger aspect ratio—the 'effective aspect ratio' A_{eF}—because the bound vortices are less curved on the fin in the presence of body and tailplane than on the fin alone.

This is due to the fact that some vortices continue along body and tailplane and less trailing vortices are leaving the fin. An estimate of the effective aspect ratio is given in section 8. For isolated swept wings the value of a is smaller at the centre and larger at the tips than the value $a_s = a_0 \cos \varphi$ for an infinite sheared wing which holds at that part of the wing which is unaffected by centre and tip effects. On fin-body-tailplane arrangements with swept-back fin, the chordwise load distributions near the fin-fuselage and fin-tailplane junctions are similar to those at the centre of swept-back and swept-forward wings, *i.e.*, the sectional lift slope is decreased near the body, increased at the tailplane junction near the body, decreased at the far side junction and increased at the tip compared with the value a_s that holds away from the junctions. The value a_s can therefore be taken as a mean value of $a(z)$.

The aim of this note is also to give calculated examples which are generally applicable. We require therefore a value of the integral in equation (42) which is independent of any special $a(z)$ variation. An approximate value is obtained by replacing $a(z)$ by a mean value a, for which a_s is appropriate. With $a_s = $ const.,

$$\frac{\omega a}{A_F} = 8 \frac{\beta_i}{\beta} \int_{R/h}^{(R/h)+1} \frac{|y_4(z)|}{1 + \dfrac{1}{(z/R)^2} - \dfrac{\beta_i}{\beta}} d\left(\frac{z}{h}\right) \qquad \ldots \quad (43)$$

By this equation $\omega a/A_F$ is a function of β_i/β, R/h, b/h, h_1/h, all of which are given quantities, except β_i/β which is thus determined as a function of $\omega a/A_F$. The equation does not allow β_i/β to be expressed explicitly as a function of $\omega a/A_F$, R/h, b/h, h_1/h, but numerical values of the integral in equation (43) can be determined for various β_i/β and graphs prepared, from which β_i/β can be read when $\omega a/A_F$, R/h, b/h and h_1/h are known. Such diagrams are given in Figs. 7a to 7n.

For the side-force distribution over the body the discussion in Ref. 1 indicated that a side-wash factor $\omega_B = 2$ seems generally more appropriate, and that as an approximation the two different values of ω and ω_B could be taken into account by subtracting from the side-force distribution in equation (35) the term:

$$\frac{\Delta C_{YB}\, c}{\bar{C}_{YF}\, \bar{c}_F} = - \frac{\omega_B - \omega}{\omega} \frac{4R/h}{J_{YF}} \sqrt{\left\{1 - \left(\frac{z}{R}\right)^2\right\}} \qquad \ldots \quad (44)$$

and from the overall side-force on the body

$$\frac{\Delta \bar{C}_{YB}}{\beta} = - \frac{\omega_B - \omega}{\omega} \frac{2}{\omega} \frac{\beta_i}{\beta} \,.\, 2\pi A_F \left(\frac{R}{h}\right)^2 . \qquad \ldots \quad (45)$$

There remains the question whether the above equations give the total side-force on the body or the part of the side-force induced by the fin, *i.e.*, whether the forces on nose and rear end of the body are included.

The determination of C_Y from the difference in potential on the two surfaces of the vortex sheet in the Trefftz-plane by equation (25) is based on the assumption $\phi(x = -\infty) = 0$. This is true if the cylinder representing the body does not reach to infinity far forward, *i.e.*, the nose of the body is taken as of finite length. Hence, some nose load is included.

The next question concerns the forces at the rear end of the body. We consider first the extreme case, $h \to 0$, $b \to 0$, *i.e.*, an isolated circle as the wake contour in the Trefftz-plane. This can be regarded as a cross-section through an isolated body.

The transformation of equation (2) leads to the potential function

$$F_1(\zeta) = - v_{y\infty}\left(\zeta + \frac{R^2}{\zeta}\right).$$

For points on the body

$$\phi_1 = -\, v_{y\,\infty} \,.\, 2y$$

and after superimposing a parallel flow in the ζ-plane:

$$\phi = \phi_1 + \phi_2 = -\, v_{y\,\infty} \,.\, y$$

$$= -\, v_{y\,\infty} R \sqrt{\left\{1 - \left(\frac{z}{R}\right)^2\right\}} \,.$$

Thus for the local side-force

$$C_{YB}\, c = \frac{2}{V_0} \Delta\phi = 4 \frac{v_{y\,\infty}}{V_0} R \sqrt{\left\{1 - \left(\frac{z}{R}\right)^2\right\}}$$

and for the total side-force referred to the area $\bar{c}\,.\,2R$:

$$\bar{C}_{YB} = \frac{\bar{F}_{YB}}{\frac{1}{2}\varrho V_0^2 \bar{c}\,.\,2R} = \frac{1}{2R} \int_{-R}^{+R} C_{YB} \frac{c}{\bar{c}}\, dz$$

$$= \frac{v_{y\,\infty}}{V_0} \pi \frac{R}{\bar{c}} \,. \qquad \ldots \qquad (46)$$

With $\dfrac{v_{y\,\infty}}{V_0} = \beta$ we obtain

$$\bar{C}_{YB} = \pi \frac{R}{\bar{c}} \beta \qquad \ldots \qquad (47)$$

which equals the nose load on the body resulting from the momentum theorem. This implies that in this case the force on the rear end of the body is not included. In this case there is no side-force on the body induced by the fin, *i.e.*, the fin induced side-force is equal to the one calculated, reduced by $\pi\,.\,R/\bar{c}\,.\,v_{y\,\infty}/V_0$.

In the other extreme case of a body at one end of a large aspect ratio fin, the calculation gives zero side-force on the body, in agreement with the fact that the fin induces no side-force on the body.

As a general approximation for the side-force on the body induced by the fin, excluding forces on the nose and rear end of the body, we take the one calculated above in equation (32), with $\omega_B = \omega$, and reduce it by

$$\Delta\bar{C}_{YB} = -\frac{\Delta\bar{F}_Y}{\frac{1}{2}\varrho V_0^2 h\bar{c}} = -\frac{v_{y\,\infty}}{V_0} \cdot 2\pi A_F \left(\frac{R}{h}\right)^2$$

$$= -\frac{2}{\omega} \beta_i \,.\, 2\pi A_F \left(\frac{R}{h}\right)^2 . \qquad \ldots \qquad (48)$$

The reduction is the same as in equation (45) for $\omega_B = 2$, $\omega = 1$. Correspondingly, the side-force distribution of equation (35) is reduced by

$$\frac{\Delta C_{YB}\, c}{\bar{C}_{YF}\, \bar{c}} = -\frac{4R/h}{J_{YF}} \sqrt{\left\{1 - \left(\frac{z}{R}\right)^2\right\}} \qquad \ldots \qquad (49)$$

This procedure is confirmed by experimental pressure distributions on a cylindrical body attached to one tip of 45-deg swept-back wings of different aspect ratios (*see* Ref. 9). The measured side-force distributions agree fairly well with those calculated from equations (35) and (49).

If calculated total side-forces are to be compared with experimental force measurements the forces at the nose and rear-end of the body have to be added. With the isolated body in inviscid flow, the nose and rear force are equal and of opposite sign. For a body attached to a fin the effective incidence at the rear end of the body is smaller than at the nose, which means a smaller force at the rear-end. A further reduction of the rear-end force can be caused by viscosity effects.

5. *The Lift Distribution on Tailplane and Body.*—Some of the bound vortices on the fin continue along the tailplane and the body. The component of these bound vortices normal to the main flow of velocity V_0 produces a force normal to the tailplane, *i.e.*, a lift. For the left part of the tailplane, as drawn in Fig. 1, the lift is negative, that is directed towards the body, for the right-hand part of the tailplane it is directed away from the body. The total lift on the tailplane is zero, but the lift forces produce a moment about the tail-fin junction. There is also a lift distribution produced along the body, with positive lift on the left-hand side and negative lift on the right.

To calculate the lift $L(y)$ as a function of the geometric side-wash angle β, we first determine it as a function of $v_{y\infty}$. This can be obtained from the difference of the potential function on upper and lower surfaces of the vortex sheet in the Trefftz-plane:

$$C_L = \frac{L}{\frac{1}{2}\varrho V_0^2 c} = \frac{2}{cV_0}(\phi_{US} - \phi_{LS}) \qquad (50)$$

$$C_{LT}\, c = 2\frac{v_{y\infty}}{V_0}\Big[- y_4(y,z)_{US} + y_4(y,z)_{LS}\Big]\, h$$

For the right-hand part of the tailplane:

$$C_{LT}\, c = 2\frac{v_{y\infty}}{V_0}\,|\Delta y_4(y)|\, h\,. \qquad (51)$$

From equations (16) to (19) the function $y(y_4)$ can be calculated and from this $\Delta y_4(y)$ can be determined graphically. Referring the local lift coefficient to the coefficient of the total side-force, as was done for the side-force coefficient in equation (34), we obtain:

$$\frac{C_{LT}\, c}{\bar{C}_{YF}\, \bar{c}_F} = \frac{2|\Delta y_4(y)|}{J_{YF}}\,. \qquad (52)$$

A few tailplane lift distributions are plotted in Fig. 8. The lift coefficients are tabulated in Table 4.

The coefficient of the total lift acting on the right-hand side of the tailplane, referred to the fin area $h\bar{c}_F$, is obtained by integration:

$$\bar{C}_{LT} = \frac{\bar{L}_T}{\frac{1}{2}\varrho V_0^2 \bar{c}_F h} = \frac{v_{y\infty}}{V_0}\cdot 2\frac{h}{\bar{c}_F}\int_0^{b/2h} |\Delta y_4(y)|\, d\left(\frac{y}{h}\right)$$

$$= \frac{v_{y\infty}}{V_0} A_F J_{LT} \qquad (53)$$

where

$$J_{LT} = 2\int_0^{b/2h} |\Delta y_4(y)|\, d\left(\frac{y}{h}\right). \qquad (54)$$

The ratio of the total lift on one half of the tailplane to the total side-force is therefore:

$$\frac{\bar{C}_{LT}}{\bar{C}_{YF}} = \frac{J_{LT}}{J_{YF}}\,. \qquad (55)$$

This ratio is plotted in Figs. 9a to 9d.

From the known lift distribution, equation (52), both the moment $\mathscr{M}$ of the lift about the fin-tailplane junction and the arm $y_0 \, . \, h/2$ of the lift force can be determined:

$$\mathscr{M} = \int_0^{b/2} L \, . \, y \, dy$$

$$= y_{0T} \bar{L}_T$$

$$\frac{y_{0T}}{h} = \frac{\int_0^{b/2h} |\Delta y_4(y)| \frac{y}{h} d\left(\frac{y}{h}\right)}{\int_0^{b/2h} |\Delta y_4(y)| \, d\left(\frac{y}{h}\right)} \, . \qquad \qquad (56)$$

y_{0T} is plotted in Fig. 10.

In the same way, the lift distribution over the body, and the total lift acting on the right-hand side of the body

$$\bar{C}_{LB} = \frac{v_{y\,\infty}}{V_0} A_F J_{LB} \qquad \qquad (57)$$

are obtained. The ratio of the total lift on the right-hand side to the total side-force

$$\frac{\bar{C}_{LB}}{\bar{C}_{YF}} = \frac{J_{LB}}{J_{YF}} \qquad \qquad (58)$$

is plotted in Fig. 11. Lift distributions and the moment arm of the lift are plotted in Fig. 12. The lift coefficients on the body are tabulated in Table 5. Since the pressures act normally to the body surface there results no moment of the body forces with respect to the body axis.

In the same way as on the fin, certain boundary conditions have to be fulfilled on the tailplane. The bound vortices produce a velocity $-\alpha_e V_0$ normal to the tailplane whilst the assumed system of trailing vortices does not produce a normal velocity. To satisfy the streamline condition, the tailplane must therefore be twisted in such a way as to produce a normal velocity $\alpha_e V_0$; neglecting the generally small velocity component v_{zB} which the flow around the isolated body produces at the position of the tailplane. The local angle of twist is related to the local lift coefficient by the sectional lift slope

$$C_L(y) = a(y) \, . \, \alpha_e(y) \, . \qquad \qquad (59)$$

To obtain an estimate of the angle of twist, we may assume that the sectional lift slope of the tailplane in the presence of fin and body is the same as for the isolated tailplane. The tailplane is twisted to positive incidences on the right-hand side and to negative incidences on the left. For the body the condition of zero total normal velocity must hold. It is, however, not yet possible to determine from this condition the required shape of the body.

Similar conditions for the bound vortices and therewith for the shape of the bodies attached to a wing hold for all arrangements producing constant induced velocities as, *e.g.*, wings with endplates and fin-fuselage combinations. The fulfilment of these conditions, however, does not seem to be important for the load distribution on the wing as is shown by comparing the experimental results on wings with untwisted plates with those calculated for plates so twisted as to achieve zero induced side-wash at the plates (*see* Ref. 8).

6. *The Limiting Cases $b \rightarrow 0$ and $R \rightarrow 0$.*—In order to be able to compare the present results with those for a body and fin without tailplane and for a fin and tailplane without body, and to facilitate the plotting of diagrams it is useful to consider the cases $b \rightarrow 0$ and $R \rightarrow 0$.

For small b, expanding in powers of b,

$$\varkappa = \frac{h_1^2 + 2h_1R + 2R^2}{h_1 + R} - \frac{R^2}{(h_1 + R)^3}\left(\frac{b}{2}\right)^2 + \ldots \qquad (60)$$

$$= \varkappa_0 + \varkappa_2\left(\frac{b}{2}\right)^2 + \ldots, \qquad (61)$$

$$\lambda = \frac{h_1^2 + 2h_1R}{(h_1 + R)^2}\frac{b}{2} + \ldots \qquad (62)$$

$$= \lambda_1\frac{b}{2} + \ldots, \qquad (63)$$

$$\mu = \frac{R^2}{(h_1 + R)^3}\left(\frac{b}{2}\right)^2 + \ldots \qquad (64)$$

$$= -\varkappa_2\left(\frac{b}{2}\right)^2 + \ldots, \qquad (65)$$

$$\varrho = \left[2R + \varkappa_0 + \tfrac{1}{2}\varkappa_2\left(\frac{b}{2}\right)^2 + \frac{\lambda_1^2}{2(2R + \varkappa_0)}\left(\frac{b}{2}\right)^2 + \ldots\right]. \qquad (66)$$

If $h_1 \neq 1$, *i.e.*, if the tailplane is not at the end of the fin,

$$\sigma = \left[\tau - \varkappa_0 - \tfrac{1}{2}\varkappa_2\left(\frac{b}{2}\right)^2 + \frac{\lambda_1^2}{2(\tau - \varkappa_0)}\left(\frac{b}{2}\right)^2 + \ldots\right]. \qquad (67)$$

In this case, both the expansions for z_3 and for y_4 from equations (13), (14), (15) for points on the body and on the fin, except $z = h_1 + R$, contain no linear order term in b, which implies that graphs of $|y_4|$, its integral, and therefore $C_{YF}c/\bar{C}_{YF}\bar{c}_F$, $C_{YB}c/(C_{YB}c)_{junction}$, J_{YF} and J_{YB} plotted against b have a horizontal tangent at $b = 0$. For points on the body where $-R < z < R$:

$$y_4(z) = \pm\sqrt{\{(2z + 2R)(\tau - 2z)\}} + \text{term in } (b/2)^2. \qquad (68)$$

For points on the fin where $R \leqslant z < R + h$:

$$y_4(z) = \frac{z + R}{z}\sqrt{(\tau z - z^2 - R^2)} + \text{term in } (b/2)^2. \qquad (69)$$

For $y = h_1 + R$, there is a linear term:

$$z_3 = \mp\lambda_1\frac{b}{2}$$

$$y_4 = \sqrt{\{(2R + \varkappa_0)(\tau - \varkappa_0)\}} \pm \frac{b}{4}\lambda_1\frac{2\varkappa_0 + 2R - \tau}{\sqrt{\{(2R + \varkappa_0)(\tau - \varkappa_0)\}}} + \ldots.$$

The lift distribution over a tailplane of small span is obtained by putting

$$\zeta = y + i(h_1 + R)$$

into equations (2), (6), (8), (15) and neglecting all higher order terms in y and $b/2$:

$$\left.\begin{aligned}
\zeta_1 &= \lambda_1 y + i\varkappa_0 + \ldots \\
\zeta_2 &= \frac{\lambda_1}{2}\left[y \mp i\sqrt{\{(b/2)^2 - y^2\}}\right] + \ldots \\
z_3 &= \mp\lambda_1\sqrt{\{(b/2)^2 - y^2\}} + \ldots \\
y_4 &= \sqrt{\{(2R + \varkappa_0)(\tau - \varkappa_0)\}} \pm \frac{b}{4}\lambda_1\frac{2\varkappa_0 + 2R - \tau}{\sqrt{\{(2R + \varkappa_0)(\tau - \varkappa_0)\}}}\sqrt{\left\{1 - \left(\frac{y}{b/2}\right)^2\right\}} + \ldots
\end{aligned}\right\} \qquad (70)$$

where the upper sign holds for the lower surface of the tailplane.

By equation (52):

$$\frac{C_{LT}c}{\bar{C}_{YF}\bar{c}_F} = \frac{2}{(J_{YF})_{b=0}}\frac{b}{2}\lambda_1\frac{2\varkappa_0 + 2R - \tau}{\sqrt{\{(2R + \varkappa_0)(\tau - \varkappa_0)\}}}\sqrt{\left\{1 - \left(\frac{y}{b/2}\right)^2\right\}}$$

$$\therefore \frac{C_{LT}c}{(C_{LT}c)_{\text{junction}}} = \sqrt{\left\{1 - \left(\frac{y}{b/2}\right)^2\right\}} \quad \ldots \quad (71)$$

The lift distribution on small tailplanes is therefore elliptic, and the moment arm is:

$$\frac{y_{0\,T}}{b/2} = \frac{4}{3\pi} \quad \ldots \quad (72)$$

For $h_1 = 1$, *i.e.*, the tailplane at the end of the fin:

$$\varkappa_0 = \tau \quad \ldots \quad (73)$$

$$\sigma = \lambda_1\frac{b}{2} + \ldots \quad \ldots \quad (74)$$

The expansions for y_4 now contain a linear term in $b/2$. From equations (13), (14) and (15) for the body

$$z_3 = 2z - \tau$$

$$y_4(z) = \sqrt{\{(2z + 2R)(\tau - 2z)\}} + \frac{b}{4}\lambda_1\sqrt{\left\{\frac{2z + 2R}{\tau - 2z}\right\}} + \ldots \quad \ldots \quad (75)$$

and for the fin,

$$z_3 = \frac{z^2 + R^2}{z} - \tau$$

$$y_4(z) = \frac{z + R}{z}\sqrt{(\tau z - z^2 - R^2)} + \frac{b}{4}\lambda_1 \cdot \frac{z + R}{\sqrt{(\tau z - z^2 - R^2)}} + \ldots \quad \ldots \quad (76)$$

except for the top of the fin, $z = 1 + R$, where $\dfrac{z^2 + R^2}{z} - \tau = 0$.

Integrating these relations,

$$J_{YB} = -\frac{1 - 4R - 4R^2}{1 + R}\sqrt{\left\{\frac{R}{1 + R}\right\}} + \left[\frac{(1 + 2R)^2}{2(1 + R)}\right]^2\left[\frac{\pi}{2} - \sin^{-1}\frac{1 - 4R - 4R^2}{(1 + 2R)^2}\right] - 2\pi R^2$$

$$+ b\frac{1 + 2R}{(1 + R)^2}\left\{-\sqrt{\left\{\frac{R}{1 + R}\right\}} + \frac{(1 + 2R)^2}{4(1 + R)}\left[\frac{\pi}{2} - \sin^{-1}\frac{1 - 4R - 4R^2}{(1 + 2R)^2}\right]\right\} + \ldots \quad (77)$$

$$J_{YF} = \frac{1 - 4R - 4R^2}{1 + R}\sqrt{\left\{\frac{R}{1 + R}\right\}} + \left[\frac{(1 + 2R)^2}{2(1 + R)}\right]^2\left[\pi + 2\sin^{-1}\frac{1}{1 + 2R}\right] + 4\pi R^2$$

$$+ b\frac{1 + 2R}{(1 + R)^2}\left\{\sqrt{\left\{\frac{R}{1 + R}\right\}} + \frac{(1 + 2R)^2}{4(1 + R)}\left[\pi + 2\sin^{-1}\frac{1}{1 + 2R}\right]\right\} + \ldots \quad \ldots \quad (78)$$

For $R = 0$:

$$J_{YF} = \frac{\pi}{2}(1 + b + \ldots) \quad \ldots \quad (79)$$

For points on the tailplane we obtain from equations (70), (15), (62), (63), (73), (74) and (52)

$$y_4(y) = \frac{1+2R}{1+R}\sqrt{\left\{\frac{1+2R}{1+R}\right\}}\sqrt{\frac{b}{2}}\sqrt{\left[1 \pm \sqrt{\left\{1-\left(\frac{y}{b/2}\right)^2\right\}}\right]}$$

$$\frac{C_{LT}\,c}{\bar{C}_{YF}\,\bar{c}_F} = \frac{2}{(J_{YF})_{b=0}}\,\frac{1+2R}{1+R}\sqrt{\left\{\frac{1+2R}{1+R}\right\}}\sqrt{b}\sqrt{\left\{1-\frac{y}{b/2}\right\}} \quad \ldots \quad (80)$$

$$\frac{C_{LT}\,c}{(C_{LT}\,c)_{\text{junction}}} = \sqrt{\left\{1-\frac{y}{b/2}\right\}} \quad \ldots \quad (81)$$

$$\frac{y_{0T}}{b/2} = 0\cdot4\,. \quad \ldots \quad (82)$$

For small R, expanding in powers of R,

$$\varkappa = h_1 + R + \ldots$$

$$\lambda = \frac{b}{2} + \text{term in } R^2$$

$$\mu = 0 + \text{term in R}^2$$

$$\varrho = \sqrt{\{h_1^2 + (b/2)^2\}} + \frac{3h_1}{\sqrt{\{h_1^2 + (b/2)^2\}}}\,R + \ldots$$

$$\sigma = \sqrt{\{(1-h_1)^2 + \; b/2)^2\}} + \text{term in } R^2\,.$$

For the fin:

$$z_3 = \mp\sqrt{\{(z-h_1-R)^2 + (b/2)^2\}}$$

$$y_4 = \begin{bmatrix} -(z-h_1)^2 - \left(\frac{b}{2}\right)^2 + \sqrt{\left\{\left[h_1^2+\left(\frac{b}{2}\right)^2\right]\left[(1-h_1)^2+\left(\frac{b}{2}\right)^2\right]\right\}} \\ \pm\sqrt{\left\{(z-h_1)^2+\left(\frac{b}{2}\right)^2\right\}}\left[\sqrt{\left\{h_1^2+\left(\frac{b}{2}\right)^2\right\}} - \sqrt{\left\{(1-h_1)^2+\left(\frac{b}{2}\right)^2\right\}}\right] \end{bmatrix}^{1/2}$$

$$+\,R\,\frac{\begin{bmatrix} 2(z-h_1) + 3h_1\left[\sqrt{\left\{\frac{(1-h_1)^2+(b/2)^2}{h_1^2+(b/2)^2}\right\}} \pm \sqrt{\left\{\frac{(z-h_1)^2+(b/2)^2}{h_1^2+(b/2)^2}\right\}}\right] \\ \pm(z-h_1)\left[\sqrt{\left\{\frac{(1-h_1)^2+(b/2)^2}{(z-h_1)^2+(b/2)^2}\right\}} - \sqrt{\left\{\frac{h_1^2+(b/2)^2}{(z-h_1)^2+(b/2)^2}\right\}}\right] \end{bmatrix}}{\begin{bmatrix} -(z-h_1)^2 - \left(\frac{b}{2}\right)^2 + \sqrt{\left\{\left[h_1^2+\left(\frac{b}{2}\right)^2\right]\left[(1-h_1)^2+\left(\frac{b}{2}\right)^2\right]\right\}} \\ \pm\sqrt{\left\{(z-h_1)^2+\left(\frac{b}{2}\right)^2\right\}}\left[\sqrt{\left\{h_1^2+\left(\frac{b}{2}\right)^2\right\}} - \sqrt{\left\{(1-h_1)^2+\left(\frac{b}{2}\right)^2\right\}}\right] \end{bmatrix}^{1/2}} \quad \ldots \quad (83)$$

where the upper signs hold for points of the fin between body and tailplane $R \leqslant z \leqslant R + h_1$ and the lower signs for $R + h_1 \leqslant z < R + h$. For $b \to 0$, $R \to 0$ equation (83) gives

$$y_4 \to \sqrt{(z - z^2)} \quad \ldots \quad (84)$$

as for an elliptic fin.

For the body, $-R < z < R$, R and z are of the same order, so that for small R:

$$z_3 = -\sqrt{\{(2z - h_1 - R)^2 + (b/2)^2\}}$$

$$y_4(z) = \sqrt{\left[(z + R)2h_1\left\{1 + \frac{\sqrt{\{(1 - h_1)^2 + (b/2)^2\}}}{\sqrt{\{h_1^2 + (b/2)^2\}}}\right\}\right]} . \quad \ldots \quad (85)$$

At the fin-body junction, $z = R$:

$$y_4(R) = \sqrt{\left[4Rh_1\left\{1 + \frac{\sqrt{\{(1 - h_1)^2 + (b/2)^2\}}}{\sqrt{\{h_1^2 + (b/2)^2\}}}\right\}\right]} . \quad \ldots \quad (86)$$

In equation (27)

$$C_{YB}(z)c = 4\frac{v_{y\infty}}{V_0}h\left[y_4(z) - \sqrt{\left\{\left(\frac{R}{h}\right)^2 - \left(\frac{z}{h}\right)^2\right\}}\right]$$

the second term is negligible compared with the first one for small R. Thus for small R

$$\frac{C_{YB}\,c}{(C_{YB}\,c)_{\text{junction}}} = \sqrt{\left\{\frac{1 + z/R}{2}\right\}} \quad \ldots \quad (87)$$

independent of b.

It follows from equation (85):

$$\frac{C_{LB}\,c}{(C_{LB}\,c)_{\text{junction}}} = \frac{\Delta y_4(y)}{\Delta y_4(y = 0)}$$

$$= \frac{1}{\sqrt{2}}\left[\sqrt{\left\{1 + \sqrt{[1 - (y/R)^2]}\right\}} - \sqrt{\left\{1 - \sqrt{[1 - (y/R)^2]}\right\}}\right]$$

$$= \sqrt{(1 - y/R)} . \quad \ldots \quad (88)$$

For the tailplane, from equations (2), (6), (8), (15)

$$\zeta = y + i(R + h_1)$$

$$z_3 = \mp\sqrt{\left\{\left(\frac{b}{2}\right)^2 - y^2\right\}}$$

$$y_4 = \left[\begin{array}{l} -(b/2)^2 + y^2 + \sqrt{\{h_1^2 + (b/2)^2\}}\sqrt{\{(1 - h_1)^2 + (b/2)^2\}} \\ \pm\sqrt{\{(b/2)^2 - y^2\}}[\sqrt{\{h_1^2 + (b/2)^2\}} - \sqrt{\{(1 - h_1)^2 + (b/2)^2\}}] \end{array}\right]^{1/2}$$

$$+ R\,\frac{\dfrac{3h_1\left[\sqrt{\{(1 - h_1)^2 + (b/2)^2\}} \pm \sqrt{\left\{\left(\frac{b}{2}\right)^2 - y^2\right\}}\right]}{2\sqrt{\{h_1^2 + (b/2)^2\}}}}{\left[\begin{array}{l} -(b/2)^2 + y^2 + \sqrt{\{h_1^2 + (b/2)^2\}}\sqrt{\{(1 - h_1)^2 + (b/2)^2\}} \\ \pm\sqrt{\{(b/2)^2 - y^2\}}[\sqrt{\{h_1^2 + (b/2)^2\}} - \sqrt{\{(1 - h_1)^2 + (b/2)^2\}}] \end{array}\right]^{1/2}} \quad \ldots \quad (89)$$

In the special case $h_1 = 0\cdot5$

$$\frac{C_{LT}(y)c(y)}{(C_{LT}\,c)_{\text{junction}}} = \sqrt{\left[\frac{1 - \left(\dfrac{y}{b/2}\right)^2}{1 + \left(\dfrac{b}{h}\right)^2\left(\dfrac{y}{b/2}\right)^2}\right]} . \quad \ldots \quad (90)$$

7. *The Special Case of the Tailplane in the Symmetry Line of the Body.*—When the tailplane passes through the centre of the body, *i.e.*, when $h_1 = -R$, the conformal transformation takes a slightly simpler form. It is therefore convenient to consider this case separately.

The transformation of equation (1)

$$\zeta_1 = \zeta - \frac{R^2}{\zeta}$$

transforms the body ADC into the z_1-axis from A_1 to C_1 (*see* Fig. 3), the fin CG into the z_1-axis from C_1 to G_1 and the tailplane into the y_1-axis from J_1 to E_1. This transform of the tailplane can be transformed without an approximation into a full circle, by the transformation

$$\zeta_2 = \frac{1}{2}\left[\zeta_1 \mp \sqrt{(\zeta_1{}^2 - \bar{\lambda}^2)}\right] \quad \ldots \quad (91)$$

where

$$\bar{\lambda} = \frac{b}{2} - \frac{R^2}{b/2}. \quad \ldots \quad (92)$$

The negative sign holds for $z < 0$ and the positive sign for $z > 0$. The centre of the circle $D_2E_2F_2$ is at the origin, and its radius is $\bar{\lambda}/2$. The z_1-axis from A_1 to D_1 and F_1 to G_1 is transformed into the z_2-axis from A_2 to D_2 and F_2 to G_2.

We then transform the circle $D_2E_2F_2$ into the z_3-axis from D_3 to F_3, and the z_2-axis from A_2 to D_2 and F_2 to G_2 into the z_3-axis from A_3 to D_3 and F_3 to G_3 by the transformation

$$\zeta_3 = \zeta_2 - \frac{\bar{\lambda}^2}{4\zeta_2}. \quad \ldots \quad (93)$$

Finally, the slit in the ζ_3-plane is transformed as before into a slit along the y_4-axis by the transformation of equation (9)

$$\zeta_4 = \sqrt{\left\{\left(\zeta_3 + i\,\frac{\bar{\varrho} - \bar{\sigma}}{2}\right)^2 + \left(\frac{\bar{\varrho} + \bar{\sigma}}{2}\right)^2\right\}} \quad \ldots \quad (94)$$

where

$$\bar{\varrho} = -z_{A3} = \sqrt{(4R^2 + \bar{\lambda}^2)} \quad \ldots \quad (95)$$

$$\bar{\sigma} = z_{G3} = \sqrt{(\tau^2 + \bar{\lambda}^2)} \quad \ldots \quad (96)$$

$$\tau = z_{G1} = \frac{1 + 2R + 2R^2}{1 + R}. \quad \ldots \quad (12)$$

Thus the relation between points on the wake contour and the slit in the ζ_4-plane is known. Points on the body, $-R < z < R$, are related to points on the z_3-axis, by the relation

$$z_3(z) = \mp \sqrt{\{(2z)^2 + \bar{\lambda}^2\}} \quad \ldots \quad (97)$$

with the minus sign for $-R < z < 0$ and the positive sign for $0 < z < R$; points on the fin, $R < z < R + 1$ by the relation:

$$z_3(z) = \sqrt{\left\{\left(\frac{z^2 + R^2}{z}\right)^2 + \bar{\lambda}^2\right\}} \quad \ldots \quad (98)$$

and points on the tailplane, $R < |y| < b/2$, by the relation

$$z_3(y) = \pm \sqrt{\left\{\bar{\lambda}^2 - \left(\frac{y^2 - R^2}{y}\right)^2\right\}} \quad \ldots \quad (99)$$

with the minus sign for the lower surface of the tailplane and the positive sign for the upper surface. For all points the relation between points on the z_3-axis and the y_4-axis reads:

$$y_4 = \pm \sqrt{\{ - z_3^2 - (\bar{\varrho} - \bar{\sigma})z_3 + \bar{\varrho}\bar{\sigma}\}} \,. \qquad \ldots \ldots \ldots \ldots \quad (100)$$

The calculation of the force distributions on fin, body and tailplane proceeds in the same way as before and the results are included in the charts.

We consider again the limiting case of small tailplane span and body diameter. Expanding in powers of $b - 2R$:

$$\bar{\lambda} = b - 2R + \ldots$$

$$\bar{\varrho} = 2R + \ldots$$

$$\bar{\sigma} = \tau + \ldots .$$

For points on the body, except $z = 0$,

$$y_4(z) = \sqrt{\{(\tau - 2z)(2R + 2z)\}} + \text{term in } (b - 2R)^2 ; \ldots \ldots \ldots \quad (101)$$

for $z = 0$

$$y_4(0) = \sqrt{(2R\tau)} \mp \frac{b - 2R}{2} \frac{\tau - 2R}{\sqrt{(2R\tau)}} + \ldots . \qquad \ldots \ldots \ldots \ldots \quad (102)$$

For points on the fin:

$$y_4(z) = \frac{z + R}{z} \sqrt{(\tau z - R^2 - z^2)} + \text{term in } (b - 2R)^2 . \qquad \ldots \ldots \quad (103)$$

This means that curves of J_{YF}, J_{YB}, $C_{YF}c/\bar{C}_{YF}\bar{c}_F$ and $C_{YB}c/(C_{YB}c)_{\text{junction}}$ plotted against b have a horizontal tangent at $b = 2R$.

For points on the tailplane we obtain by expanding in powers of $(y - 2R)$ and $(b - 2R)$:

$$y_4(y) = \sqrt{(2R\tau)} \mp \frac{b - 2R}{2} \frac{\tau - 2R}{\sqrt{(2R\tau)}} \sqrt{\left\{1 - \left(\frac{2y - 2R}{b - 2R}\right)^2\right\}} \qquad \ldots \ldots \quad (104)$$

$$\frac{C_{LT}\,c}{\bar{C}_{YF}\,\bar{c}_F} = - \frac{2}{(J_{YF})_{b=2R}} (b - 2R) \frac{\tau - 2R}{\sqrt{(2R\tau)}} \sqrt{\left\{1 - \left(\frac{2y - 2R}{b - 2R}\right)^2\right\}} \ldots \ldots \quad (105)$$

$$\frac{C_{LT}\,c}{(C_{LT}\,c)_{\text{junction}}} = \sqrt{\left\{1 - \left(\frac{2y - 2R}{b - 2R}\right)^2\right\}} \qquad \ldots \ldots \ldots \ldots \ldots \ldots \quad (106)$$

and the moment arm is

$$\frac{y_0}{b/2} = \frac{R}{b/2} + \frac{4}{3\pi}\left(1 - \frac{R}{b/2}\right) . \qquad \ldots \ldots \ldots \ldots \ldots \ldots \quad (107)$$

For small R, expanding in powers of R,

$$\bar{\lambda} = \frac{b}{2} + \ldots$$

$$\bar{\varrho} = \frac{b}{2} + \ldots$$

$$\bar{\sigma} = \sqrt{\{1 + (b/2)^2\}} + \frac{R}{\sqrt{\{1 + (b/2)^2}} + \ldots .$$

For points on the fin

$$y_4(z) = \sqrt{\left\{-z^2 - \left(\frac{b}{2}\right)^2 + \frac{b}{2}\sqrt{\left\{1 + \left(\frac{b}{2}\right)^2\right\}} + \sqrt{\left\{z^2 + \left(\frac{b}{2}\right)^2\right\}}\left[\sqrt{\left\{1 + \left(\frac{b}{2}\right)^2\right\}} - \frac{b}{2}\right]\right\}}$$

$$+ \frac{R}{2}\frac{\frac{b}{2} + \sqrt{\left\{z^2 + \left(\frac{b}{2}\right)^2\right\}}}{\sqrt{\left\{1 + \left(\frac{b}{2}\right)^2\right\}}}\frac{1}{\left[-z^2 - \left(\frac{b}{2}\right)^2 + \frac{b}{2}\sqrt{\left\{1 + \left(\frac{b}{2}\right)^2\right\}} + \sqrt{\left\{z^2 + \left(\frac{b}{2}\right)^2\right\}}\left[\sqrt{\left\{1 + \left(\frac{b}{2}\right)^2\right\}} - \frac{b}{2}\right]\right]^{1/2}} . \quad (108)$$

$y_4(z, R = 0)$ from equation (108) agrees with $y_4(z, R = 0)$ from equation (83), for $h_1 = 0$.

For points on the body, R and z are of the same order, so that for small R:

$$z_3(z) = \mp \frac{b}{2} + \ldots ,$$

for $-R < z < 0$:

$$y_4(z) = 0 + \text{terms in } R^2 \text{ and } z^2 , \quad \ldots \quad (109)$$

for $0 < z < R$

$$y_4(z) = \sqrt{\left[2\frac{b}{2}\sqrt{\left\{1 + \left(\frac{b}{2}\right)^2\right\}} - 2\left(\frac{b}{2}\right)^2\right]} + \frac{R \,.\, b/2}{\sqrt{\left\{1 + \left(\frac{b}{2}\right)^2\right\}}\sqrt{\left[2\frac{b}{2}\sqrt{\left\{1 + \left(\frac{b}{2}\right)^2\right\}} - 2\left(\frac{b}{2}\right)^2\right]}} . \quad (110)$$

Thus for small R

$$\frac{C_{YB}\,c}{(C_{YB}\,c)_{\text{junction}}} = 1 . \quad \ldots \quad (111)$$

8. *The Calculation Procedure.*—The above calculations have been made for those arrangements which produce a system of trailing vortices giving constant v_y-velocities at the fin and zero v_z-velocities at the tailplane. This implies a restriction on the geometry (plan-forms of the fin and the tailplane, twist of the tailplane, and shape of the body). However, in the limit $A \to 0$ (*i.e.*, aspect ratios of fin and tailplane $\to 0$) the flow in the Trefftz-plane can be interpreted as representing the flow in sections through the actual fin-tailplane so that $\beta_i = \beta =$ const. whatever the given shape as long as fin and tailplane are plane surfaces. This implies that the twist of the tailplane tends to zero as $A \to 0$ and that the body tends to a cylindrical shape. Hence, the calculation is exact in the limiting case $A \to 0$, and differences between any given arrangement and the constant induced side-wash arrangement appear only when the aspect ratio is not small. However, an approximate calculation can be made even for arrangements with large aspect ratio when the differences between a given arrangement and the constant induced side-wash arrangement can be expected to be appreciable.

An estimate of the side-force distribution on a given arrangement is obtained by dividing the force distribution calculated by equation (34) by the given $c/\bar{c}_F$ values. A better approximation is generally obtained by adding the difference between the side-force on the fin calculated for the fin-body-tailplane arrangement and the side-force for an elliptic fin to the side-force on the given fin alone, which can be calculated by the usual methods (*see* Ref. 12):

$$\frac{\Delta C_{YF}}{\beta}\frac{c}{\bar{c}_F} = \frac{2}{\omega}\frac{\beta_i}{\beta}A_F J_{YF}\left[\frac{C_{YF}\,c}{\bar{C}_{YF}\,\bar{c}_F}\right] - \left(\frac{2}{\omega}\frac{\beta_i}{\beta}\right)_{\substack{R=0\\b=0}} A_F \frac{\pi}{2}\frac{4}{\pi}\sqrt{\left\{1 - \left(\frac{z - (R + h/2)}{h/2}\right)^2\right\}} \quad \ldots \quad (112)$$

where the first term on the right-hand side is obtained from equations (29) and (31), and the second term is simply the elliptic load distribution over the height of the fin. This procedure has proved successful in similar cases (*see* Refs. 6, 7, 8 and 9).

The known quantities for a given fin-body-tailplane combination are: the aspect ratio A_F of the fin outside the body, the angle of sweep φ of the mid-chord line of the fin, and the ratios of the body radius R, the total tailplane span b and the vertical distance h_1 of the tailplane from the fin-body junction to the height h of the fin. The first value to be determined is $\omega a/2\pi A_F$.

The side-wash factor ω and the sectional lift slope a are related to the chordwise load distribution. They are, therefore, different for the fin-body-tailplane arrangement and the isolated fin. For isolated wings ω and a have been expressed in Ref. 12 as functions of the aspect ratio A. The change in a and ω due to the presence of body and tailplane can thus be taken into account by introducing an 'effective aspect ratio' A_{eF} and calculating a and ω by the formulae for an isolated wing of aspect ratio A_{eF}.

The effect of the tailplane on the chordwise side-force distribution on the fin depends of course on the span of the tailplane. It depends also on the chord of the tailplane and the position of the tailplane leading edge with respect to the leading edge of the fin. The change in effective aspect ratio increases with increasing tailplane span and tailplane chord; it is greater for tailplanes which have their leading edge forward of the fin leading edge than for tailplanes in rearward positions.

To obtain an estimate of A_{eF}/A_F, we consider some limiting cases. With zero span of the tailplane, $b = 0$, the relation of Ref. 1 is applicable:

$$b = 0: \qquad A_{eF}/A_F = 1 + \frac{R/h}{1 + R/h}. \qquad \text{(113)}$$

With a large tailplane on top of the fin, $h_1 = h$, the arrangement is equivalent to Hartley's case of two bodies at the tips of a wing[6]. In this case an effective aspect ratio

$$h_1 = h\,, \quad b \to \infty: \quad A_{eF}/A_F = 2(1 + R/h) \qquad \text{(114)}$$

has proved reasonable in practice. The tailplane at the middle of the fin, $h_1 = 0 \cdot 5h$, has no effect for zero body diameter

$$h_1 = 0 \cdot 5h\,, \quad R = 0: \quad A_{eF}/A_F = 1\,. \qquad \text{(115)}$$

A reasonable estimate for $R \neq 0$ is

$$h_1 = 0 \cdot 5h\,, \quad R \neq 0: \quad A_{eF}/A_F = 1 + \tfrac{1}{2}\frac{R/h}{1 + R/h}. \qquad \text{(116)}$$

An interpolation formula which includes the limiting cases is:

$$0 \cdot 5 < h_1/h < 1: \frac{A_{eF}}{A_F} = 1 + \frac{h_1}{h}\frac{R/h}{1 + R/h} + \left(2\frac{h_1}{h} - 1\right)\frac{b/h}{2 + b/h}\left[1 + 2\frac{R}{h} - \frac{R/h}{1 + R/h}\right]. \qquad \text{(117)}$$

A corresponding formula for the case where the tailplane is at the centre of the body is

$$h_1 = -R: \frac{A_{eF}}{A_F} = 1 + \frac{R/h}{1 + R/h} + \frac{b/h - 2R/h}{2 + b/h - 2R/h}\left[1 + 2\frac{R}{h} - \frac{R/h}{1 + R/h}\right]. \qquad \text{(118)}$$

For tailplanes where the leading edge is appreciably behind the fin leading edge so that a smaller change in A_{eF} is to be expected, the calculations can be done for A_{eF} from equations (117), (118) to give one limiting case, and for $A_{eF} = A_F$ for the other limiting case. Any given case can then be calculated with A_{eF} taken between these two limits.

The sectional lift slope a depends also on the two-dimensional lift slope a_0 and the angle of sweep. A good approximation is given by

$$a_0 = k \cdot 2\pi \left(1 + 0\cdot 8 \frac{t/c}{\cos \varphi_e}\right) \quad \ldots \quad (119)$$

where t/c is the thickness/chord ratio of the fin, k is a factor for the lift reduction due to the boundary layer, which changes with Reynolds number ($k = 0\cdot 92$ for $R_e \simeq 2 \times 10^6$ and $t/c \simeq 0\cdot 1$) and φ_e is an effective angle of sweep (*see* Ref. 12).

$$\varphi_e = \frac{\varphi}{\left\{1 + \left(\frac{a_0 \cos \varphi}{\pi A_{eF}}\right)^2\right\}^{1/4}} \quad \ldots \quad (120)$$

With the defined values of a_0, A_{eF}, φ_e the values of a and ω can be calculated:

$$a_s = \frac{2a_0 n \cos \varphi_e}{1 - \pi n \cot \pi n} \quad \ldots \quad (121)$$

where

$$n = 1 - \frac{1}{2\left\{1 + \left[\frac{a_0 \cos \varphi_e}{\pi A_{eF}}\right]^2\right\}^{\frac{1}{4\left(1 + \frac{|\varphi_e|}{\pi/2}\right)}}} \quad \ldots \quad (122)$$

and

$$\omega = 2n \,. \quad \ldots \quad (123)$$

For the special case $a_0 = 2\pi$, the term $\omega a/2\pi A_F$ is plotted in Fig. 13 for various values of the geometric angle of sweep of the mid-chord line.

With the calculated $\omega a/2\pi A_F$ the induced side-wash β_i/β for given values of R/h, h_1/h, b/h can be found by plotting the values interpolated from Figs. 7a to 7n against R/h. There are no curves given for $h_1 = 0\cdot 5h$, $R = 0$ and $R = 0\cdot 1h$, since for small R/h β_i/β is practically independent of b/h and equal to the values for $h_1 = h$, $b = 0$. The value of J_{YF} for given R/h, h_1/h, b/h can be found from Figs. 4a to 4d, and the coefficient for the total side-force on the fin from

$$\frac{\bar{C}_{YF}}{\beta} = \frac{2}{\omega} \frac{\beta_i}{\beta} A_F J_{YF} \,. \quad \ldots \quad (124)$$

The ratio J_{YB}/J_{YF} for $\omega_B = \omega$ is interpolated from Fig. 5 and the overall side-force coefficient, excluding the forces on the nose and rear end of the body is

$$\frac{\bar{C}_Y}{\beta} = \frac{2}{\omega} \frac{\beta_i}{\beta} A_F \left[J_{YF} + J_{YB} - 2\pi \left(\frac{R}{h}\right)^2\right] . \quad \ldots \quad (125)$$

The additional side-force distributions are obtained from equation (112) where $C_{YF} c/\bar{C}_{YF} \bar{c}_F$ is interpolated from Table 2. The value $\left(\frac{2}{\omega} \frac{\beta_i}{\beta}\right)_{\substack{R=0 \\ b=0}}$ for the fin alone can be determined from Fig. 7a, using the values of ω and a which correspond to the wing alone. These can first be calculated by equations (119) to (123) using the given A_F and φ. These additional distributions are to be added to the side-force of the fin alone. Otherwise, the total side-force distribution can be approximated by

$$\frac{C_{YF}(z)}{\beta}\frac{c(z)}{\bar{c}_F} = \frac{\bar{C}_{YF}}{\beta}\left[\frac{C_{YF}c}{\bar{C}_{YF}\bar{c}_F}\right]. \qquad (126)$$

The side-force distribution on the body with nose and tail forces excluded is

$$\frac{C_{YB}}{\beta}\frac{c}{\bar{c}_F} = \left(\frac{C_{YF}}{\beta}\frac{c}{\bar{c}_F}\right)_{z=R}\cdot\frac{C_{YB}c}{(C_{YB}c)_{\text{junction}}} - \frac{2}{\omega}\frac{\beta_i}{\beta}A_F\,.\,4\frac{R}{h}\sqrt{\left\{1-\left(\frac{z}{R}\right)^2\right\}} \qquad (127)$$

where $\dfrac{C_{YB}c}{(C_{YB}c)_{\text{junction}}}$ can be interpolated from Table 3.

Finally, the coefficient of the total lift acting on one half of the tailplane or body, referred to the fin area, can be calculated from

$$\bar{C}_{LT} = \frac{\bar{C}_{LT}}{\bar{C}_{YF}}\bar{C}_{YF} \qquad (128)$$

$$\bar{C}_{LB} = \frac{\bar{C}_{LB}}{\bar{C}_{YF}}\bar{C}_{YF} \qquad (129)$$

where $\bar{C}_{LT}/\bar{C}_{YF}$ and $\bar{C}_{LB}/\bar{C}_{YF}$ are read from Figs. 9 and 11. The lift distributions can be interpolated from Tables 4 and 5. The lift coefficient $(C_{LT}c)_{\text{junction}}$ at the fin-tailplane junction, by which the lift coefficients have been divided, is equal to half the difference of the side-force $(C_{YF}c)$ at the two sides of the tailplane, and the lift coefficient $(C_{LB}c)_{\text{junction}}$ is equal to half the side-force coefficient $(C_{YF}c)$ at the body-fin junction $z = R$. The moment arm of the lift forces can be determined from Fig. 10.

To facilitate the estimate of the tailplane effect for varying tailplane position by interpolating between the calculated examples, the shapes and positions of 'neutral' tailplanes are given in Fig. 14. They are stagnation streamlines in the flow around body and fin and thus do not affect the side-force distributions on fin and body nor do they take any lift forces.

For arrangements that give constant side-wash v_y along fin and body, the relation between induced drag and total side-force is:

$$\bar{C}_{Di} = \tfrac{1}{2}\frac{v_{y\infty}}{V_0}\bar{C}_Y. \qquad (130)$$

With

$$\bar{C}_Y = \frac{v_{y\infty}}{V_0}A_F\left[J_{YF}+J_{YB}-2\pi\left(\frac{R}{h}\right)^2\right] \qquad (131)$$

we obtain

$$\bar{C}_{Di} = \frac{\bar{C}_Y^2}{\pi A_F}\frac{\pi}{2\left[J_{YF}+J_{YB}-2\pi\left(\frac{R}{h}\right)^2\right]}. \qquad (132)$$

The factor $\dfrac{\pi}{2\left[J_{YF}+J_{YB}-2\pi\left(\frac{R}{h}\right)^2\right]}$ giving the reduction of the induced drag compared with that of the fin alone is plotted in Fig. 15. Experience has shown that the reduction factor is not very different for non-constant induced side-wash arrangements, especially if the aspect ratio is small, as is usually the case for fin-fuselage arrangements.

As an example the side-force on the fin has been calculated for an arrangement where experimental results are available for a systematic variation of the tailplane position. Calculated results are given in Table 6. The total side-force on the fin can be determined in a quarter of an hour, and the side-force distribution in about an hour. The experimental and theoretical results are plotted together in Fig. 16; they show good agreement. The position of the tailplane, for which the side-force on the fin is the same with or without tailplane, is taken as the position of the junction between tailplane and fin or body for neutral tailplanes, as plotted in Fig. 14. The side-force distributions on fin and fuselage, calculated by equations (126) and (127), are plotted in Fig. 17; the distributions on the fuselage differ from those in Fig. 6 by the term

$$\frac{2}{\omega}\frac{\beta_i}{\beta}A_E \,.\, 4\,\frac{R}{h}\sqrt{\left\{1-\left(\frac{z}{R}\right)^2\right\}}\,.$$

The figure illustrates how large is the effect of fuselage and tailplane on the side-force on the fin. The fuselage increases the total side-force on the fin by a factor 1·6 and for the tailplane on top of the fin, tailplane and fuselage together increase it by a factor 2·2. The effect of the tailplane on the side-force of the fin-fuselage arrangement depends of course not only on the position of the tailplane but also on the other parameters: aspect ratio and sweep of the fin, diameter of the body, span of the tailplane, so that it cannot strictly be described by one single curve as given in Ref. 9.

LIST OF SYMBOLS

x, y, z		Rectangular system of co-ordinates, x in the wind direction, y spanwise, z positive upwards; origin on the body axis
ζ	$=$	$y + iz$, complex co-ordinate in the Trefftz-plane
ζ_ν	$=$	$y_\nu + iz_\nu$, complex co-ordinate in one of the transformed Trefftz-planes
c		Local chord
$\bar{c}_F$		Mean chord of the fin outside the body
h		Height of the fin outside the body
R		Body radius
b		Tailplane span
h_1		Distance of tailplane from wing-body junction
A_F	$=$	$h/\bar{c}_F$, aspect ratio of the fin outside the body
A_{eF}		Effective aspect ratio
φ		Angle of sweep of the mid-chord line on the fin
φ_e		Effective angle of sweep (*see* equation (120))
β		Geometric side-wash angle

β_B		Additional side-wash angle produced by the flow around the isolated body
β_i		Induced side-wash angle at the fin
β_e		Effective side-wash angle
V_0		Velocity of the main flow
$v_{y\,\infty}$		Side-wash velocity in the Trefftz-plane
ϕ		Velocity potential
$C_{Y\,F}$		Side-force coefficient on the fin
$\bar{C}_{Y\,F}$		Coefficient of the total side-force on the fin
$C_{Y\,B}$		Side-force coefficient on the body
$\bar{C}_{Y\,B}$		Coefficient of the total side-force on the body referred to the fin area $h\bar{c}_F$
$\bar{C}_Y$	=	$\bar{C}_{Y\,F} + \bar{C}_{Y\,B}$, coefficient of the total side-force
$C_{L\,T}$		Lift coefficient on the tailplane
$\bar{C}_{L\,T}$		Coefficient of the total lift on one half of the tailplane referred to the fin area $h\bar{c}_F$
$C_{L\,B}$		Lift coefficient on the body
$\bar{C}_{L\,B}$		Coefficient of the total lift on one half of the body referred to the fin area $h\bar{c}_F$
$\bar{C}_{D\,i}$		Coefficient of the total induced drag referred to the fin area $h\bar{c}_F$
$J_{Y\,F}$	=	$\bar{C}_{Y\,F}/(A_F v_{y\,\infty}/V_0)$
a	=	$dC_Y/d\beta_e = dC_L/d\alpha_e$, local sectional lift slope
a_0		Lift slope coefficient of the two-dimensional aerofoil
ω	=	$\beta_i/\frac{1}{2}(v_{y\,\infty}/V_0)$, side-wash factor
ω_B		Side-wash factor for the body
$y_{0\,T}$	=	$\mathscr{M}/\bar{L}_T$, moment arm of the lift on the tailplane

Suffices

$_F$	Fin
$_B$	Body
$_T$	Tailplane
$_e$	Effective
$_i$	Induced

REFERENCES

No.	*Author*	*Title, etc.*
1	J. Weber	Theoretical load distribution on a wing with a cylindrical body at one end. R. & M. 2889. June, 1952.
2	W. Mangler	The distribution of lift over an aerofoil with end-plates. *L.F.F.* Vol. 14, p. 564. A.R.C. 3414. 1938.
3	W. Mangler and J. Rotta ..	Aerofoils with tip plates. AVA Monograph F_1, 1·6. Reports and Translations. 1023. 1947.
4	V. M. Falkner and Sir Charles Darwin	The design of minimum drag tip fins. R. & M. 2279. March, 1945.
5	J. Rotta	Luftkräfte am Tragflügel mit einer seitlichen Scheibe. *Ing. Arch.*, Vol. 13, p. 119. 1942.
6	D. E. Hartley	Theoretical load distributions on wings with cylindrical bodies at the tips. C.P. 147. June, 1952.
7	J. Weber	Theoretical load distribution on a wing with vertical plates. R. & M. 2960. March, 1954.
8	D. Küchemann and D. J. Kettle	The effect of endplates on swept wings. C.P.104. June, 1951.
9	J. A. Lawford	Low-speed wind-tunnel measurements of the lift on a 45-deg sweptback half wing and cylindrical body. R.A.E. Tech. Note Aero. 2243. July, 1953.
10	A. E. Bryson, jr.	Stability derivatives for a slender missile with application to a wing-body-vertical-tail configuration. *J. Ae. Sci.* Vol. 20, No. 5, p. 297. 1953.
11	M. T. Landahl	Analysis of some wing-body-vertical tail interference problems for non-symmetric steady flow using slender-body theory. K.T.H. Aero. Tech. Note 32. July, 1953.
12	D. Küchemann	A simple method of calculating the span and chordwise loading on straight and swept wings of any given aspect ratio at subsonic speeds. R. & M. 2935. August, 1952.
13	J. Weber, D. A. Kirby and D. J. Kettle	An extension of Multhopp's method of calculating the spanwise loading of wing fuselage combinations. R. & M. 2872. November, 1951.
14	R. T. Jones	Properties of low-aspect-ratio pointed wings at speeds below and above the speed of sound. N.A.C.A. Report 835. 1946.

TABLE 1

Position of Certain Points in the Various ζ-planes

	$\zeta =$	$\zeta_1 =$	$\zeta_2 =$
A	$-iR$	$-i\,.\,2R$	$-i\,.\,\frac{1}{2}[2R+\varkappa+\sqrt{\{(2R+\varkappa)^2+\lambda^2\}}]$
B	R	0	$-i\,.\,\frac{1}{2}[\varkappa+\sqrt{(\varkappa^2+\lambda^2)}]$
C	iR	$i\,.\,2R$	$i\,.\,\frac{1}{2}[2R-\varkappa-\sqrt{\{(2R-\varkappa)^2+\lambda^2\}}]$
D	$i(h_1+R)$	$i\dfrac{h_1^2+2h_1R+2R^2}{h_1+R}$	$i\,.\,\frac{1}{2}[\mu-\sqrt{(\mu^2+\lambda^2)}]$
E	$\dfrac{b}{2}+i(h_1+R)$	$\lambda+i\varkappa$	$\dfrac{\lambda}{2}$
F	$i(h_1+R)$	$i\dfrac{h_1^2+2h_1R+2R^2}{h_1+R}$	$i\,.\,\frac{1}{2}[\mu+\sqrt{(\mu^2+\lambda^2)}]$
G	$i(1+R)$	$i\tau$	$i\,.\,\frac{1}{2}[\tau-\varkappa+\sqrt{\{(\tau-\varkappa)^2+\lambda^2\}}]$

	$\zeta_3 =$	$\zeta_4 =$
A	$-i\,.\,\varrho$	0
B	$-i\,.\,\frac{1}{2}\left[\varkappa+\mu+\sqrt{(\varkappa^2+\lambda^2)}+\dfrac{\mu^2+\lambda^2}{\varkappa+\mu+\sqrt{(\varkappa^2+\lambda^2)}}\right]$	
C	$-i\,.\,\frac{1}{2}\left[\begin{array}{l}-2\mathrm{R}+\varkappa+\mu+\sqrt{\{(2R-\varkappa)^2+\lambda^2\}} \\ \qquad+\dfrac{\mu^2+\lambda^2}{-2R+\varkappa+\mu\sqrt{\{(2R-\varkappa)^2+\lambda^2\}}}\end{array}\right]$	
D	$-i\sqrt{(\mu^2+\lambda^2)}$	$\sqrt{[-\mu^2-\lambda^2+\sqrt{\{\mu^2+\lambda^2\}}(\varrho-\sigma)+\varrho\sigma]}$
E	$-i\,.\,\mu$	$\sqrt{[-\mu^2+(\varrho-\sigma)\mu+\varrho\sigma]}$
F	$i\sqrt{(\mu^2+\lambda^2)}$	$\sqrt{[-\mu^2-\lambda^2-\sqrt{\{\mu^2+\lambda^2\}}(\varrho-\sigma)+\varrho\sigma]}$
G	$i\,.\,\sigma$	0

TABLE 2

Values of $\dfrac{C_{YF}(z)c(z)}{\bar{C}_{YF}\bar{c}_F}$

$h_1 = h$

$\dfrac{z-R}{h}$	$b=0$: $\dfrac{R}{h}=0$	$0\cdot1$	$0\cdot25$	$0\cdot5$	$b=h$: $\dfrac{R}{h}=0$	$0\cdot1$	$0\cdot25$	$0\cdot5$	$b=2h$: $\dfrac{R}{h}=0$	$0\cdot1$	$0\cdot25$	$0\cdot5$	$b=3h$: $\dfrac{R}{h}=0$	$0\cdot1$	$0\cdot25$	$0\cdot5$	$b=\infty$: $R=0$
0	0	1·088	1·254	1·306	0	0·841	0·986	1·038	0	0·809	0·948	0·996	0	0·803	0·940	0·988	0
0·05	0·555	1·100	1·253	1·303	0·417	0·854	0·988	1·037	0·403	0·828	0·951	0·997	0·399	0·822	0·942	0·989	0·398
0·1	0·764	1·122	1·249	1·296	0·580	0·877	0·991	1·036	0·562	0·846	0·954	0·997	0·558	0·841	0·945	0·990	0·555
0·2	1·019	1·160	1·234	1·267	0·788	0·928	0·998	1·031	0·771	0·901	0·968	0·998	0·767	0·897	0·959	0·992	0·764
0·3	1·167	1·179	1·207	1·224	0·930	0·972	1·004	1·024	0·916	0·951	0·982	0·999	0·912	0·948	0·979	0·995	0·909
0·4	1·248	1·175	1·165	1·167	1·032	1·006	1·007	1·014	1·024	0·994	0·996	1·000	1·020	0·993	0·994	0·999	1·019
0·5	1·273	1·144	1·106	1·095	1·106	1·031	1·008	1·005	1·107	1·028	1·007	1·001	1·104	1·029	1·008	1·002	1·103
0·6	1·248	1·084	1·027	1·006	1·160	1·048	1·006	0·991	1·168	1·055	1·017	1·001	1·168	1·058	1·020	1·005	1·167
0·7	1·167	0·988	0·921	0·892	1·195	1·058	1·002	0·978	1·216	1·077	1·024	1·002	1·215	1·081	1·029	1·007	1·215
0·8	1·019	0·846	0·777	0·746	1·218	1·064	0·997	0·968	1·247	1·090	1·029	1·002	1·248	1·097	1·036	1·009	1·248
0·9	0·764	0·625	0·566	0·539	1·231	1·066	0·994	0·962	1·266	1·099	1·032	1·002	1·267	1·105	1·039	1·010	1·267
0·95	0·555	0·450	0·406	0·385	1·234	1·067	0·993	0·960	1·270	1·100	1·032	1·002	1·271	1·107	1·041	1·010	1·272
1·0	0	0	0	0	1·235	1·067	0·993	0·959	1·272	1·102	1·033	1·001	1·273	1·108	1·041	1·010	1·273

TABLE 2—*continued*

Values of $\dfrac{C_{YF}(z)c(z)}{\bar{C}_{YF}\bar{c}_F}$

$h_1 = 0\cdot75h$

$\dfrac{z-R}{h}$	$b=0$				$b=h$				$b=2h$				$b=3h$			
	$\dfrac{R}{h}=0$	0·1	0·25	0·5	$\dfrac{R}{h}=0$	0·1	0·25	0·5	$\dfrac{R}{h}=0$	0·1	0·25	0·5	$\dfrac{R}{h}=0$	0·1	0·25	0·5
0	0	1·088	1·254	1·306	0	1·058	1·219	1·268	0	1·058	1·216	1·270	0	1·060	1·221	1·278
0·05	0·555	1·100	1·253	1·303	0·543	1·073	1·221	1·267	0·545	1·075	1·219	1·270	0·547	1·076	1·225	1·278
0·1	0·764	1·122	1·249	1·296	0·752	1·100	1·224	1·265	0·756	1·104	1·223	1·270	0·759	1·107	1·230	1·279
0·2	1·019	1·160	1·234	1·267	1·020	1·158	1·230	1·259	1·029	1·170	1·238	1·272	1·033	1·177	1·246	1·281
0·3	1·167	1·179	1·207	1·224	1·194	1·207	1·235	1·249	1·210	1·228	1·253	1·272	1·216	1·233	1·263	1·284
0·4	1·248	1·175	1·165	1·167	1·324	1·244	1·237	1·238	1·337	1·274	1·266	1·274	1·344	1·280	1·278	1·288
0·5	1·273	1·144	1·106	1·095	1·391	1·268	1·237	1·228	1·424	1·307	1·277	1·274	1·432	1·316	1·291	1·291
0·6	1·248	1·084	1·027	1·006	1·440	1·283	1·236	1·219	1·479	1·329	1·284	1·275	1·488	1·339	1·299	1·292
0·7	1·167	0·988	0·921	0·892	1·463	1·290	1·235	1·214	1·506	1·340	1·287	1·275	1·515	1·349	1·303	1·294
0·75	1·103	0·924	0·854	0·824	1·466	1·291	1·235	1·214	1·509	1·342	1·288	1·275	1·518	1·350	1·304	1·294
					0·646	0·480	0·399	0·355	0·558	0·382	0·288	0·231	0·533	0·351	0·249	0·185
0·8	1·019	0·846	0·777	0·746	0·633	0·470	0·391	0·347	0·546	0·374	0·282	0·227	0·522	0·345	0·244	0·182
0·9	0·764	0·625	0·566	0·539	0·516	0·383	0·318	0·282	0·446	0·306	0·230	0·185	0·426	0·280	0·200	0·149
0·95	0·555	0·450	0·406	0·385	0·386	0·286	0·249	0·211	0·335	0·229	0·172	0·139	0·320	0·210	0·150	0·112
1·0	0	0	0	0	0	0	0	0	0	0	0	0	0	0	0	0

TABLE 2—*continued*

Values of $\dfrac{C_{YF}(z)c(z)}{\bar{C}_{YF}\bar{c}_F}$

$h_1 = 0 \cdot 5h$

$\dfrac{z-R}{h}$	$b = 0$				$b = h$				$b = 2h$				$b = 3h$			
	$\dfrac{R}{h} = 0$	0·1	0·25	0·5	$\dfrac{R}{h} = 0$	0·1	0·25	0·5	$\dfrac{R}{h} = 0$	0·1	0·25	0·5	$\dfrac{R}{h} = 0$	0·1	0·25	0·5
0	0	1·088	1·254	1·306	0	1·138	1·352	1·433	0	1·174	1·425	1·560	0	1·191	1·468	1·625
0·05	0·555	1·100	1·253	1·303	0·555	1·159	1·354	1·433	0·555	1·188	1·430	1·560	0·555	1·215	1·474	1·626
0·1	0·764	1·122	1·249	1·296	0·764	1·180	1·356	1·432	0·764	1·220	1·434	1·560	0·764	1·238	1·479	1·626
0·2	1·019	1·160	1·234	1·267	1·019	1·234	1·362	1·426	1·019	1·279	1·444	1·561	1·019	1·298	1·491	1·628
0·3	1·167	1·179	1·207	1·224	1·167	1·276	1·367	1·421	1·167	1·325	1·453	1·562	1·167	1·346	1·503	1·630
0·4	1·248	1·175	1·165	1·167	1·248	1·301	1·370	1·414	1·248	1·353	1·460	1·562	1·248	1·374	1·513	1·631
0·5	1·273	1·144	1·106	1·095	1·273	1·309 0·966	1·371 0·819	1·414 0·742	1·273	1·362 0·899	1·466 0·686	1·562 0·560	1·273	1·385 0·882	1·516 0·638	1·632 0·476
0·6	1·248	1·084	1·027	1·006	1·248	0·946	0·800	0·726	1·248	0·880	0·676	0·550	1·248	0·862	0·624	0·467
0·7	1·167	0·988	0·921	0·892	1·167	0·883	0·747	0·676	1·167	0·824	0·636	0·514	1·167	0·805	0·585	0·438
0·8	1·019	0·846	0·777	0·746	1·019	0·769	0·648	0·585	1·019	0·719	0·550	0·448	1·019	0·701	0·511	0·384
0·9	0·764	0·625	0·566	0·539	0·764	0·575	0·482	0·434	0·764	0·537	0·412	0·338	0·764	0·523	0·384	0·289
0·95	0·555	0·450	0·406	0·385	0·555	0·417	0·350	0·313	0·555	0·388	0·299	0·246	0·555	0·372	0·275	0·210
1·0	0	0	0	0	0	0	0	0	0	0	0	0	0	0	0	0

TABLE 2—*continued*

Values of $\dfrac{C_{YF}(z)c(z)}{\bar{C}_{YF}\bar{c}_F}$

$h_1 = -R$

$\dfrac{z-R}{h}$	$b = 2R$				$b = h$				$b = 2h$				$b = 3h$			
	$\dfrac{R}{h} = 0$	0·1	0·25	0·5	$\dfrac{R}{h} = 0$	0·1	0·25	0·5	$\dfrac{R}{h} = 0$	0·1	0·25	0·5	$\dfrac{R}{h} = 0$	0·1	0·25	0·5
0	0	1·088	1·254	1·306	1·235	1·253	1·278	1·306	1·280	1·292	1·307	1·313	1·273	1·296	1·313	1·319
0·05	0·555	1·100	1·253	1·303	1·234	1·250	1·275	1·303	1·273	1·289	1·305	1·310	1·271	1·292	1·306	1·316
0·1	0·764	1·122	1·249	1·296	1·231	1·246	1·268	1·296	1·266	1·281	1·294	1·300	1·267	1·284	1·299	1·307
0·2	1·019	1·160	1·234	1·267	1·218	1·238	1·246	1·267	1·247	1·256	1·263	1·271	1·248	1·257	1·267	1·276
0·3	1·167	1·179	1·207	1·224	1·195	1·202	1·212	1·224	1·216	1·218	1·222	1·226	1·215	1·219	1·224	1·229
0·4	1·248	1·175	1·165	1·167	1·160	1·161	1·164	1·167	1·168	1·166	1·165	1·168	1·168	1·166	1·166	1·169
0·5	1·273	1·144	1·106	1·095	1·106	1·103	1·101	1·095	1·107	1·100	1·096	1·093	1·104	1·104	1·095	1·092
0·6	1·248	1·084	1·027	1·006	1·032	1·026	1·018	1·006	1·024	1·014	1·007	1·002	1·020	1·011	1·004	1·001
0·7	1·167	0·988	0·921	0·892	0·930	0·922	0·909	0·892	0·916	0·904	0·896	0·888	0·912	0·900	0·891	0·886
0·8	1·019	0·846	0·777	0·746	0·788	0·779	0·765	0·746	0·771	0·761	0·749	0·741	0·767	0·755	0·746	0·738
0·9	0·764	0·625	0·566	0·539	0·580	0·570	0·558	0·539	0·562	0·553	0·544	0·538	0·558	0·546	0·540	0·532
0·95	0·555	0·450	0·406	0·385	0·417	0·407	0·399	0·385	0·403	0·396	0·389	0·385	0·399	0·391	0·387	0·378
1·0	0	0	0	0	0	0	0	0	0	0	0	0	0	0	0	0

TABLE 3

Values of $\dfrac{C_{YB}(z)c(z)}{(C_{YB}c)_{\text{junction}}}$ *for* $\omega_B = \omega$

$h_1 = h$

z/R_0	$b = 0$				$b = h$				$b = 2h$				$b = 3h$			
	$\frac{R}{h} = 0$	0·1	0·25	0·5	$\frac{R}{h} = 0$	0·1	0·25	0·5	$\frac{R}{h} = 0$	0·1	0·25	0·5	$\frac{R}{h} = 0$	0·1	0·25	0·5
−1·0	0	0	0	0	0	0	0	0	0	0	0	0	0	0	0	0
−0·9	0·224	0·194	0·209	0·250	0·224	0·193	0·195	0·215	0·224	0·191	0·190	0·198	0·224	0·190	0·188	0·192
−0·8	0·316	0·274	0·293	0·348	0·316	0·273	0·275	0·300	0·316	0·272	0·268	0·278	0·316	0·270	0·267	0·271
−0·6	0·447	0·387	0·409	0·478	0·447	0·386	0·387	0·416	0·447	0·385	0·379	0·389	0·447	0·387	0·379	0·380
−0·4	0·548	0·474	0·494	0·568	0·548	0·474	0·471	0·499	0·548	0·475	0·464	0·470	0·548	0·477	0·465	0·462
−0·2	0·633	0·549	0·563	0·634	0·633	0·550	0·542	0·566	0·633	0·551	0·536	0·536	0·633	0·554	0·538	0·529
0	0·707	0·615	0·622	0·685	0·707	0·619	0·605	0·621	0·707	0·622	0·601	0·596	0·707	0·625	0·604	0·591
0·2	0·775	0·678	0·675	0·725	0·775	0·684	0·664	0·669	0·775	0·688	0·661	0·649	0·775	0·692	0·667	0·648
0·4	0·837	0·738	0·725	0·756	0·837	0·747	0·721	0·715	0·837	0·752	0·722	0·702	0·837	0·755	0·728	0·704
0·6	0·894	0·800	0·776	0·786	0·894	0·811	0·781	0·762	0·894	0·816	0·786	0·758	0·894	0·820	0·792	0·764
0·8	0·949	0·870	0·839	0·822	0·949	0·881	0·850	0·822	0·949	0·886	0·858	0·829	0·949	0·889	0·863	0·837
0·9	0·975	0·913	0·883	0·856	0·975	0·923	0·896	0·868	0·975	0·927	0·903	0·879	0·975	0·929	0·909	0·886
1·0	1·0	1·0	1·0	1·0	1·0	1·0	1·0	1·0	1·0	1·0	1·0	1·0	1·0	1·0	1·0	1·0

TABLE 3—*continued*

Values of $\dfrac{C_{YB}(z)c(z)}{(C_{YB}c)_{\text{junction}}}$ *for* $\omega_B = \omega$

$h_1 = 0 \cdot 5h$

z/R	$b = 0$				$b = h$				$b = 2h$				$b = 3h$			
	$\frac{R}{h} = 0$	0·1	0·25	0·5	$\frac{R}{h} = 0$	0·1	0·25	0·5	$\frac{R}{h} = 0$	0·1	0·25	0·5	$\frac{R}{h} = 0$	0·1	0·25	0·5
−1·0	0	0	0	0	0	0	0	0	0	0	0	0	0	0	0	0
−0·9	0·224	0·194	0·209	0·250	0·224	0·192	0·195	0·219	0·224	0·194	0·190	0·199	0·224	0·196	0·191	0·195
−0·8	0·316	0·274	0·293	0·348	0·316	0·271	0·276	0·306	0·316	0·272	0·270	0·279	0·316	0·274	0·271	0·273
−0·6	0·447	0·387	0·409	0·478	0·447	0·384	0·387	0·423	0·447	0·385	0·380	0·387	0·447	0·387	0·383	0·380
−0·4	0·548	0·474	0·494	0·568	0·548	0·471	0·469	0·504	0·548	0·472	0·463	0·467	0·548	0·475	0·465	0·462
−0·2	0·633	0·549	0·563	0·634	0·633	0·545	0·538	0·568	0·633	0·547	0·533	0·531	0·633	0·548	0·537	0·528
0	0·707	0·615	0·622	0·685	0·707	0·613	0·599	0·619	0·707	0·616	0·596	0·586	0·707	0·618	0·601	0·588
0·2	0·775	0·678	0·675	0·725	0·775	0·676	0·657	0·662	0·775	0·679	0·654	0·636	0·775	0·681	0·661	0·640
0·4	0·837	0·738	0·725	0·756	0·837	0·739	0·710	0·701	0·837	0·742	0·711	0·687	0·837	0·743	0·719	0·694
0·6	0·894	0·800	0·776	0·786	0·894	0·802	0·767	0·743	0·894	0·805	0·773	0·742	0·894	0·807	0·781	0·753
0·8	0·949	0·870	0·839	0·822	0·949	0·872	0·838	0·803	0·949	0·875	0·845	0·813	0·949	0·876	0·852	0·825
0·9	0·975	0·913	0·883	0·856	0·975	0·916	0·887	0·852	0·975	0·919	0·893	0·866	0·975	0·920	0·899	0·877
1·0	1·0	1·0	1·0	1·0	1·0	1·0	1·0	1·0	1·0	1·0	1·0	1·0	1·0	1·0	1·0	1·0

TABLE 3—*continued*

Values of $\dfrac{C_{YB}(z)c(z)}{(C_{YB}c)_{\text{junction}}}$ *for* $\omega_B = \omega$

for $h_1 = -R$

z/R	$b = 2R$: $\frac{R}{h} = 0{\cdot}1$	0·25	0·5	$b = h$: $\frac{R}{h} = 0$	0·1	0·25	0·5	$b = 2h$: $\frac{R}{h} = 0$	0·1	0·25	0·5	$b = 3h$: $\frac{R}{h} = 0$	0·1	0·25	0·5
—1·0	0	0	0	0	0	0	0	0	0	0	0	0	0	0	0
—0·9	0·194	0·209	0·250	0	0·081	0·175	0·250	0	0·058	0·131	0·224	0	0·055	0·104	0·201
—0·8	0·274	0·293	0·348	0	0·113	0·243	0·348	0	0·074	0·175	0·309	0	0·067	0·147	0·276
—0·6	0·387	0·409	0·478	0	0·151	0·330	0·478	0	0·100	0·233	0·415	0	0·091	0·197	0·369
—0·4	0·474	0·494	0·568	0	0·174	0·385	0·568	0	0·115	0·268	0·479	0	0·106	0·227	0·423
—0·2	0·549	0·563	0·634	0	0·186	0·417	0·634	0	0·123	0·287	0·517	0	0·114	0·245	0·460
0	0·615	0·622	0·685	0	0·190	0·427	0·685	0	0·125	0·292	0·528	0	0·115	0·249	0·462
				1·0	0·894	0·775		1·0	0·914	0·842	0·798	1·0	0·920	0·859	0·840
0·2	0·678	0·675	0·725	1·0	0·896	0·780	0·725	1·0	0·915	0·845	0·806	1·0	0·922	0·861	0·839
0·4	0·738	0·725	0·756	1·0	0·903	0·795	0·756	1·0	0·920	0·851	0·811	1·0	0·926	0·864	0·838
0·6	0·800	0·776	0·786	1·0	0·915	0·820	0·786	1·0	0·929	0·863	0·820	1·0	0·933	0·874	0·840
0·8	0·870	0·839	0·822	1·0	0·936	0·861	0·822	1·0	0·945	0·888	0·841	1·0	0·948	0·896	0·853
0·9	0·913	0·883	0·856	1·0	0·954	0·897	0·856	1·0	0·958	0·914	0·868	1·0	0·961	0·919	0·875
1·0	1·0	1·0	1·0	1·0	1·0	1·0	1·0	1·0	1·0	1·0	1·0	1·0	1·0	1·0	1·0

TABLE 4

$$Values\ of\ \frac{C_{LT}(y)c(y)}{(C_{LT}c)_{\text{junction}}}$$

$$h_1 = h$$

$\frac{y}{b/2}$	$b = 0$	$b = h$: $\frac{R}{h} = 0$	$b = h$: 0·1	$b = h$: 0·25	$b = h$: 0·5	$b = 2h$: $\frac{R}{h} = 0$	$b = 2h$: 0·1	$b = 2h$: 0·25	$b = 2h$: 0·5	$b = 3h$: $\frac{R}{h} = 0$	$b = 3h$: 0·1	$b = 3h$: 0·25	$b = 3h$: 0·5
0	1·0	1·0	1·0	1·0	1·0	1·0	1·0	1·0	1·0	1·0	1·0	1·0	1·0
0·2	0·894	0·85	0·86	0·87	0·875	0·77	0·81	0·835	0·855	0·715	0·755	0·795	0·84
0·4	0·775	0·685	0·71	0·735	0·74	0·59	0·63	0·675	0·705	0·505	0·56	0·615	0·675
0·6	0·632	0·525	0·555	0·585	0·595	0·43	0·47	0·515	0·55	0·345	0·395	0·45	0·50
0·8	0·447	0·35	0·375	0·40	0·41	0·27	0·30	0·34	0·37	0·21	0·245	0·28	0·325
1·0	0	0	0	0	0	0	0	0	0	0	0	0	0

$$h_1 = 0·5h$$

$\frac{y}{b/2}$	$b = 0$	$b = h$: $\frac{R}{h} = 0$	$b = h$: 0·1	$b = h$: 0·25	$b = h$: 0·5	$b = 2h$: $\frac{R}{h} = 0$	$b = 2h$: 0·1	$b = 2h$: 0·25	$b = 2h$: 0·5	$b = 3h$: $\frac{R}{h} = 0$	$b = 3h$: 0·1	$b = 3h$: 0·25	$b = 3h$: 0·5
0	1·0	1·0	1·0	1·0	1·0	1·0	1·0	1·0	1·0	1·0	1·0	1·0	1·0
0·2	0·980	0·961	0·965	0·965	0·97	0·910	0·93	0·94	0·95	0·840	0·88	0·915	0·94
0·4	0·917	0·851	0·87	0·885	0·895	0·716	0·765	0·805	0·835	0·587	0·65	0·715	0·785
0·6	0·800	0·686	0·71	0·735	0·755	0·512	0·56	0·605	0·66	0·389	0·435	0·500	0·575
0·8	0·600	0·469	0·495	0·515	0·535	0·318	0·345	0·385	0·435	0·231	0·265	0·295	0·335
1·0	0	0	0	0	0	0	0	0	0	0	0	0	0

TABLE 4—*continued*

Values of $\dfrac{C_{LT}(y)c(y)}{(C_{LT}c)_{\text{junction}}}$

$h_1 = 0{\cdot}75h; \quad R = 0$

$\dfrac{y}{b/2}$	$b = 0$	$b = h$	$b = 2h$	$b = 3h$
1·0	1·0	1·0	1·0	1·0
0·8	0·980	0·945	0·875	0·805
0·6	0·917	0·825	0·68	0·56
0·4	0·800	0·650	0·49	0·375
0·2	0·600	0·445	0·31	0·235
0	0	0	0	0

$h_1 = -R$

$\dfrac{y-R}{\frac{b}{2}-R}$	$b = 2R$	$b = h$				$b = 2h$				$b = 3h$			
		$\dfrac{R}{h} = 0$	0·1	0·25	0·5	$\dfrac{R}{h} = 0$	0·1	0·25	0·5	$\dfrac{R}{h} = 0$	0·1	0·25	0·5
0	1·0	1·0	1·0	1·0	1·0	1·0	1·0	1·0	1·0	1·0	1·0	1·0	1·0
0·2	0·980	0·85	0·92	0·945	0·980	0·77	0·86	0·92	0·96	0·715	0·80	0·875	0·93
0·4	0·917	0·685	0·79	0·865	0·917	0·59	0·68	0·775	0·86	0·505	0·59	0·69	0·79
0·6	0·800	0·525	0·625	0·72	0·800	0·43	0·505	0·60	0·71	0·345	0·42	0·51	0·625
0·8	0·600	0·35	0·43	0·515	0·600	0·27	0·33	0·405	0·50	0·21	0·26	0·325	0·42
1·0	0	0	0	0	0	0	0	0	0	0	0	0	0

TABLE 5

Values of $\dfrac{C_{L\,B}(y)c(y)}{(C_{L\,B}\,c)_{\text{junction}}}$

$h_1 = h$

y/R	$b = 0$				$b = h$				$b = 2h$				$b = 3h$			
	$\frac{R}{h} = 0$	0·1	0·25	0·5	$\frac{R}{h} = 0$	0·1	0·25	0·5	$\frac{R}{h} = 0$	0·1	0·25	0·5	$\frac{R}{h} = 0$	0·1	0·25	0·5
0	1·0	1·0	1·0	1·0	1·0	1·0	1·0	1·0	1·0	1·0	1·0	1·0	1·0	1·0	1·0	1·0
0·2	0·894	0·874	0·850	0·812	0·894	0·877	0·861	0·840	0·894	0·879	0·868	0·855	0·894	0·881	0·873	0·862
0·4	0·775	0·742	0·702	0·639	0·775	0·749	0·724	0·680	0·775	0·752	0·735	0·705	0·775	0·754	0·744	0·715
0·6	0·632	0·595	0·546	0·474	0·632	0·607	0·575	0·522	0·632	0·613	0·588	0·551	0·632	0·617	0·597	0·565
0·8	0·447	0·414	0·369	0·307	0·447	0·425	0·394	0·345	0·447	0·430	0·406	0·370	0·447	0·432	0·412	0·383
1·0	0	0	0	0	0	0	0	0	0	0	0	0	0	0	0	0

$h_1 = 0{\cdot}5h$

y/R	$b = 0$				$b = h$				$b = 2h$				$b = 3h$			
	$\frac{R}{h} = 0$	0·1	0·25	0·5	$\frac{R}{h} = 0$	0·1	0·25	0·5	$\frac{R}{h} = 0$	0·1	0·25	0·5	$\frac{R}{h} = 0$	0·1	0·25	0·5
0	1·0	1·0	1·0	1·0	1·0	1·0	1·0	1·0	1·0	1·0	1·0	1·0	1·0	1·0	1·0	1·0
0·2	0·894	0·874	0·850	0·812	0·894	0·871	0·857	0·827	0·894	0·869	0·863	0·847	0·894	0·869	0·867	0·855
0·4	0·775	0·742	0·702	0·639	0·775	0·741	0·714	0·665	0·775	0·739	0·725	0·693	0·775	0·738	0·732	0·704
0·6	0·632	0·595	0·546	0·474	0·632	0·600	0·561	0·496	0·632	0·602	0·575	0·534	0·632	0·602	0·582	0·553
0·8	0·447	0·414	0·369	0·307	0·447	0·418	0·381	0·321	0·447	0·420	0·394	0·354	0·447	0·420	0·398	0·372
1·0	0	0	0	0	0	0	0	0	0	0	0	0	0	0	0	0

TABLE 5—*continued*

Values of $\dfrac{C_{LB}(y)c(y)}{(C_{LB}c)_{\text{junction}}}$

$h_1 = -R$

y/R	$b = 2R$			$b = h$				$b = 2h$				$b = 3h$			
	$\frac{R}{h} = 0\cdot1$	$0\cdot25$	$0\cdot5$	$\frac{R}{h} = 0$	$0\cdot1$	$0\cdot25$	$0\cdot5$	$\frac{R}{h} = 0$	$0\cdot1$	$0\cdot25$	$0\cdot5$	$\frac{R}{h} = 0$	$0\cdot1$	$0\cdot25$	$0\cdot5$
0	1·0	1·0	1·0	1·0	1·0	1·0	1·0	1·0	1·0	1·0	1·0	1·0	1·0	1·0	1·0
0·2	0·874	0·850	0·812	1·0	0·938	0·872	0·812	1·0	0·956	0·898	0·820	1·0	0·958	0·914	0·833
0·4	0·742	0·702	0·639	1·0	0·880	0·742	0·639	1·0	0·913	0·800	0·665	1·0	0·917	0·831	0·695
0·6	0·595	0·546	0·474	1·0	0·823	0·618	0·474	1·0	0·870	0·711	0·531	1·0	0·877	0·751	0·575
0·8	0·414	0·369	0·307	1·0	0·765	0·490	0·307	1·0	0·828	0·629	0·405	1·0	0·840	0·676	0·471
1·0	0	0	0	1·0	0·705	0·347	0	1·0	0·788	0·550	0·270	1·0	0·804	0·610	0·378

TABLE 6

Calculation Example

$A_F = 1 \cdot 37, \ \varphi = 0, \ R/h = 0 \cdot 22, \ b/h = 1 \cdot 93, \ h_1/h = 1 \cdot 0, \ a_0 = 2\pi$

	From	Fin Alone	Fin and Body	Fin-Body-Tailplane
A_{eF}	Equation (117)	1·37	1·62	2·46
n	Equation (122)	0·624	0·604	0·560
ω	Equation (123)	1·248	1·208	1·12
a	Equation (121)	4·35	4·62	5·27
$\frac{\omega a}{2\pi A_F}$		0·631	0·648	0·685
β_i/β	Figs. 7a to 7d	0·558	0·498	0·332
J_{YF}	Figs. 4a to 4d	1·57	2·73	5·25
$\frac{\bar{C}_{YF}}{\beta}$	Equation (124)	1·92	3·08	4·26

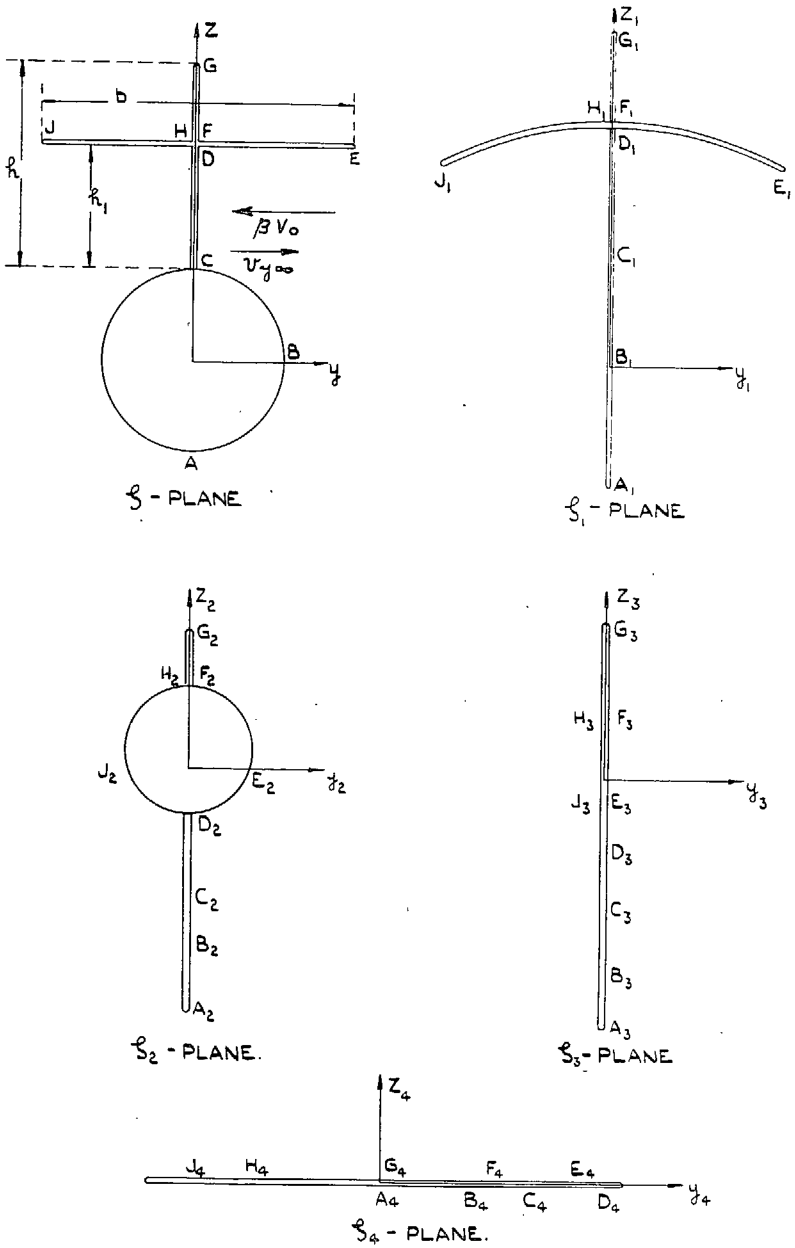

FIG. 1. Sketch of the conformal transformations of the Trefftz-plane.

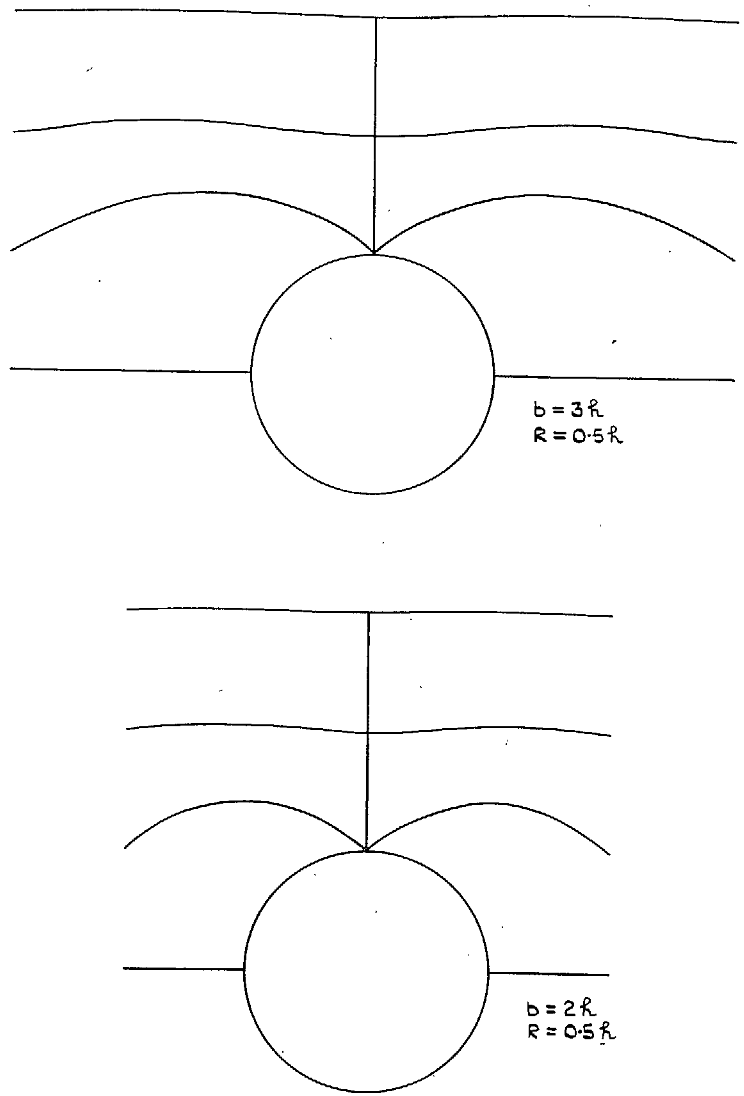

FIG. 2. Tailplane shapes which lead to circular arcs in the ζ_1-plane.

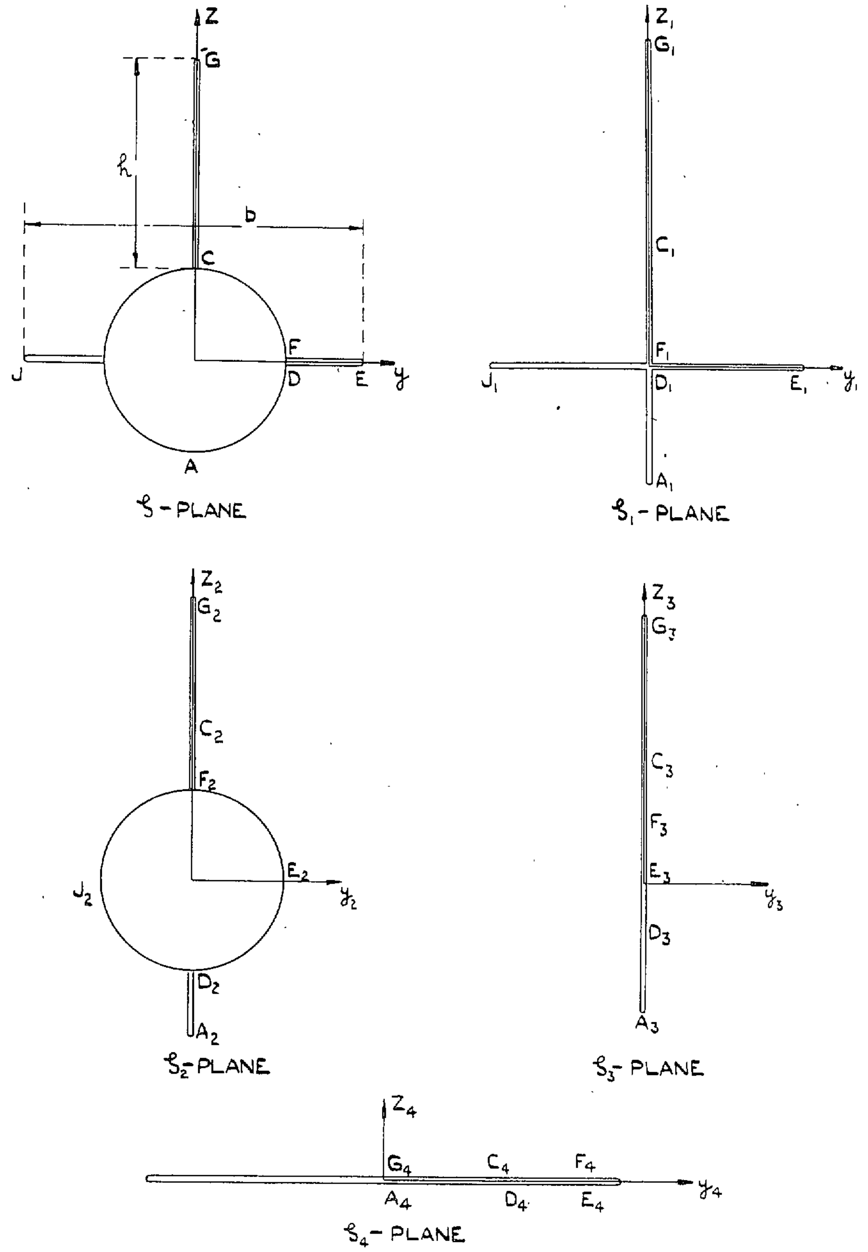

FIG. 3. Sketch of the conformal transformations of the Trefftz-plane for the special case $h_1 = - R$.

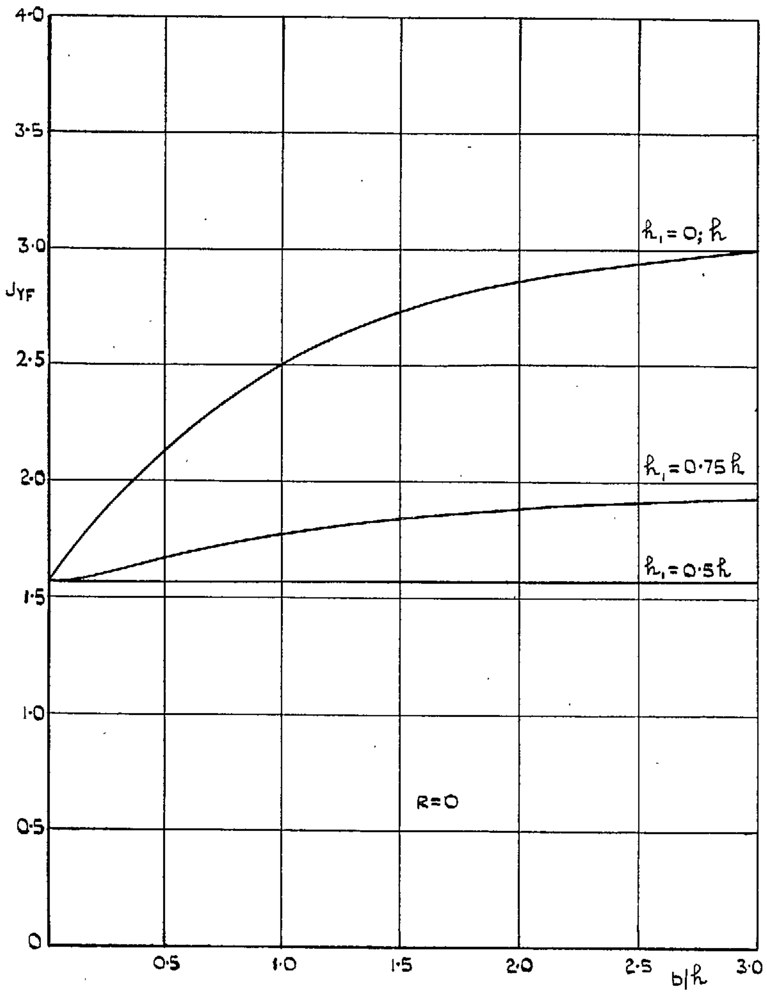

FIG. 4a. Coefficient for calculating the side-force on the fin;
$$\overline{C}_{YF} = \frac{2}{\omega}\frac{\beta_i}{\beta} A_F J_{YF}.$$

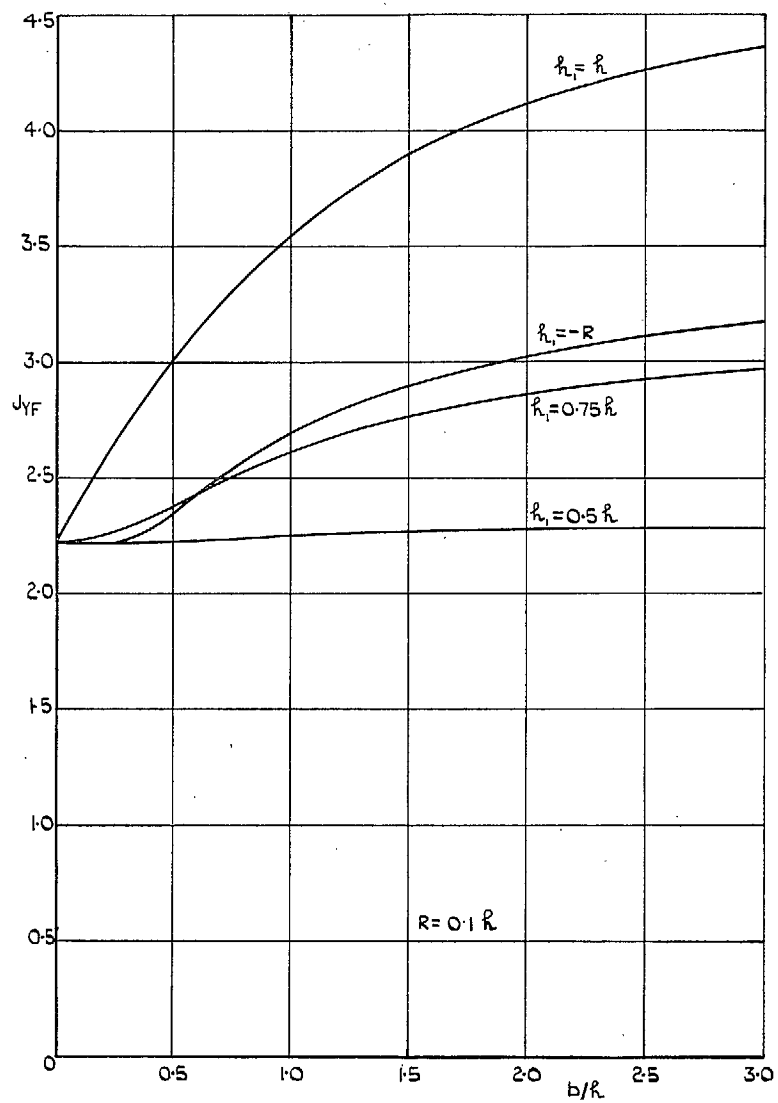

FIG. 4b. Coefficient for calculating the side-force on the fin;
$$\overline{C}_{YF} = \frac{2}{\omega}\frac{\beta_i}{\beta} A_F J_{YF}.$$

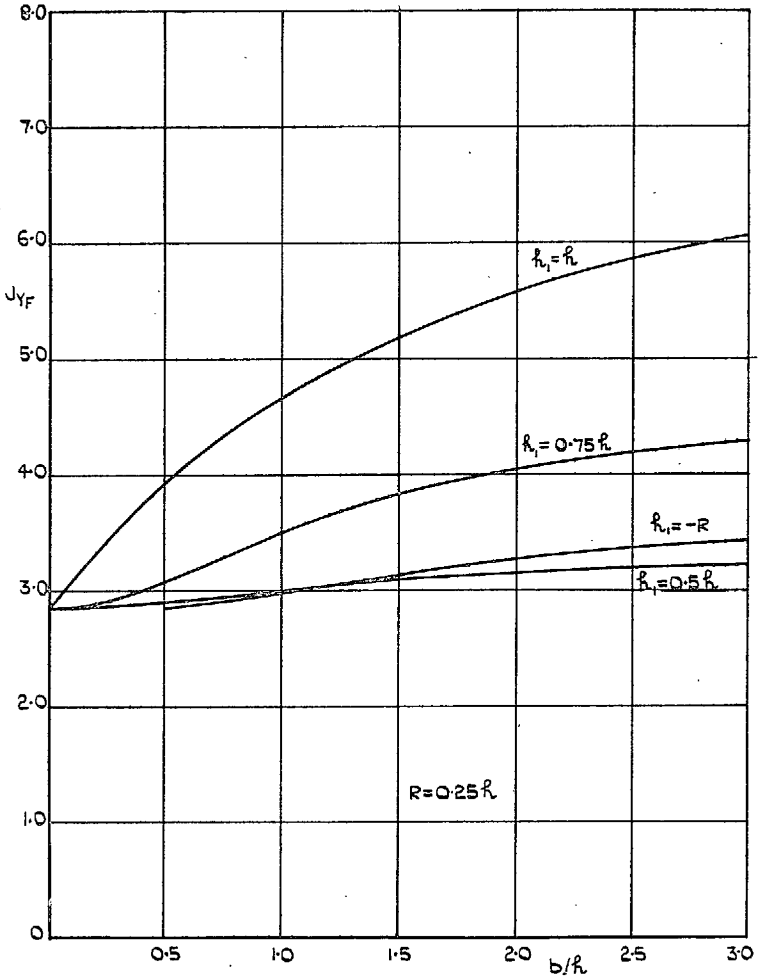

FIG. 4c. Coefficient for calculating the side-force on the fin; $\overline{C}_{YF} = \frac{2}{\omega}\frac{\beta_i}{\beta} A_F J_{YF}$.

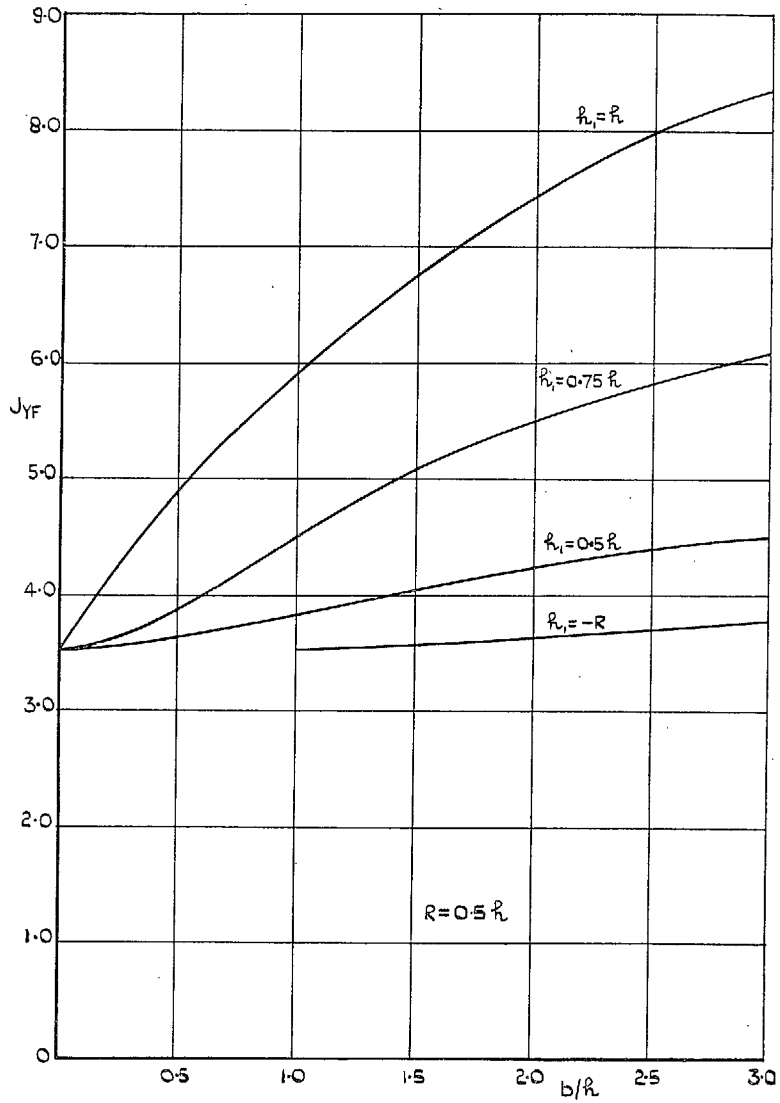

FIG. 4d. Coefficient for calculating the side-force on the fin; $\overline{C}_{YF} = \frac{2}{\omega}\frac{\beta_i}{\beta} A_F J_{YF}$.

(4754)

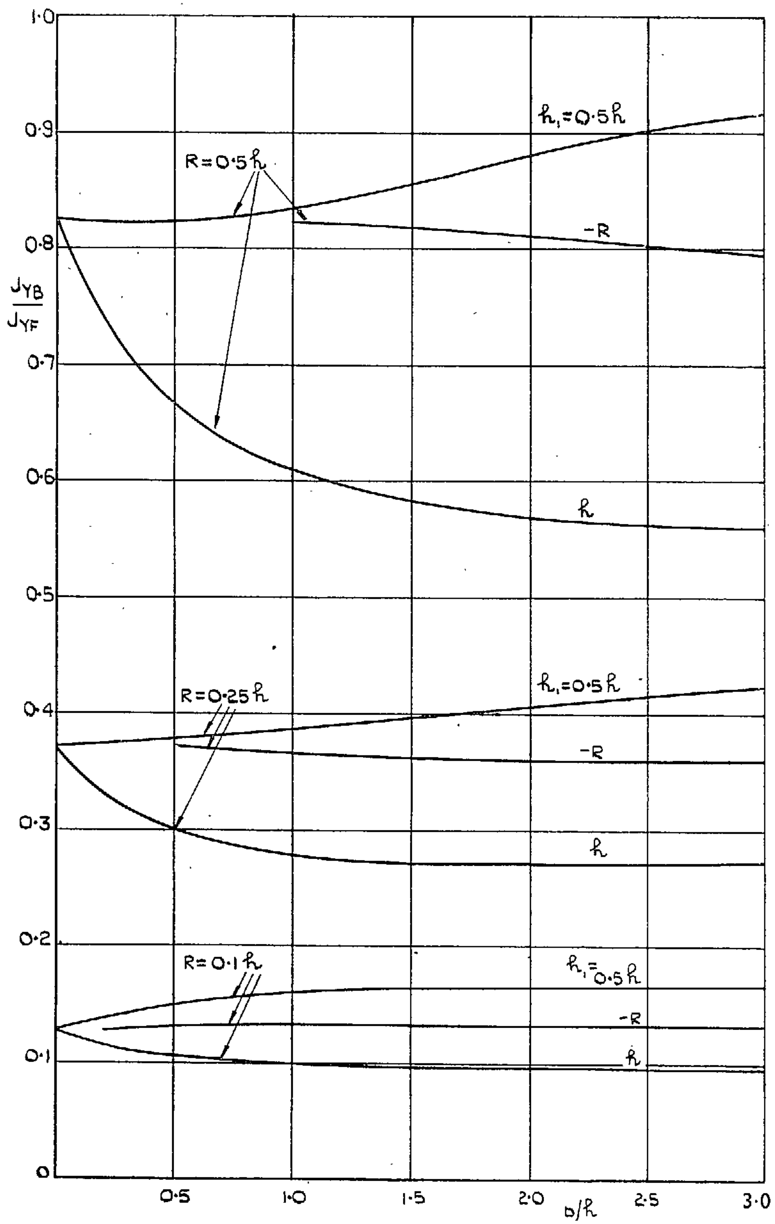

FIG. 5. Ratio between the side-forces on body and fin, $\omega_B = \omega$.

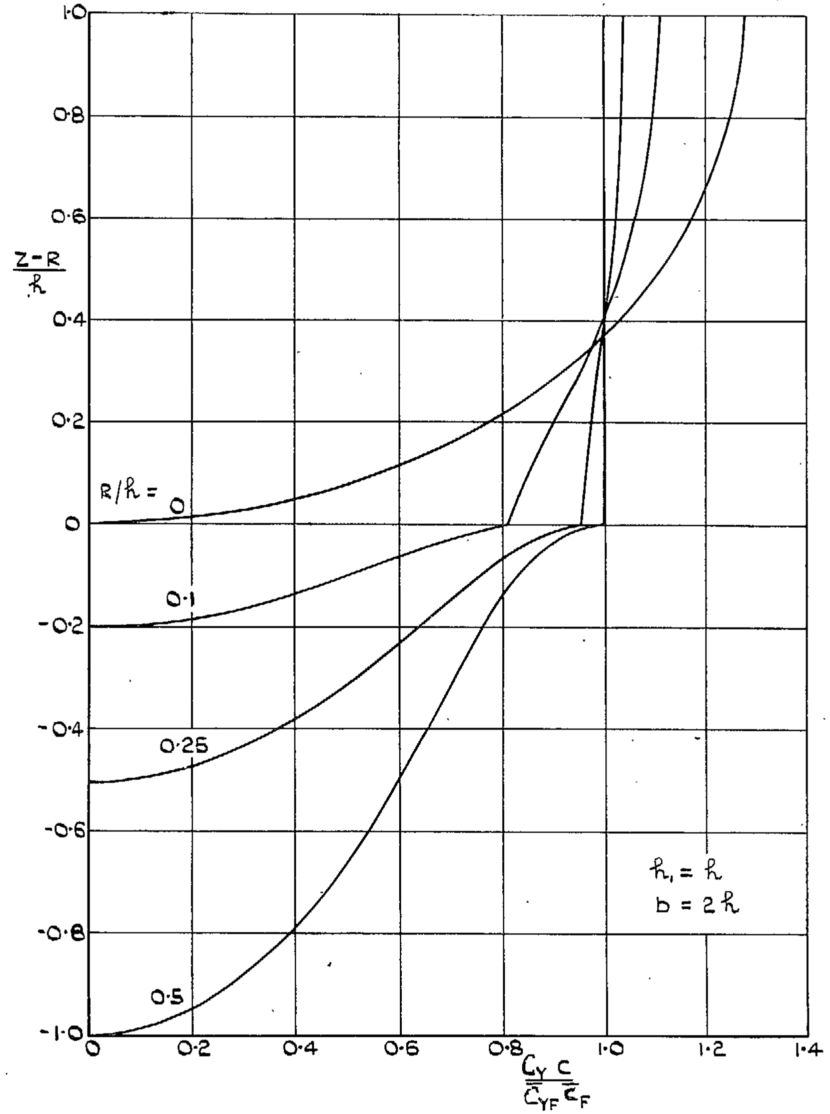

FIG. 6a. Side-force distributions for $\omega_B = \omega$.

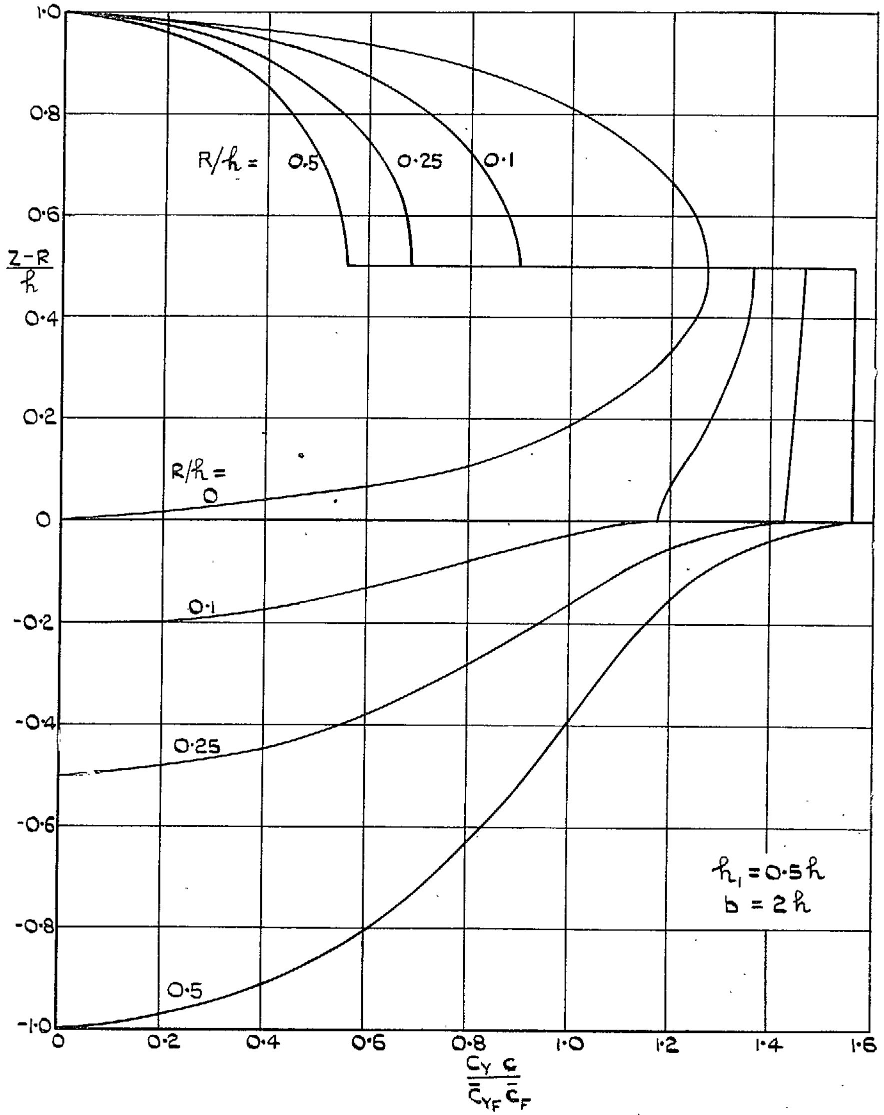

FIG. 6b. Side-force distributions for $\omega_B = \omega$.

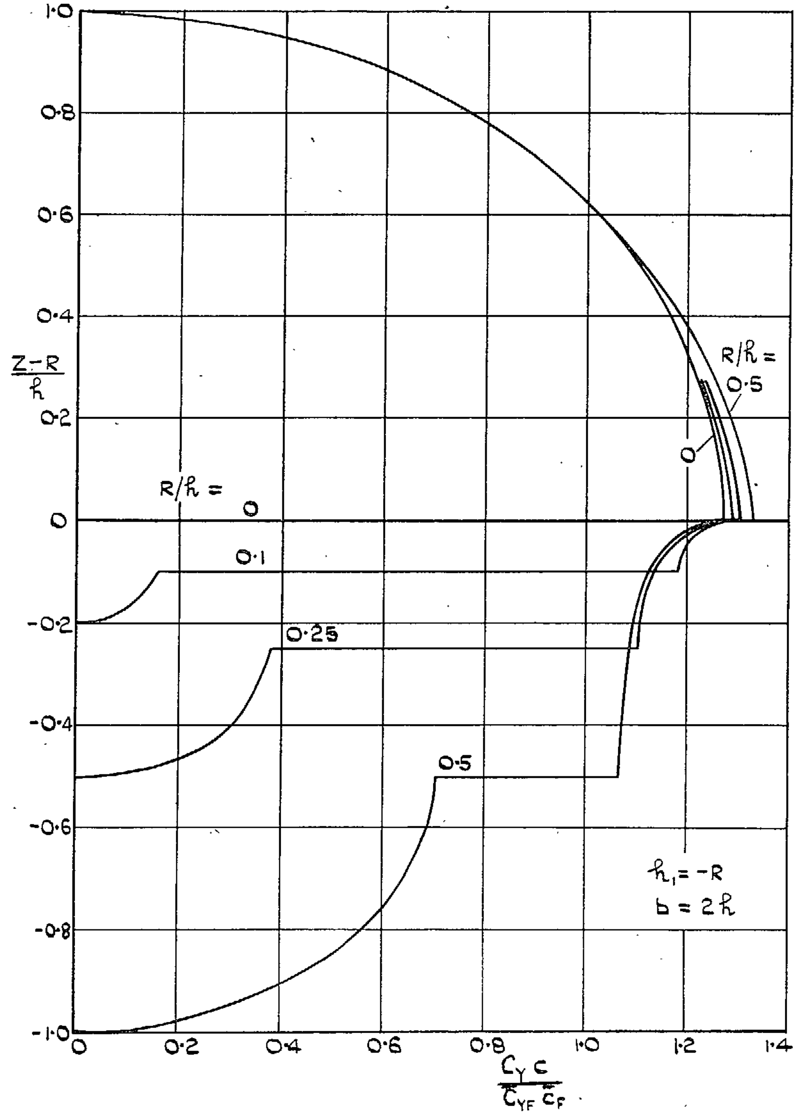

FIG. 6c. Side-force distributions for $\omega_B = \omega$.

(4754)

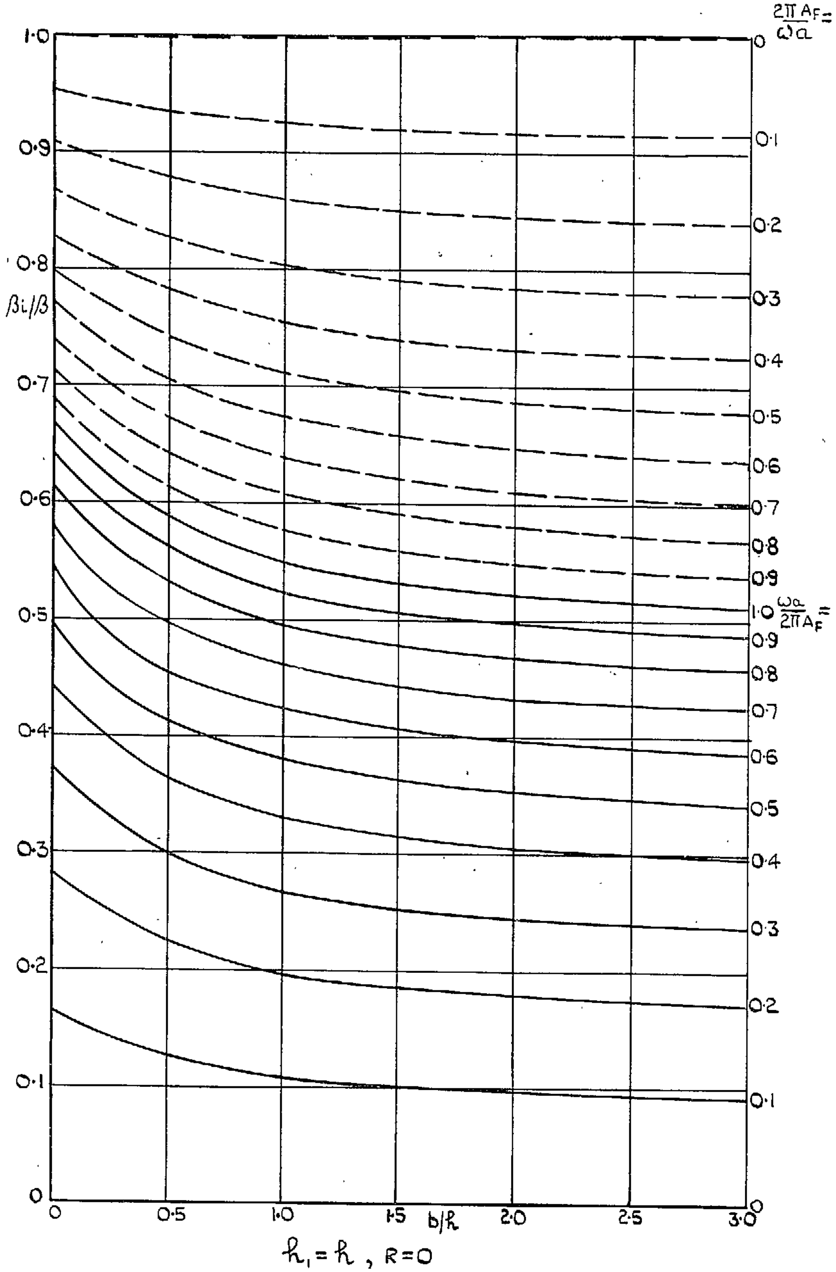

FIG. 7a. Induced side-wash.

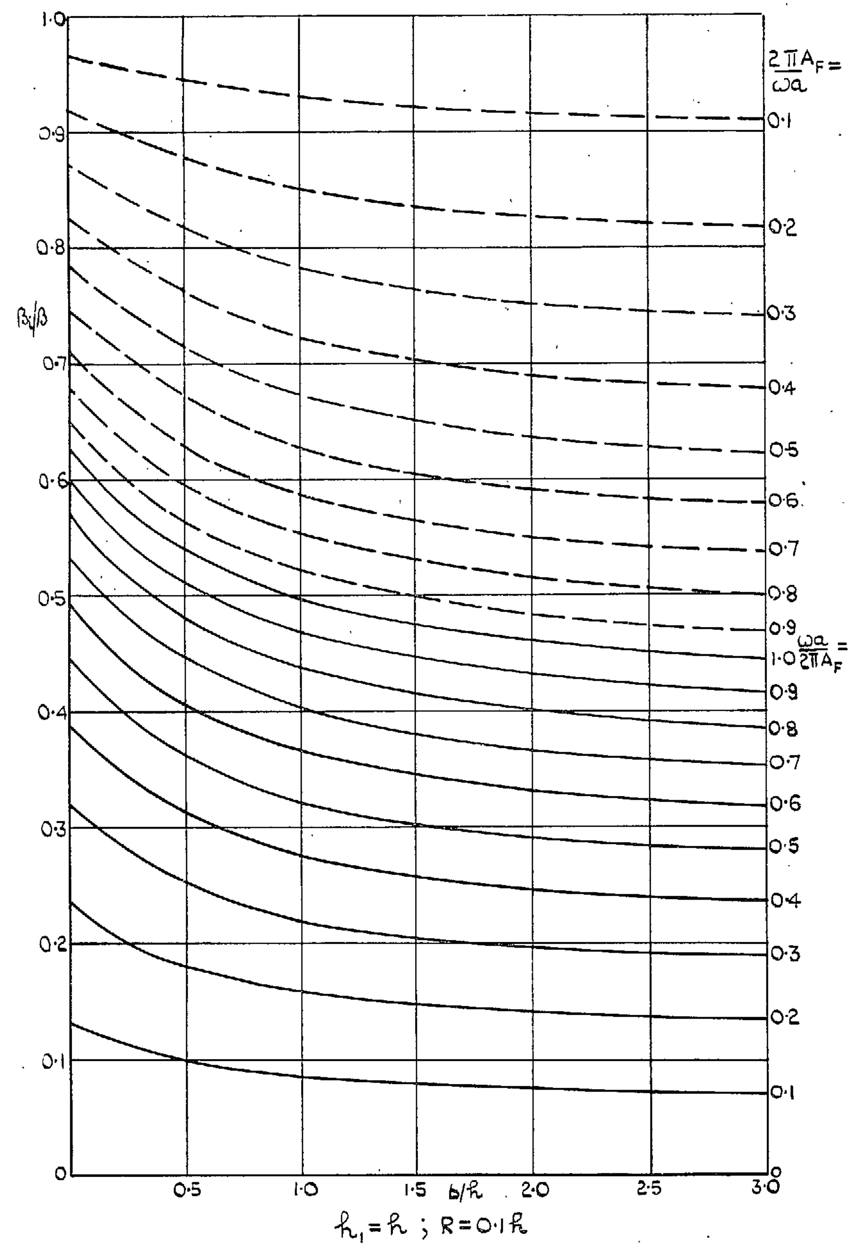

FIG. 7b. Induced side-wash.

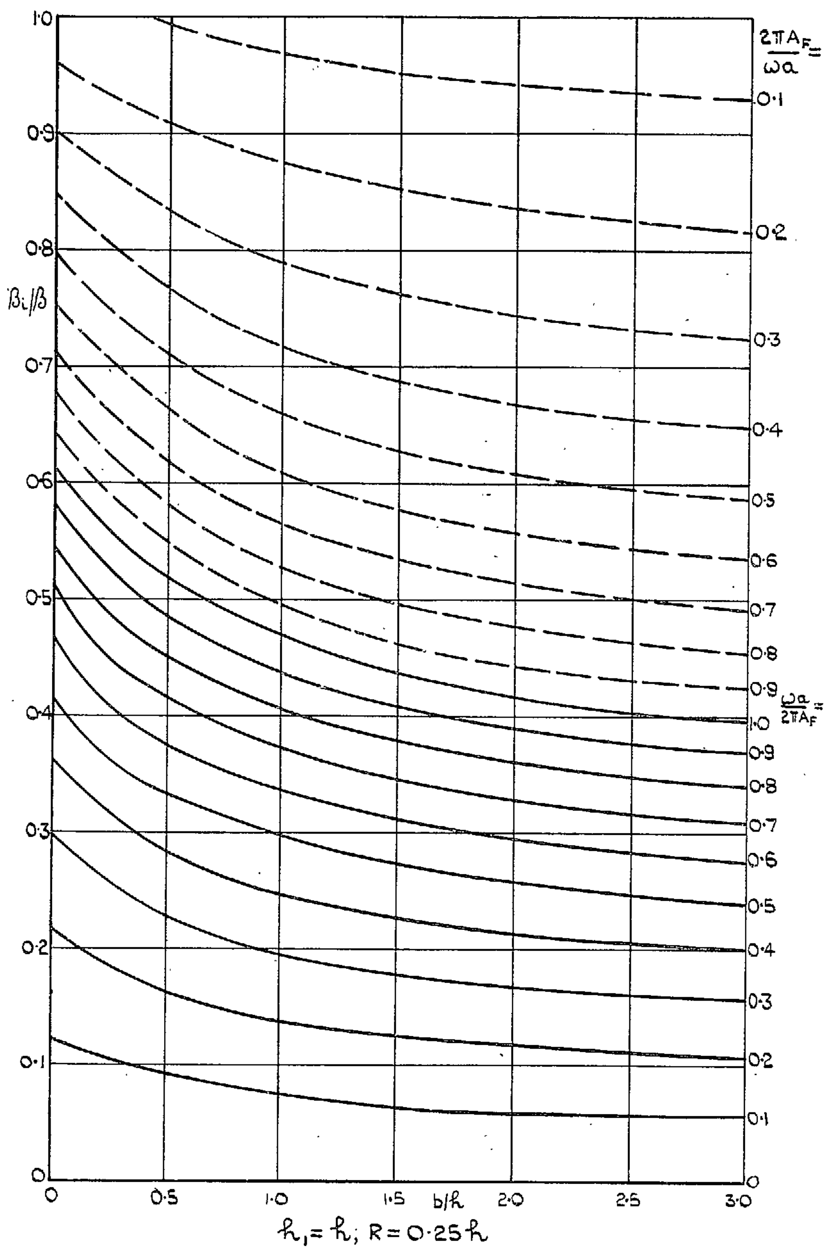

FIG. 7c. Induced side-wash.

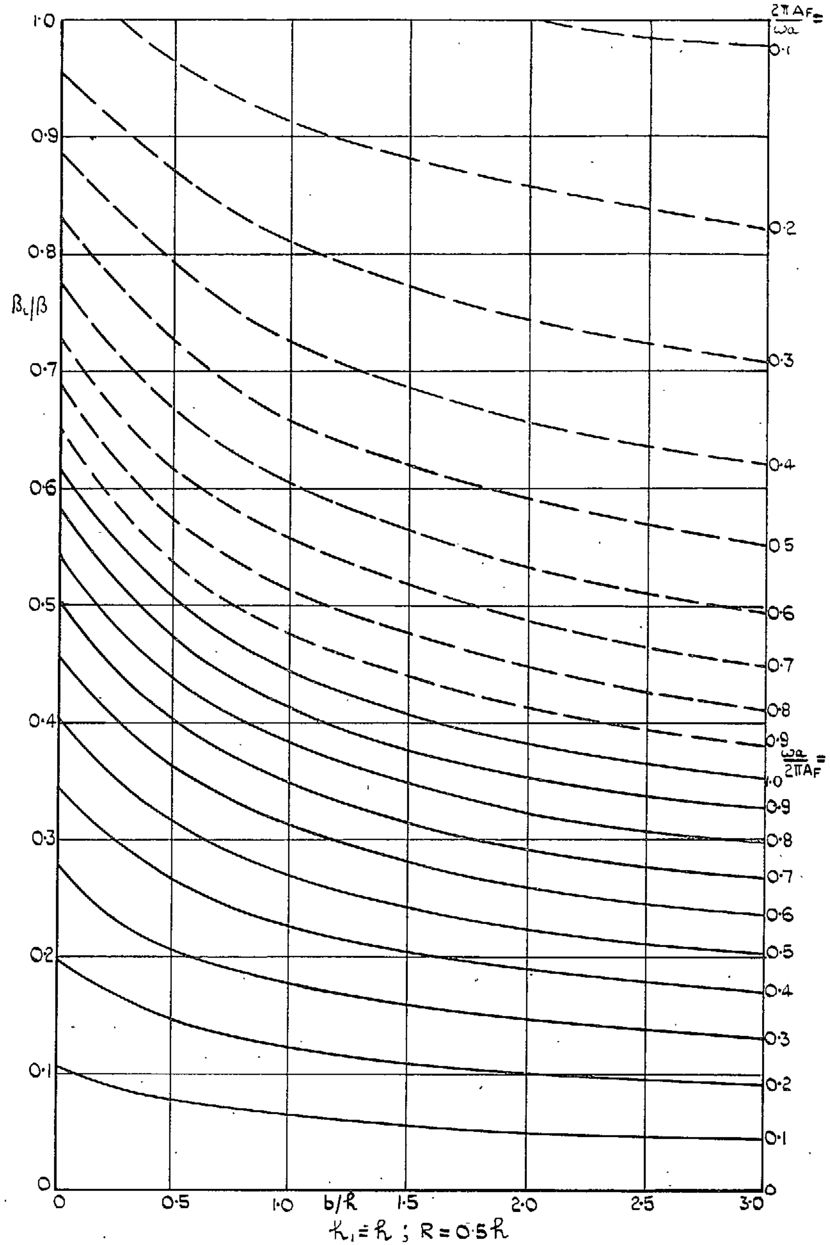

FIG. 7d. Induced side-wash.

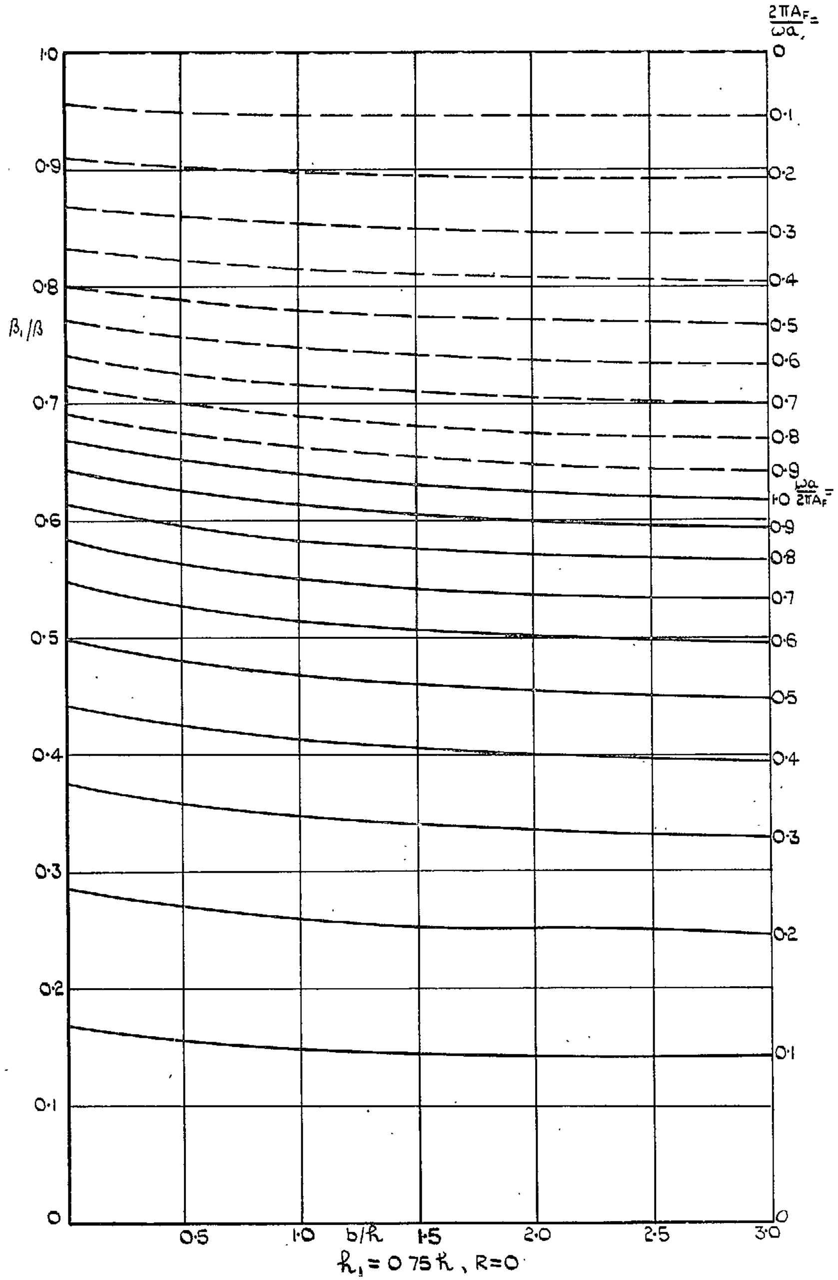

FIG. 7e. Induced side-wash.

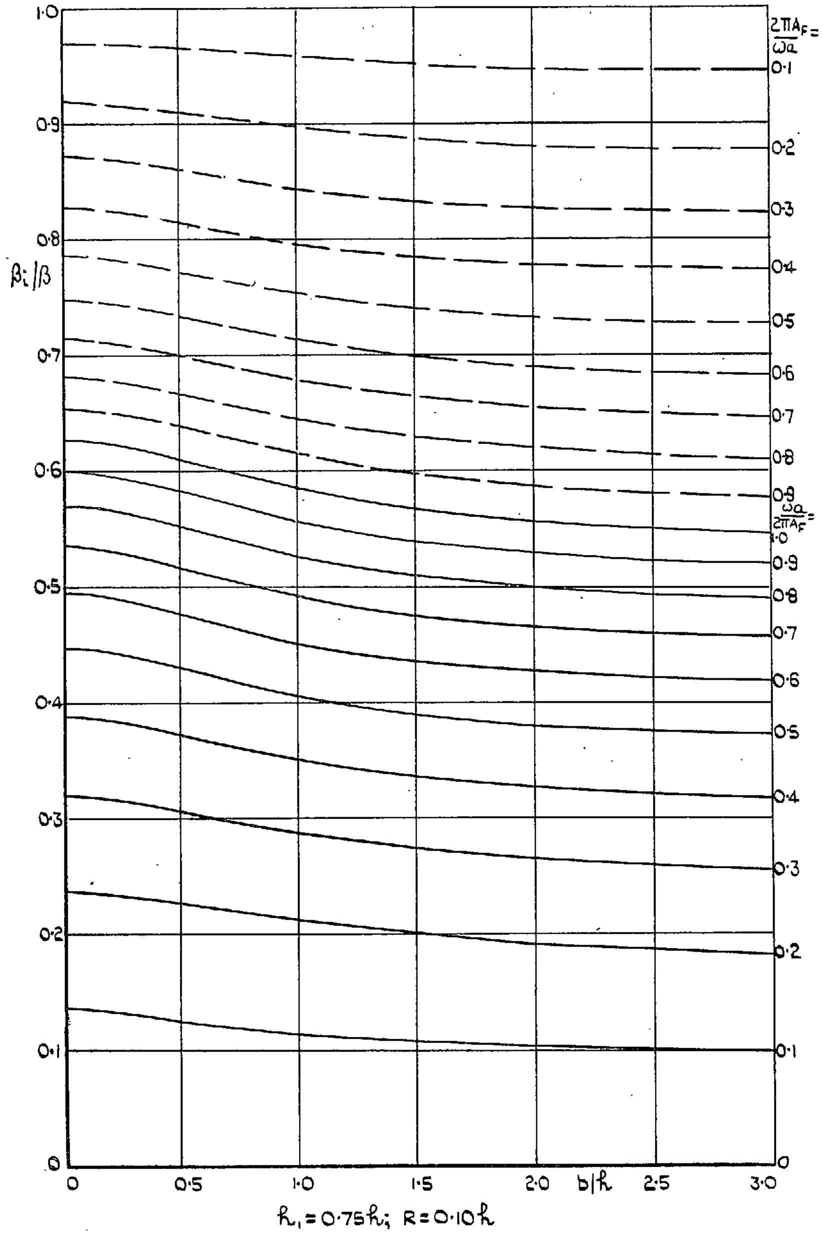

FIG. 7f. Induced side-wash.

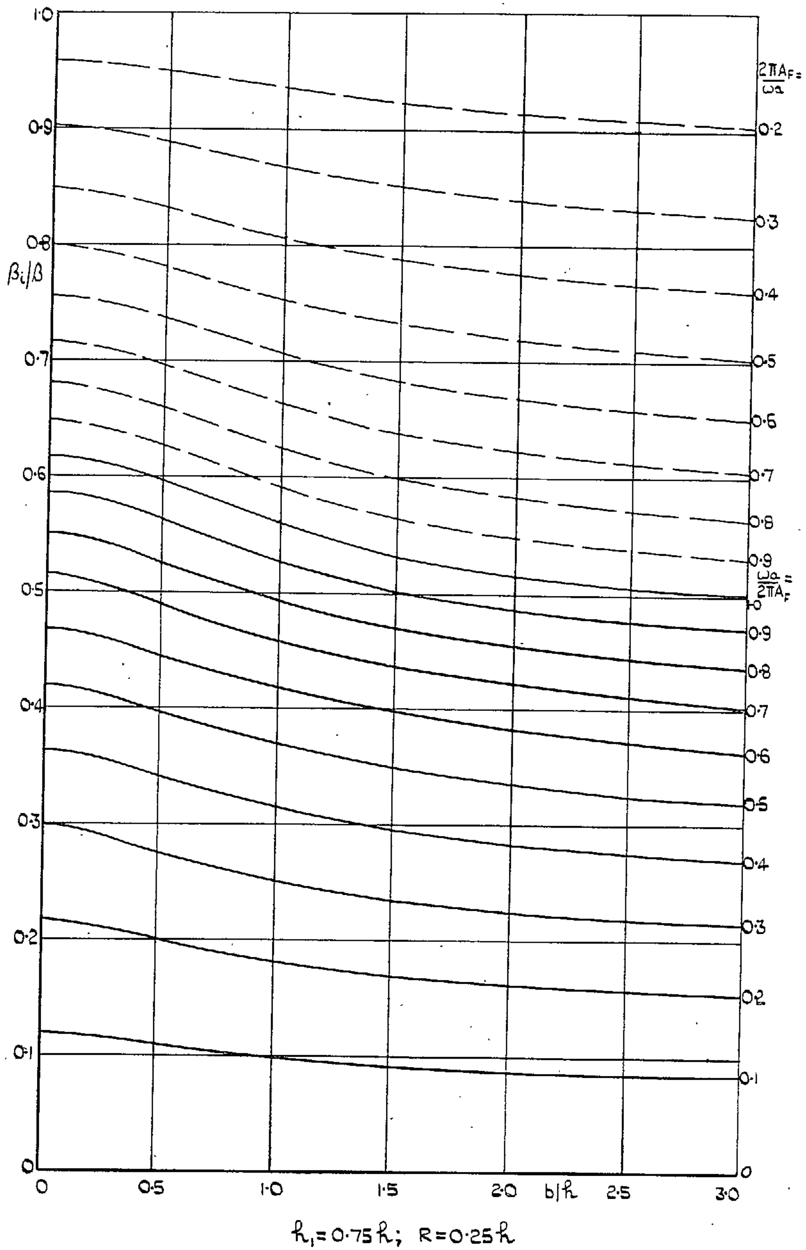

FIG. 7g. Induced side-wash.

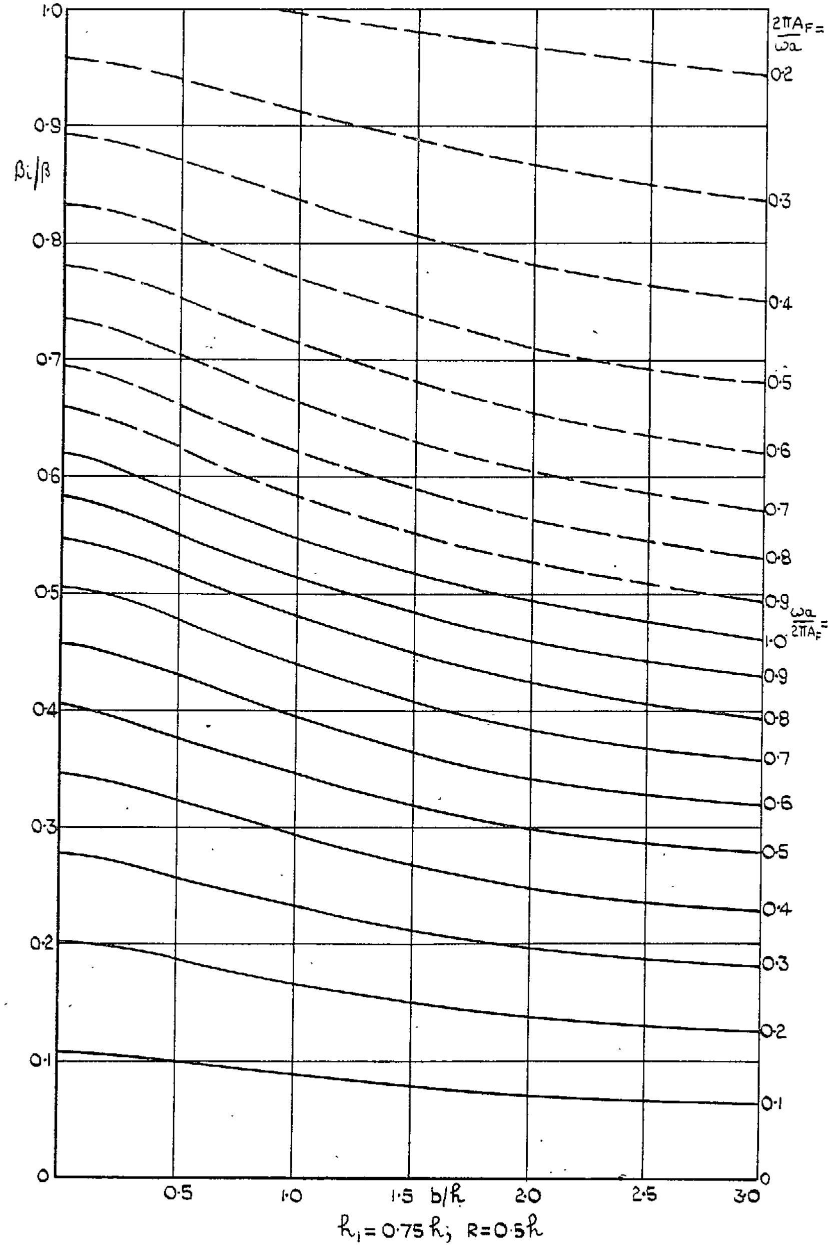

FIG. 7h. Induced side-wash.

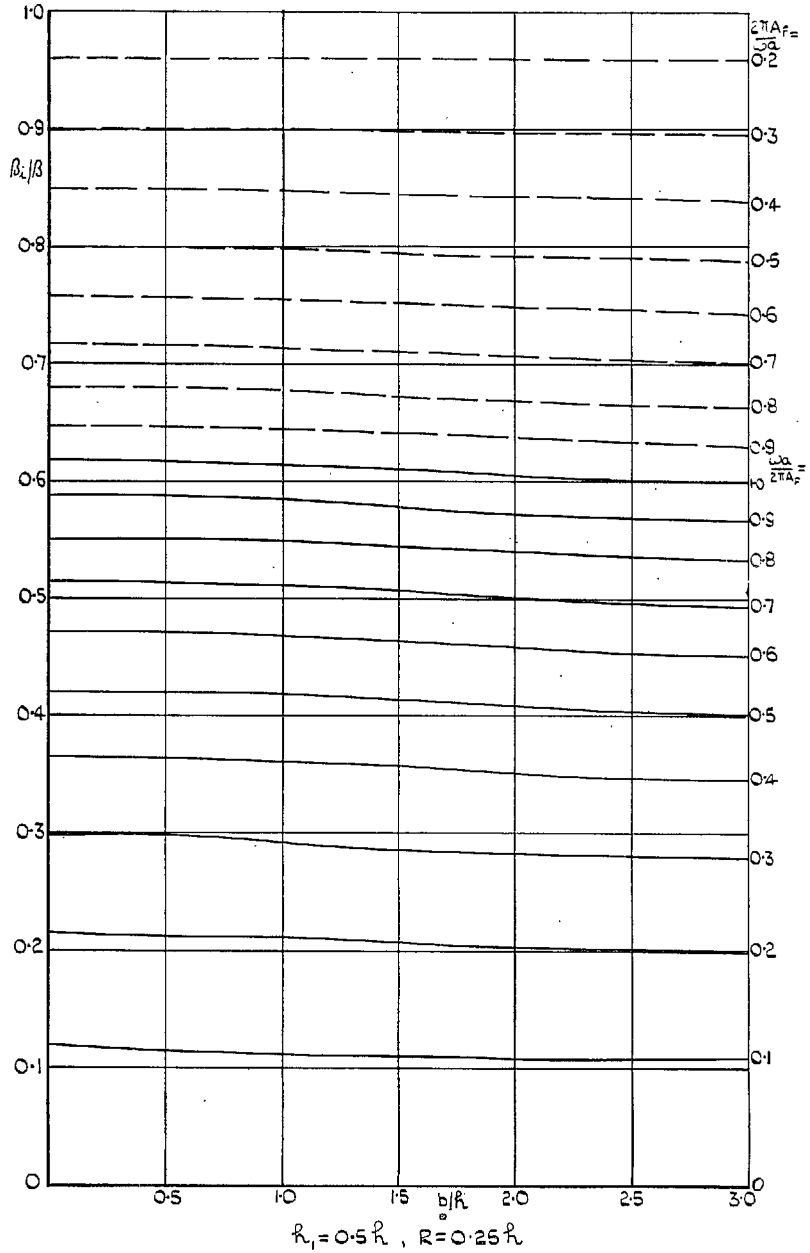

FIG. 7i. Induced side-wash.

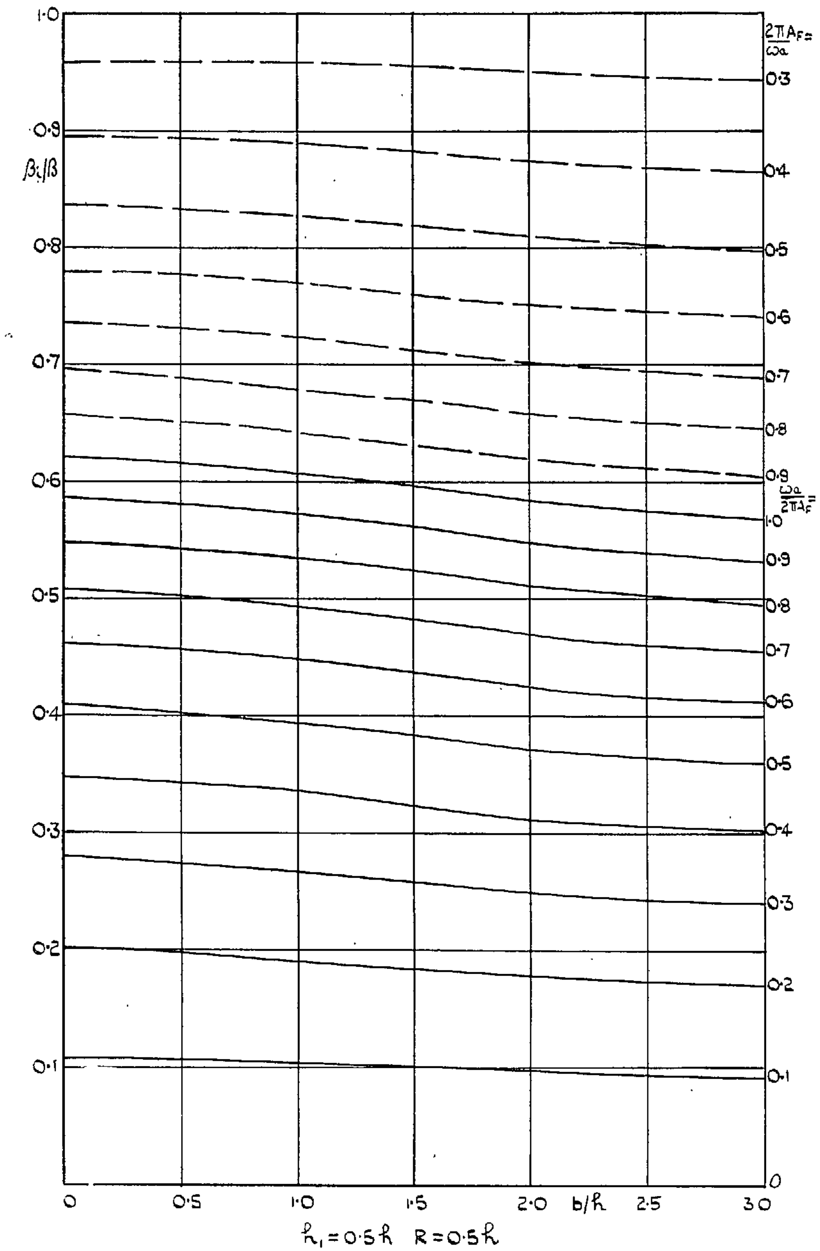

FIG. 7k. Induced side-wash.

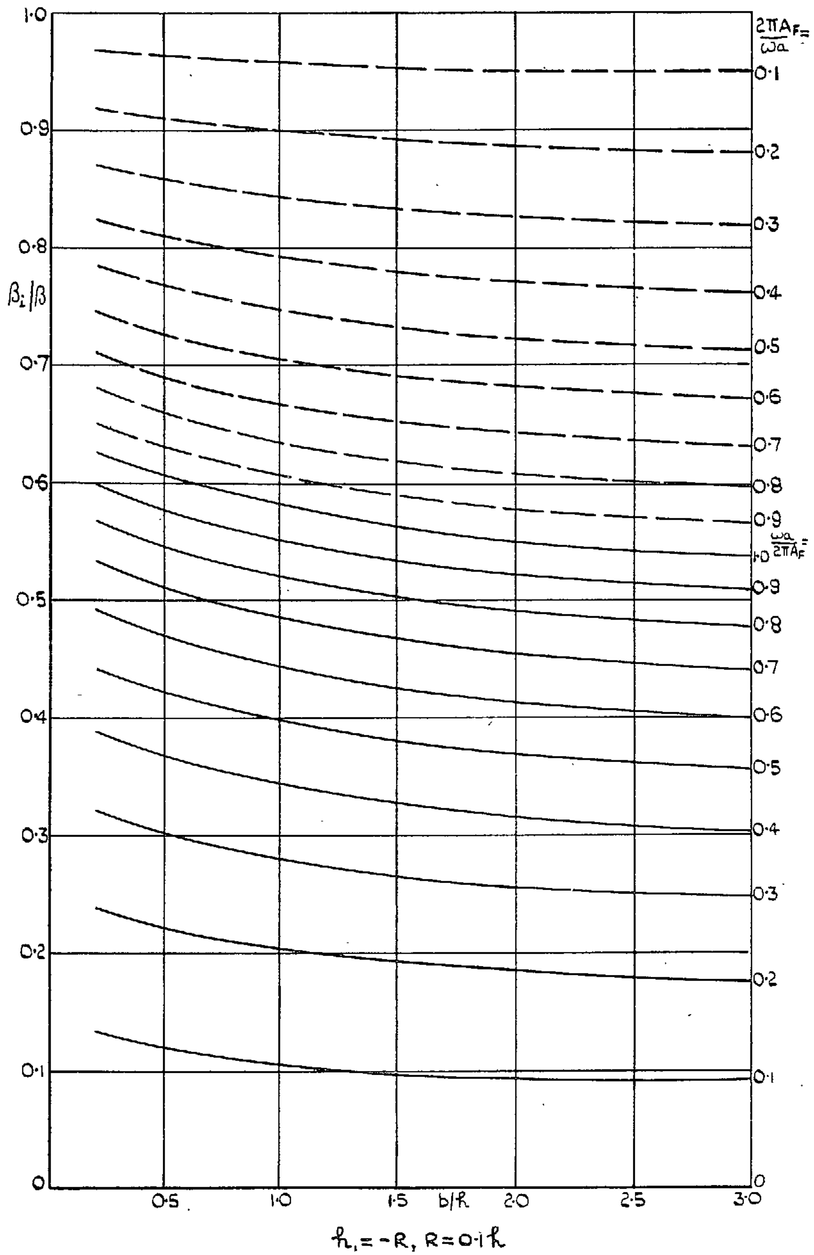

FIG. 7l. Induced side-wash.

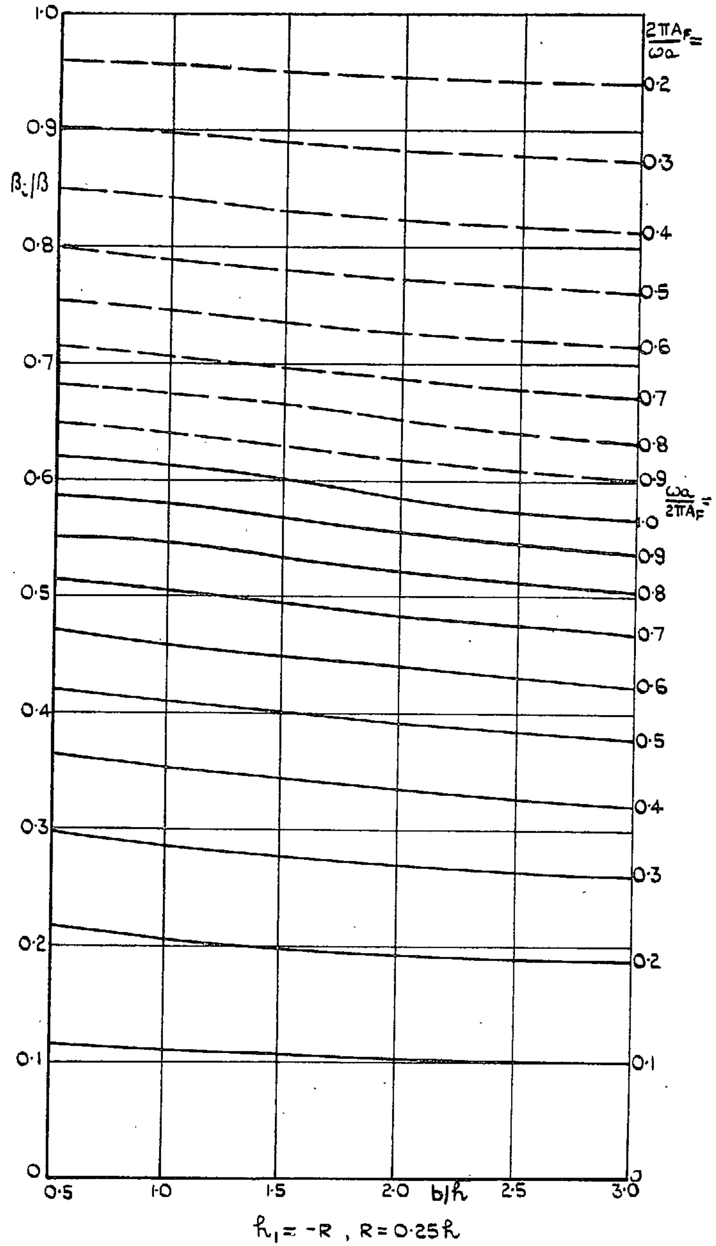

FIG. 7m. Induced side-wash.

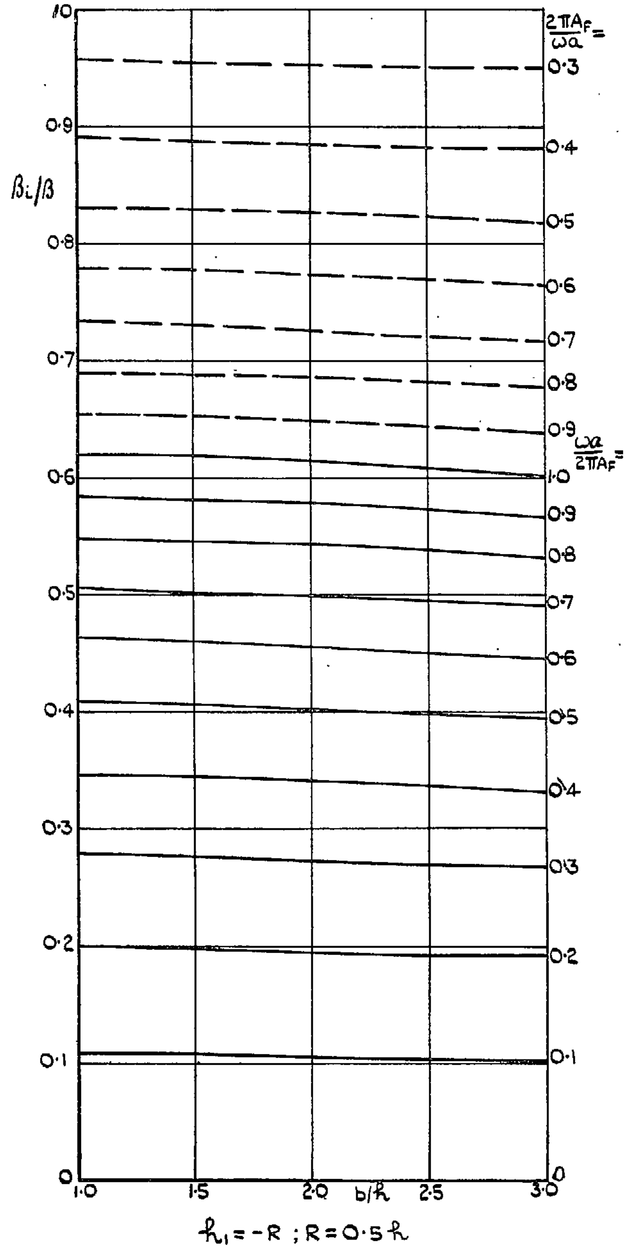

FIG. 7n. Induced side-wash.

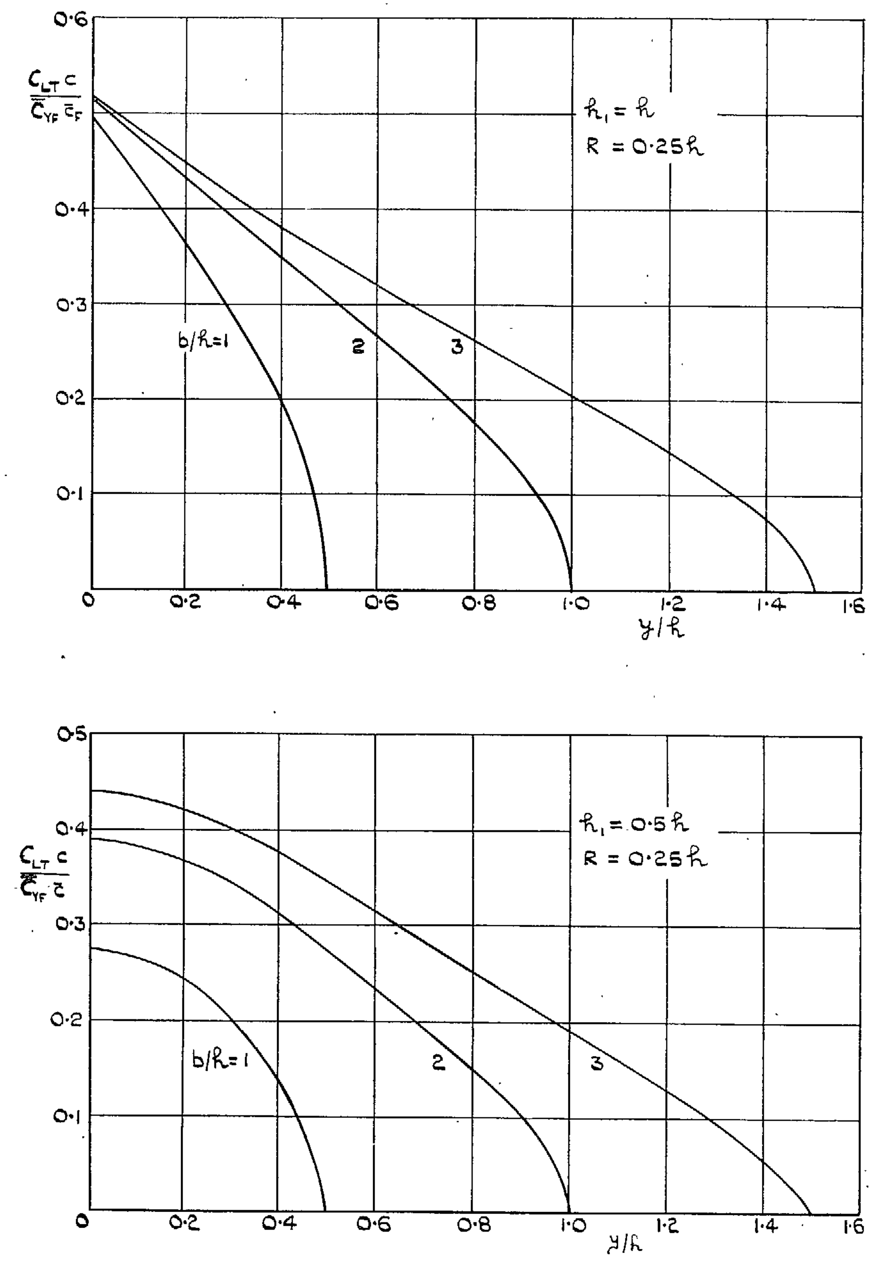

FIG. 8. Lift distribution on the tailplane.

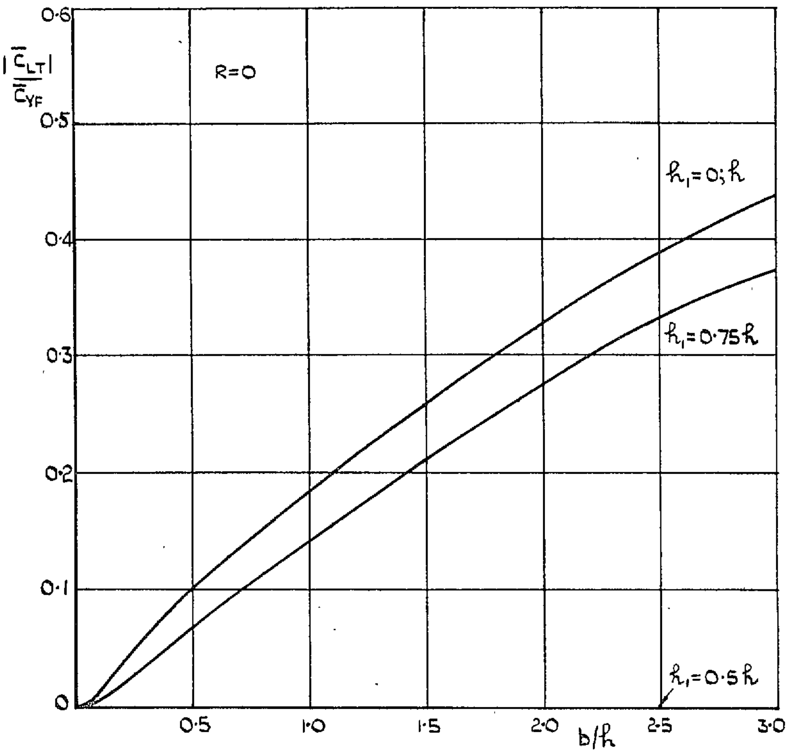

FIG. 9a. Ratio between the lift on one half of the tailplane and the side-force on the fin.

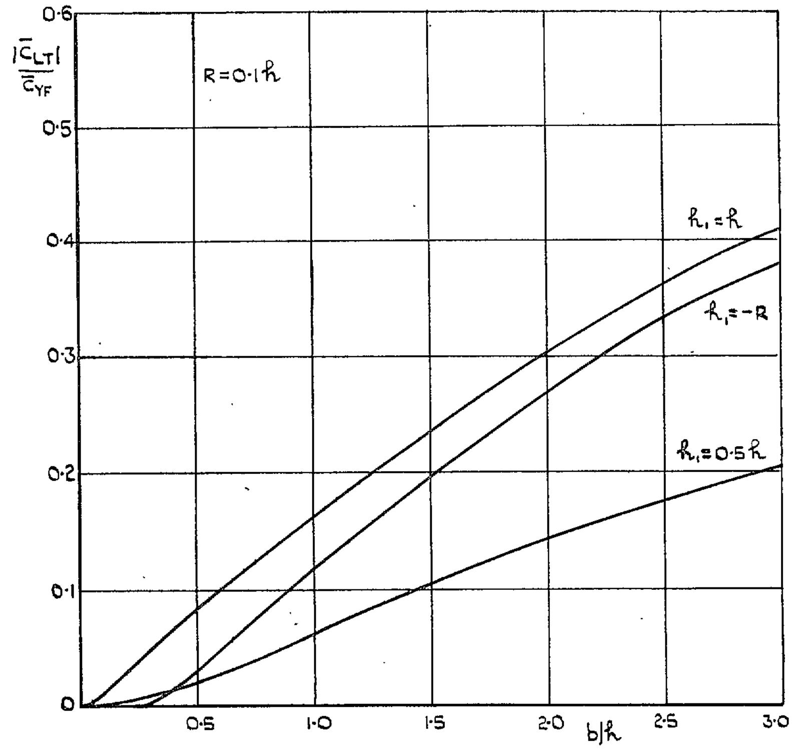

FIG. 9b. Ratio between the lift on one half of the tailplane and the side-force on the fin.

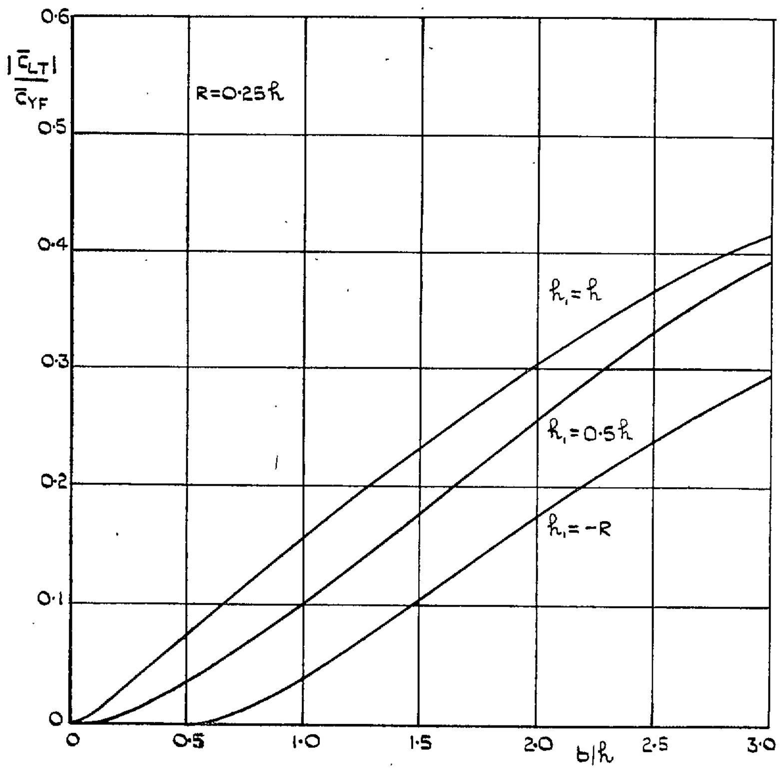

FIG. 9c. Ratio between the lift on one half of the tailplane and the side-force on the fin.

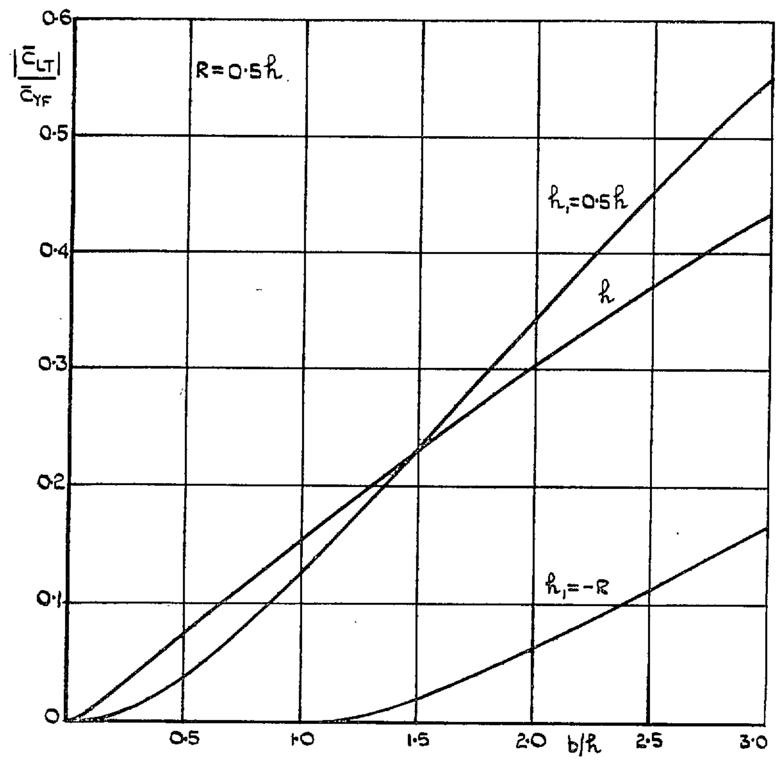

FIG. 9d. Ratio between the lift on one half of the tailplane and the side-force on the fin.

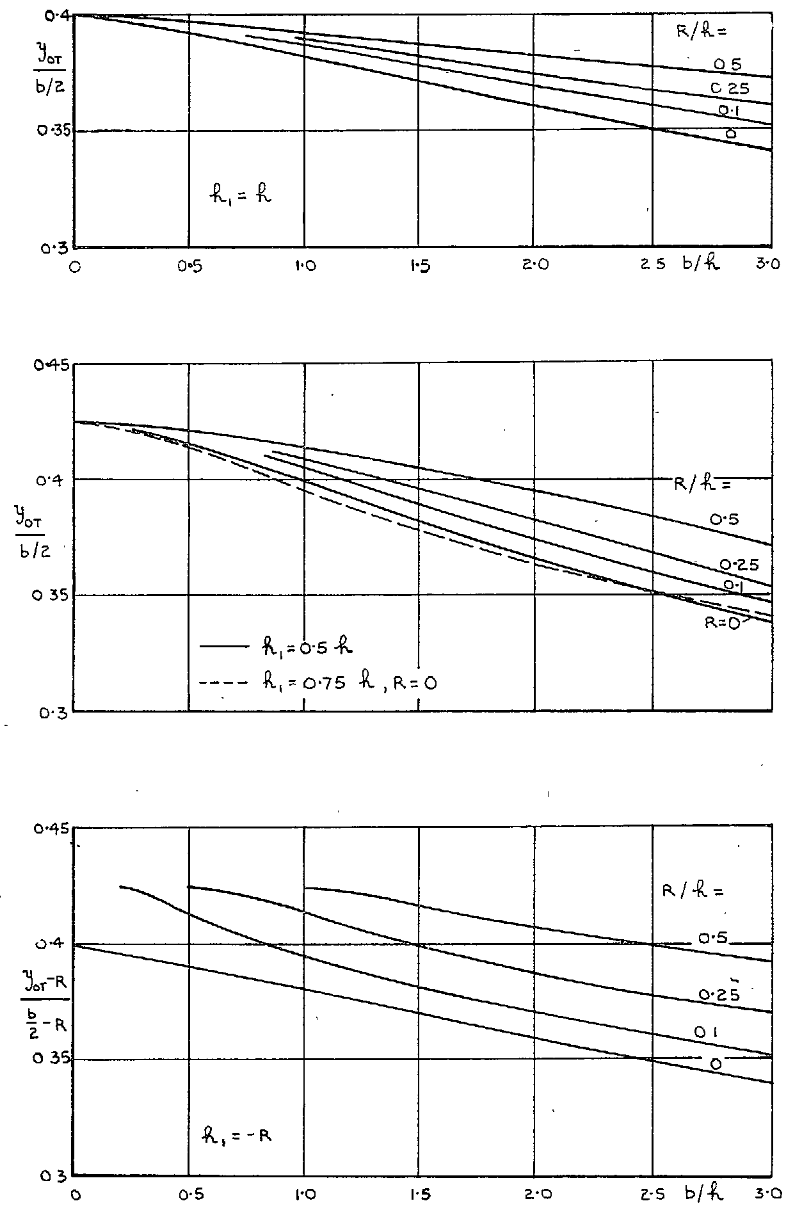

FIG. 10. Moment arm of the lift distribution on the tailplane.

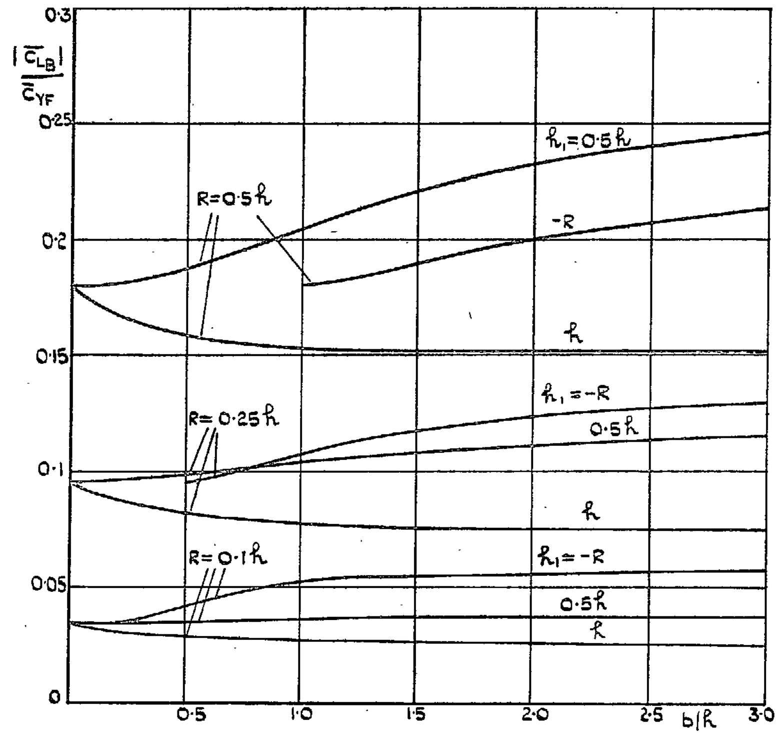

FIG. 11. Ratio between the lift on one half of the body and the side-force on the fin.

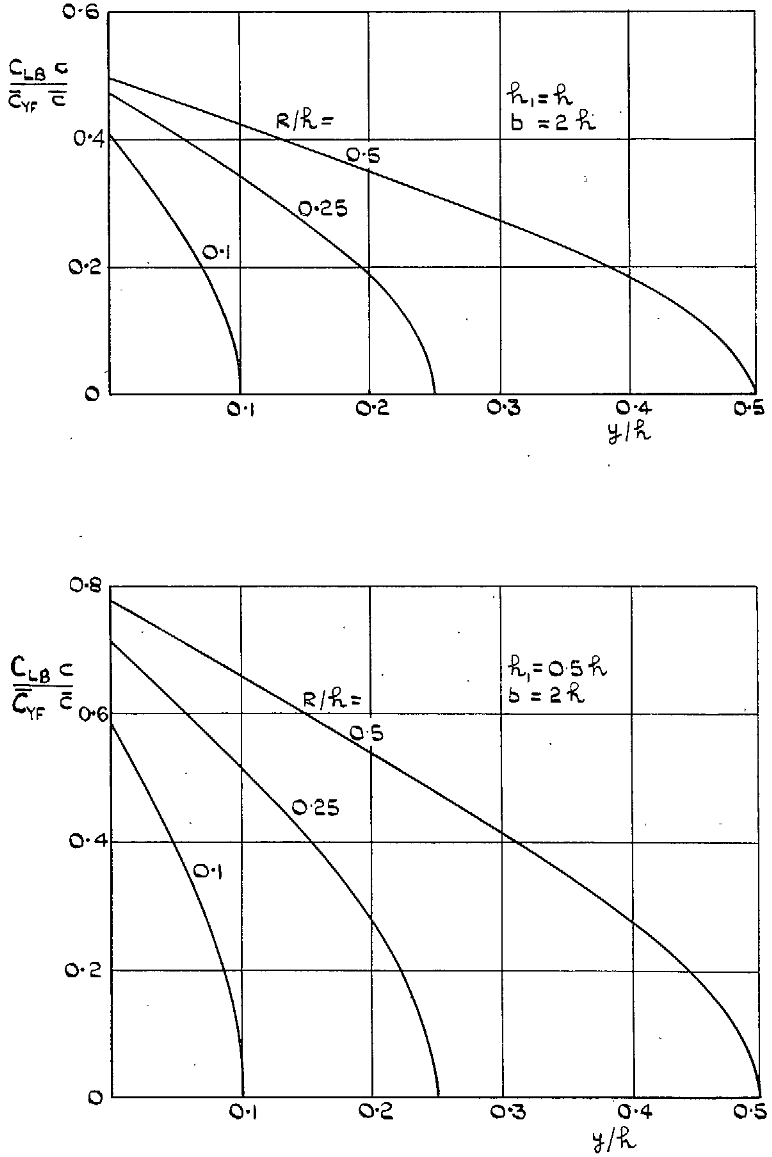

FIG. 12. Lift distribution on the body.

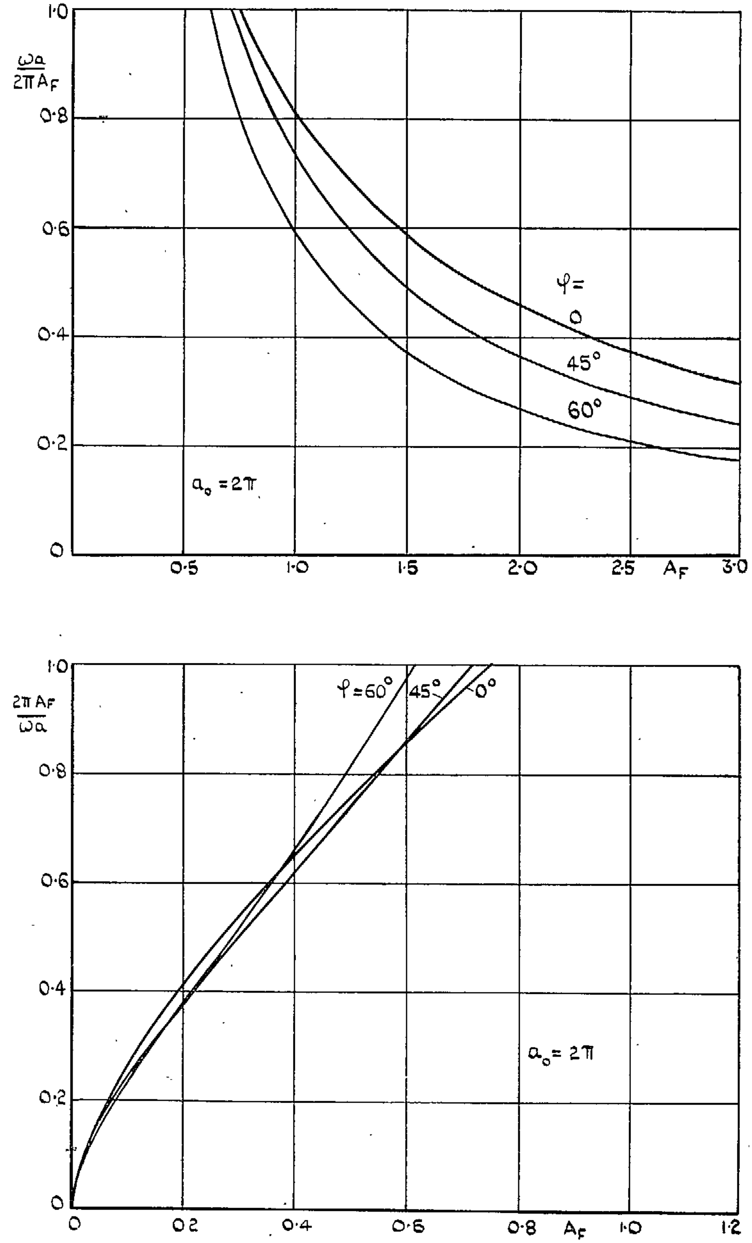

FIG. 13. The parameter $\omega a/2\pi A_F$.

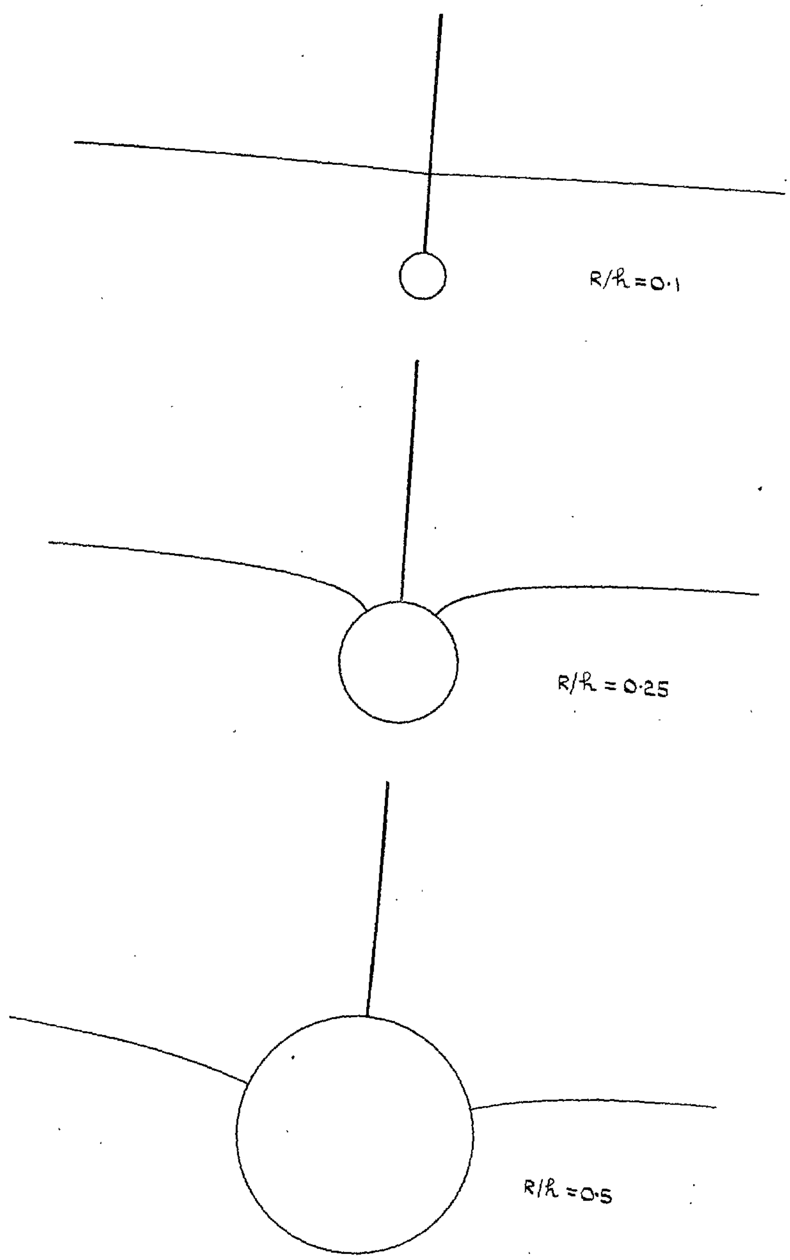

FIG. 14. Neutral tailplanes.

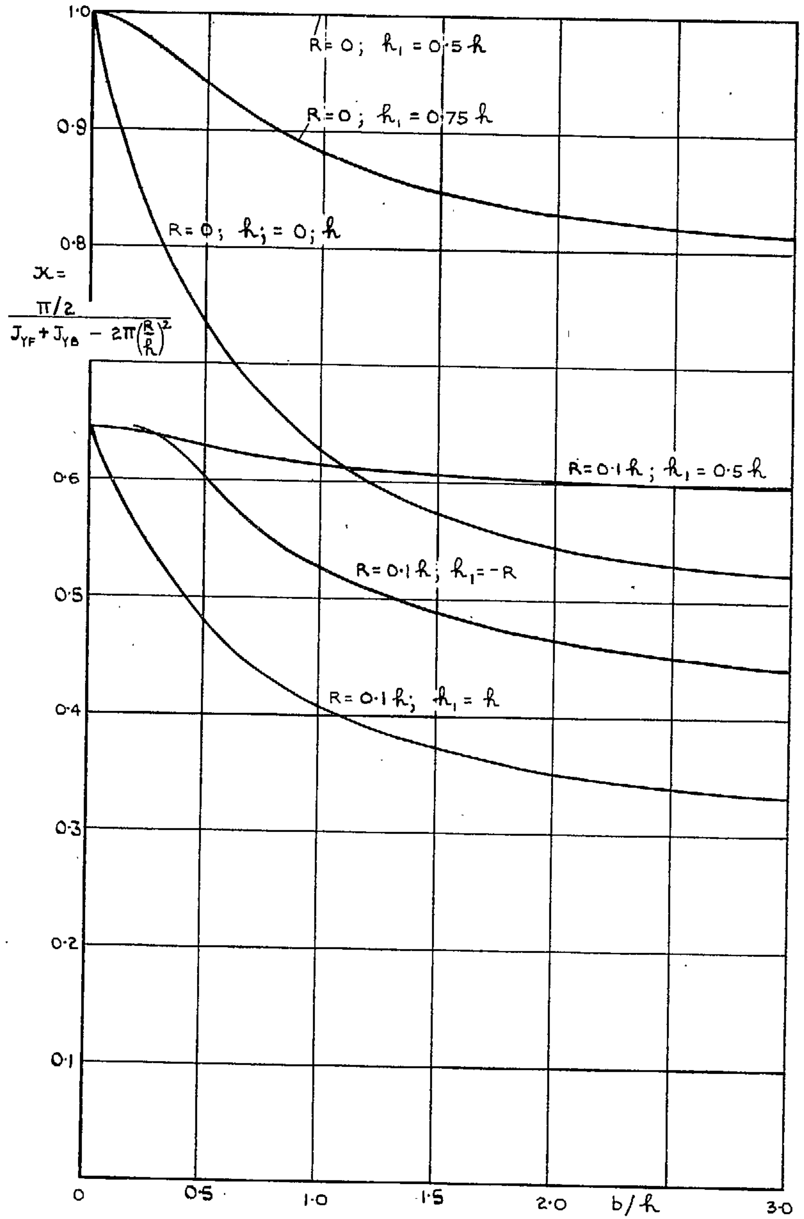

FIG. 15a. Induced drag reduction.
$\bar{C}_{Di} = \varkappa \, . \, \bar{C}_Y{}^2/\pi A_F.$

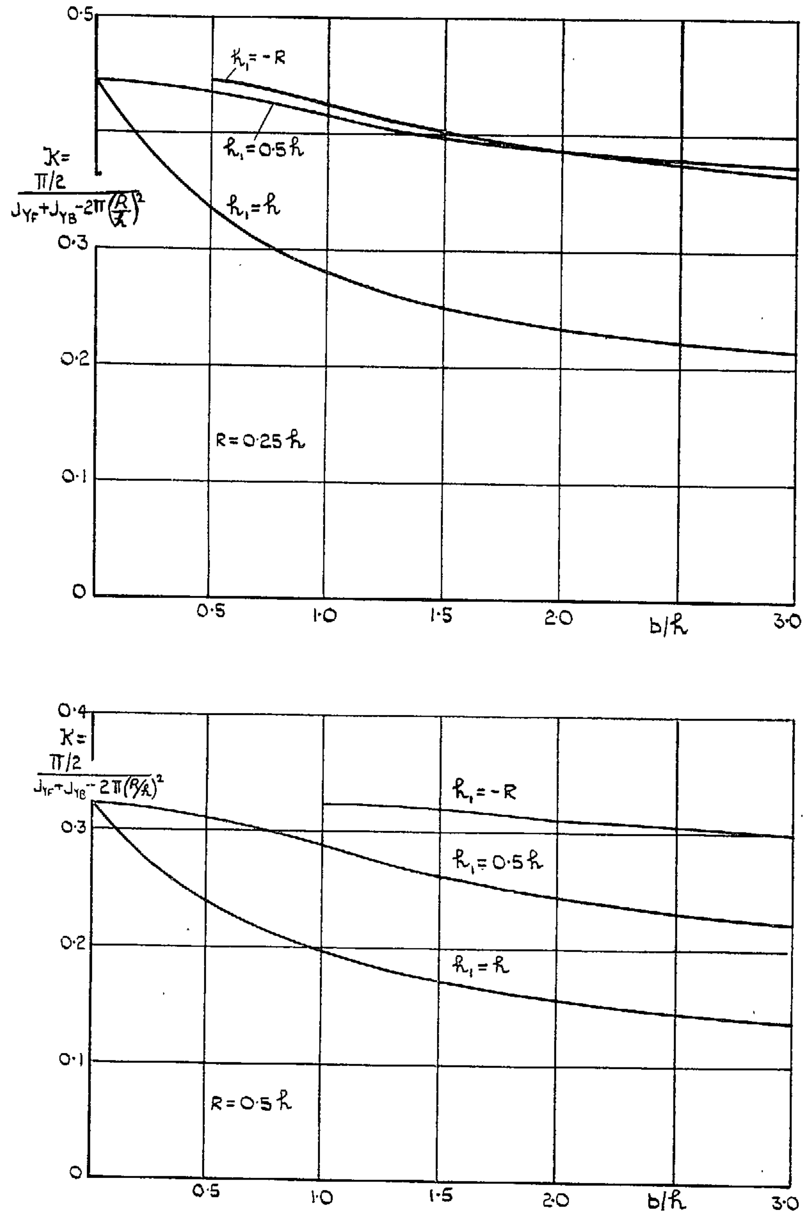

FIG. 15b. Induced drag reduction.
$\bar{C}_{Di} = \varkappa \, . \, \bar{C}_Y{}^2/\pi A_F.$

(4754) Wt. 20/9086 K.7 3/57 Hw.

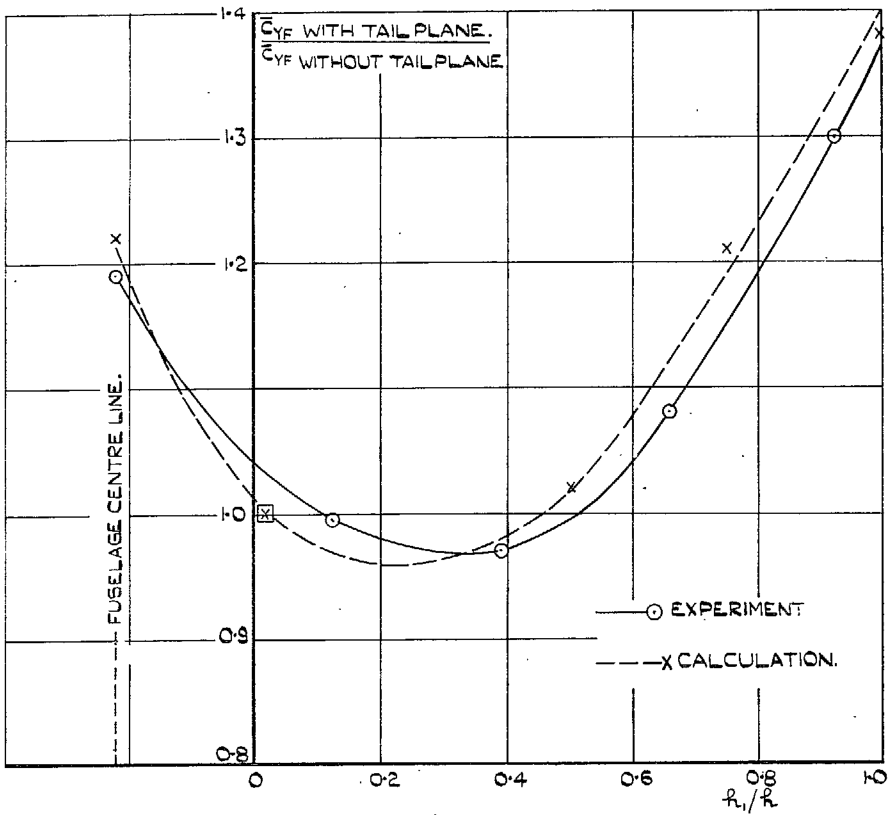

$A_F = 1{\cdot}37$, $\varphi = 0$, $R/h = 0{\cdot}22$
$b/h = 1{\cdot}93$ FOR $h_1 > 0$
$b/h = 2{\cdot}28$ FOR $h_1 < 0$

FIG. 16. Comparison of experimental and calculated side-force coefficients.

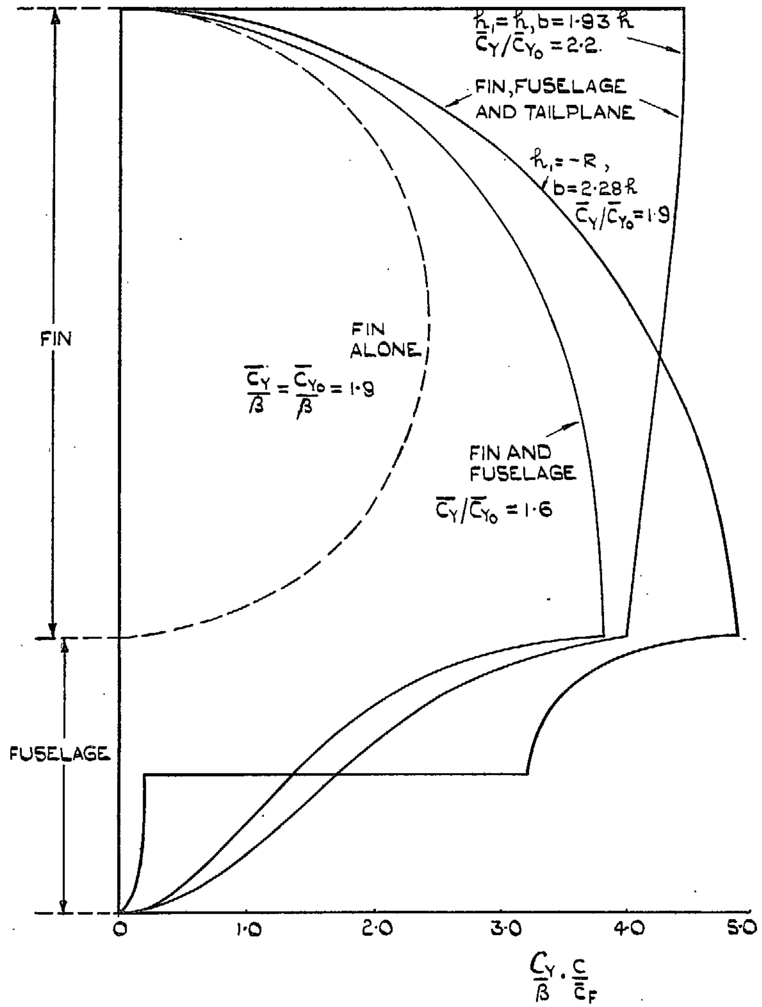

$A_F = 1{\cdot}37$, $\varphi = 0$, $R/h = 0{\cdot}22$

FIG. 17. Side-force distributions.

PRINTED IN GREAT BRITAIN

Publications of the Aeronautical Research Council

ANNUAL TECHNICAL REPORTS OF THE AERONAUTICAL RESEARCH COUNCIL (BOUND VOLUMES)

1939 Vol. I. Aerodynamics General, Performance, Airscrews, Engines. 50*s.* (51*s.* 9*d.*).
Vol. II. Stability and Control, Flutter and Vibration, Instruments, Structures, Seaplanes, etc. 63*s.* (64*s.* 9*d.*)

1940 Aero and Hydrodynamics, Aerofoils, Airscrews, Engines, Flutter, Icing, Stability and Control Structures, and a miscellaneous section. 50*s.* (51*s.* 9*d.*)

1941 Aero and Hydrodynamics, Aerofoils, Airscrews, Engines, Flutter, Stability and Control Structures. 63*s.* (64*s.* 9*d.*)

1942 Vol. I. Aero and Hydrodynamics, Aerofoils, Airscrews, Engines. 75*s.* (76*s.* 9*d.*)
Vol. II. Noise, Parachutes, Stability and Control, Structures, Vibration, Wind Tunnels. 47*s.* 6*d.* (49*s.* 3*d.*)

1943 Vol. I. Aerodynamics, Aerofoils, Airscrews. 80*s.* (81*s.* 9*d.*)
Vol. II. Engines, Flutter, Materials, Parachutes, Performance, Stability and Control, Structures. 90*s.* (92*s.* 6*d.*)

1944 Vol. I. Aero and Hydrodynamics, Aerofoils, Aircraft, Airscrews, Controls. 84*s.* (86*s.* 3*d.*)
Vol. II. Flutter and Vibration, Materials, Miscellaneous, Navigation, Parachutes, Performance, Plates and Panels, Stability, Structures, Test Equipment, Wind Tunnels. 84*s.* (86*s.* 3*d.*)

1945 Vol. I. Aero and Hydrodynamics, Aerofoils. 130*s.* (132*s.* 6*d.*)
Vol. II. Aircraft, Airscrews, Controls. 130*s.* (132*s.* 6*d.*)
Vol. III. Flutter and Vibration, Instruments, Miscellaneous, Parachutes, Plates and Panels, Propulsion. 130*s.* (132*s.* 3*d.*)
Vol. IV. Stability, Structures, Wind Tunnels, Wind Tunnel Technique. 130*s.* (132*s.* 3*d.*)

Annual Reports of the Aeronautical Research Council—

1937 2*s.* (2*s.* 2*d.*) 1938 1*s.* 6*d.* (1*s.* 8*d.*) 1939–48 3*s.* (3*s.* 3*d.*)

Index to all Reports and Memoranda published in the Annual Technical Reports, and separately—

April, 1950 - - - - R. & M. 2600 2*s.* 6*d.* (2*s.* 8*d.*)

Author Index to all Reports and Memoranda of the Aeronautical Research Council—

1909—January, 1954 R. & M. No. 2570 15*s.* (15*s.* 6*d.*)

Indexes to the Technical Reports of the Aeronautical Research Council—

December 1, 1936—June 30, 1939	R. & M. No. 1850	1*s.* 3*d.* (1*s.* 5*d.*)
July 1, 1939—June 30, 1945	R. & M. No. 1950	1*s.* (1*s.* 2*d.*)
July 1, 1945—June 30, 1946	R. & M. No. 2050	1*s.* (1*s.* 2*d.*)
July 1, 1946—December 31, 1946	R. & M. No. 2150	1*s.* 3*d.* (1*s.* 5*d.*)
January 1, 1947—June 30, 1947	R. & M. No. 2250	1*s.* 3*d.* (1*s.* 5*d.*)

Published Reports and Memoranda of the Aeronautical Research Council—

Between Nos. 2251–2349	R. & M. No. 2350	1*s.* 9*d.* (1*s.* 11*d.*)
Between Nos. 2351–2449	R. & M. No. 2450	2*s.* (2*s.* 2*d.*)
Between Nos. 2451–2549	R. & M. No. 2550	2*s.* 6*d.* (2*s.* 8*d.*)
Between Nos. 2551–2649	R. & M. No. 2650	2*s.* 6*d.* (2*s.* 8*d.*)

Prices in brackets include postage

HER MAJESTY'S STATIONERY OFFICE

York House, Kingsway, London W.C.2; 423 Oxford Street, London W.1 (Post Orders: P.O. Box 569, London S.E.1) 13a Castle Street, Edinburgh 2; 39 King Street, Manchester 2; 2 Edmund Street, Birmingham 3; 109 St. Mary Street, Cardiff; Tower Lane, Bristol, 1; 80 Chichester Street, Belfast, *or through any bookseller.*

S.O. Code No. 23–2992

R. & M. No. 299